How network processing shapes photoreceptor output

An Dau

A thesis submitted for the degree of

Doctor of Philosophy

Department of Biomedical Science

The University of Sheffield

September 2013

Acknowledgement

The last four years have been a fantastic period of my life. I have been given the chance to explore some exciting bits of science, to meet amazing people and to fulfil some of my childhood dreams. There were ups and downs, but in retrospect, I would always look back and think “it was truly a great time”. First and foremost, I would like to thank Professor Mikko Juusola. He appeared out of the blue and recruited me in 2009, and ever since has been not only a generous supervisor, but also an inspiring friend and a father figure. I would not be where I am now without him.

From day one, I have been extremely lucky to share the office with wonderful colleagues, who outside the lab are also my good friends. Many thanks to Uwe Friederich, Zhuoyi Song, Marie Baxter, Sidhartha Dongre, Olivier List and Florence Blanchard. I deeply appreciate the fun time we had together and your great help during my study.

Very special thank you I would like to give to Xiaofeng Li. The adventures we went through together will live long in my memory and I am sure our brotherhood will thrive.

The work in this thesis was supported by funding from the University of Sheffield and by help from my advisors. Thank you, Matthew Holley, Alex Whitworth and Mark Bevan.

I would also like to thank my friends in Sheffield and the VietSoc Sheffield, who have made my stay in this city a cheerful time.

I am especially grateful to my friend Son Vi, who I admire and have learnt a great deal from. His love for science has inspired me in many ways.

Also, I am indebted to my best friend Dung Nguyen. Her encouragement has meant a lot during the difficult times of my study.

Everything I am, I owe it to my family. This thesis was made possible by the unfailing love and support of my parents, brother, sister-in-law, my fiancée and my soon-to-be brother-in-law. Words are not enough to thank them.

Abstract

Despite their small-sized “wetware”, flies have conquered myriads of terrains, evolving vastly varied visual lifestyles. One of the key features underlying the success of fly vision is the outstanding performance of its early stages, in which information sampling and processing is dynamically optimised to better suit the surrounding environment. Although much research on fly retina and primary interneurons has been initiated, little is known about how individual neural component contributes to their adaptive processing and how network feedback might regulate photoreceptor responses according to the encountered situation.

My PhD study elucidated the issues mentioned above by studying early vision of two dipteran species: fruitfly (*Drosophila melanogaster*) and blowfly (*Calliphora vicina*). I have measured electroretinograms from their compound eyes, performed intracellular recordings from their photoreceptors and Large Monopolar Cells (LMCs) and employed behavioural paradigms to test their optomotor responses. The recorded biological data were then analysed by advanced signal processing techniques and used to produce Volterra series models, which yield fast predictions of photoreceptor outputs.

The results presented in this thesis quantify the impacts of missing the small- and/or large-conductance calcium-activated potassium channels on response dynamics and adaptability of photoreceptor/LMCs, and on photoreceptor survival. The different adaptive regimes in early vision of different mutants were further shown to have significant influences on motion perception. In addition, temporal characteristics, spatial receptive field and spatiotemporal resolution of the *Drosophila* wild-type compound eye were compared with that of the Histidine Decarboxylase-deficient mutant, in which synaptic transmissions from photoreceptor to interneurons was non-functional, thus dynamic contributions of network processing to photoreceptor output were missing.

My study provides experimental data that support/verify theories of sensory information processing, which were previously proposed. Moreover, the important role of network feedback, as a photoreceptor’s gain controller, and the benefit of specific ion channels in improving effectiveness/robustness of neural communication were highlighted.

Table of Contents

List of Abbreviations

AC	Amacrine cell
CNS	Central nervous system
DRA	Dorsal rim area
EM	Electron microscopy
GWN	Gaussian white-noise
LICs	Light-induced currents
LMCs	Large monopolar cells
LPTC	Lobula plate tangential cells
MSE	Mean squared error
NS	Naturalistic stimuli
PDFs	Probability density functions
SEM	Standard error of mean
SNR	Signal-to-noise ratio

List of Figures

List of Supplement Figures

List of Tables

List of Symbols

α_n	Angular position of a light source
$\boldsymbol{C}$	Relative change of receptive field half-width
d	Rhabdomere diameter
$\Delta\rho$	Width at half-maximum of photoreceptor receptive field
$\Delta\varphi$	Interommatidial angle
$\Delta\varphi_e$	Effective interommatidial angle
D	Resolvability of photoreceptor's neural image/ommatidium lens diameter (see context)
f	Focal distance
F	Accuracy (fitness) of Volterra model prediction
F_s	Sampling rate
I_0	Intensity of light flash from a lighting point at the centre of the photoreceptor's receptive field
I_a	Effective intensity that is absorbed by a photoreceptor
I_n	Intensity of light flash from a lighting point at angular position α_n
k	Volterra kernel
λ	Wavelength
O	Optomotor index
P	Regression matrix
P^+	Moore-Penrose pseudoinverse matrix of the regression matrix
R	Information transfer rate
R_C	Relative change of neural image's resolvability
R_m	Photoreceptor membrane's input resistance
$\boldsymbol{RM}$	Response mean
$\boldsymbol{RV}$	Relative variation

$u(t)$	Time series of light stimuli
ν_s	Maximum resolvable spatial frequency
V	Resting potential of dark-adapted photoreceptor
$V / \log(I)$	Intracellular voltage response / logarithm of light intensity
V_0	Amplitude of photoreceptor intracellular response to light flash from a lighting point at the centre of the photoreceptor's receptive field
V_n	Amplitude of photoreceptor intracellular response to light flash from a lighting point at angular position α_n
w	Object's angular speed
S	Spatial half-width of moving object's retinal image
S_n	Sensitivity of photoreceptor to light coming from incident angle α_n
θ	Column of kernel values
θ	Least-squares estimation of kernel value column
τ	Regression time
τ	Time constant
T	Finite limit of system memory
T_h	Temporal half-width of photoreceptor voltage response
$y(t)$	Time series of photoreceptor voltage response
Y	Sequence of photoreceptor voltage values

Chapter 1: General introduction

1.1 Motivation and Objectives

The compound eyes have poor optic and the small brains of flies only possess limited computation capacities. Yet fly vision has thrived for more than 300 million years (Borst and Haag, 2002), with the ability to encode ~10^9-fold changes of surrounding light and flight manoeuvres amongst the fastest of the animal kingdom (Land and Collett, 1974). Such outstanding performance ultimately depends on how visual information is sampled and processed at the earliest stages. Thus, over the last decades, fly early vision has been used as a fruitful model to study fundamental questions of sensory processing.

Thanks to the intensive research, we now know relatively well how the absorption of photons leads to voltage response of photoreceptor, the physical wiring in the photoreceptor/interneurons network, the different pathways that visual information is routed into, and how network adaptation helps to maintain and improve coding efficiency. However, little is understood about the influence of lateral and centrifugal feedback on photoreceptor output. To make the most out of the biophysically-constrained "wetware", does network activity start refining fly vision already at the level of retina?

With this thesis, I aimed to advance knowledge in that particular issue by studying early visual processing of two species: the fruit fly *Drosophila Melanogaster* and the blowfly *Calliphora Vicina*. *In vivo* electrophysiological techniques and behavioural paradigms were combined with the advanced genetic tools in *Drosophila*, which allowed precise manipulation of specifically targeted neural function/connectivity.

I have carried out two projects during my PhD study. Firstly, I studied the impacts of removing either or both calcium-activated potassium channels, which are expressed ubiquitously in the lamina and higher order neurons but very weakly in the retina. Therefore, abnormal characteristics found in mutant photoreceptor output could be attributable to the input from their altered interneurons. Secondly, I compared photoreceptors of wild-type *Drosophila* and the Histidine Decarboxylase-deficient mutant hdc^{JK910}, in which synaptic transmissions from photoreceptor to LMCs were blocked. Discrepancies in their photoreceptors' temporal properties, spatial acuity

and retinal images of moving objects would potentially reflect the different effects caused by light-dependent (in wild-type) and tonic (in mutant) lamina feedback.

1.2 Outline of the thesis

The thesis consists of a general introduction and four result chapters, in each of them specific questions were addressed and the experiment findings were discussed. In the remaining of this chapter, the outline of the thesis is provided, followed by a brief review of relevant literature.

The study in Chapter 2 quantifies how Ca^{2+}-activated K^{+}-channels reduce network excitability (energetics), improving neural adaptability and survival for transmitting and perceiving sensory information. Despite photoreceptors of *Drosophila* BK- (*dSlo4*) and SK-channel (*dSK*) single-mutants and (*dSK*$^{-}$;;*dSlo4*) double-mutant sample light information normally, single-mutant photoreceptors are more depolarised and respond faster than double-mutant or wild-type counterparts, while post-synaptic single-mutant and wild-type LMC-interneurons respond slower than double-mutant LMCs. Moreover, during repetitive naturalistic stimulation, output ranges of different mutant photoreceptors adapt differently as the network dynamically rebalances its synaptic loads. Thus, Ca^{2+}-activated K^{+}-channels shape photoreceptor and LMC outputs through synaptic interactions, whereupon specific mutation effects are compensated homeostatically to unique adaptive regimes. We further show that these adaptive regimes limit the mutants' motion perception and through cytotoxic excessive activity can reduce photoreceptor longevity.

This work is the outcome of Juusola lab's collaboration with scientists at Cambridge University and Dartmouth College. Electrophysiological data were equally contributed by me and another member of our lab, Xiaofeng Li.

Chapter 3 further investigated potential influences of network feedback on photoreceptor temporal dynamics. I compared temporal responses characteristics of wild-type photoreceptors with those of the *hdc*^{JK910} mutant. Although mutant photoreceptors exhibited normal adaptability during light transitions, they were found to have artificial higher resting potential, most likely due excessive and tonic excitatory feedbacks. Importantly, the data presented in this chapter illustrate that wild-type photoreceptors operate in wider intensity range and encode naturalistic light modulations more robustly that those of mutants. Together with previous

studies in the literature, these findings demonstrate important roles of lamina feedback as photoreceptors' dynamic gain controller.

In Chapter 4, the comparative study on wild-type and *hdc*^{JK910} photoreceptors focused on their static spatial characteristics. Under moderate ambient illumination and the desensitisation impacts of prolonged light exposure, wild-type and mutant photoreceptors exhibited similar acceptance angle. In contrast, careful assessments on a large number of samples indicated that dark-adapted mutant photoreceptors have narrower receptive field than their wild-type counterparts. The available data are suggestive but not conclusive of a hypothesis in which, in dim condition, neural information of neighbouring cartridges is pooled together at the lamina network and fed back to photoreceptors. Specific physiological and morphological studies are recommended for future research. Besides, retinal movements of up to 3.5º in the *Drosophila* eye were also reported.

In Chapter 5, properties of retinal images in the fly eye were studied by monitoring intracellular responses of photoreceptors to actual moving objects. Compensation for neural latency and directional preference were not found at this sampling stage, emphasising that certain features of motions are only extracted/processed by higher order interneurons. Also, I examined the dependence of neural image resolutions on object speeds and verified previous theoretical studies, which predicted the existence of two domains where resolution is dictated by optic quality and object speed, respectively. Moreover, spatiotemporal performances of wild-type and *hdc*^{JK910} compound eye were compared. My data suggest that top-down regulation fine-tunes the trade-off between sensitivity and resolution of retinal images according to ambient light. Lastly, the chapter provides a detailed description of a fast modelling method where Volterra series was used to simulate photoreceptor responses.

1.3 Overview of the fly visual system

In this section, structural and functional organisation of the fly visual system will be briefly reviewed with the main focus on early processing stages. Results of studies on *Drosophila*, *Musca*, *Calliphora* and *Lucilia* are presented together as highly conserved features were commonly found in neural functions and connectivity of these species (Buschbeck and Friedrich, 2008, Takemura et al., 2008).

Light coming from the surrounding environment is sampled by three types of eyes. Whilst the compound eye and the ocelli are the only known light sensing organs in most flies and insects, there are two extra eyes, called H-B eyelet, in *Drosophila* (Hofbauer and Buchner, 1989, Yasuyama and Meinertzhagen, 1999). Nevertheless, the scope of my research is restricted on the former, which are the main eyes with panoramic visual field covering almost every direction around the fly's head. Information captured by the photoreceptors in the retina of the compound eyes is further processed by four optic neuropils: the lamina, medulla, lobula and lobula plate (**Fig. 1-1**) (Borst and Haag, 2002).

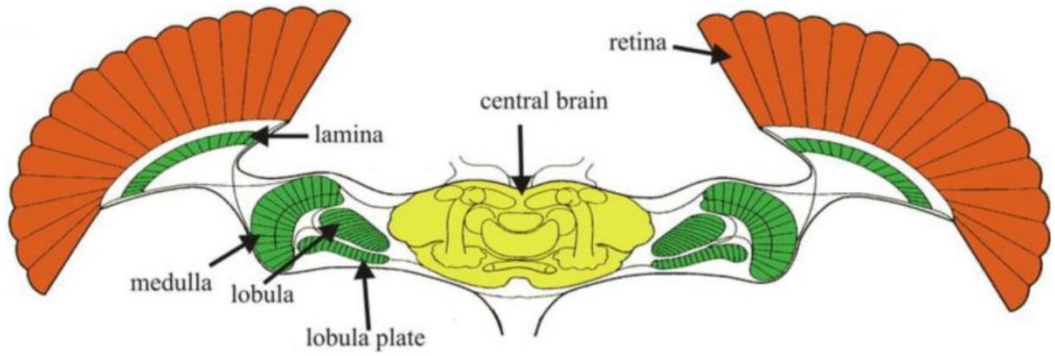

Figure 1-1. Structural organisation of the fly visual system, which consists of the compound eye and four optic neuropils: the lamina, medulla, lobula and lobula plate. Figure adapted from (Borst and Haag, 2002).

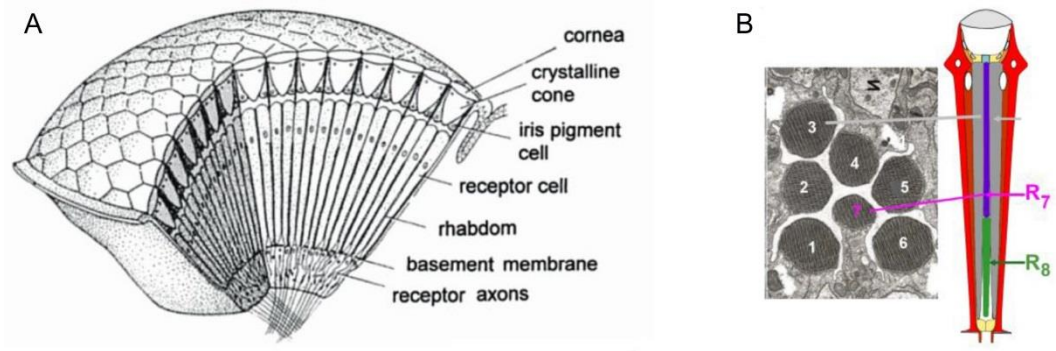

Figure 1-2. **(A)** Schematic structure of the compound eye. Figure from (Land and Nilsson, 2002).

(B) Electron micrograph (left) and schematic structure (right) of an ommatidium in the fly eye. The eight photoreceptors under one facet lens, inside an ommatidium, are aligned to seven different directions. Photoreceptors R7 and R8 lie on top of each other in the centre of the ommatidium and share the same axis. Figure from (Elyada, 2009).

The fly compound eye is made of hundreds to thousands single eyes (from *circa* 750 units in *Drosophila* to 5,000 units in *Calliphora*), each of which is a regular structure called ommatidium (Wolff and Ready, 1993, Land and Nilsson, 2002). The eight photoreceptor cells (R1-R8) inside each ommatidium share the same facet lens (**Fig. 1-2A**) but are aligned to seven different directions (**Fig. 1-2B**). Whilst the outer photoreceptor R1-R6 are most sensitive to light in the green range, spectral sensitivities of the inner cells R7 and R8, which lie on top of each other and point to the same direction, exhibit three distinctive subtypes: pale, yellow and DRA (Clandinin and Zipursky, 2002, Wernet et al., 2003, Wardill et al., 2012). Besides, variations of the eye structure are thought to be tuned for specific purposes (Land, 1989), such as the increase of interommatidial angle alongside the frontal-lateral axis that benefits processing of fast motion (Braitenberg, 1967, Elyada, 2009) and the acute zone in the eye of male fly that support chasing behaviour (Land and Eckert, 1985).

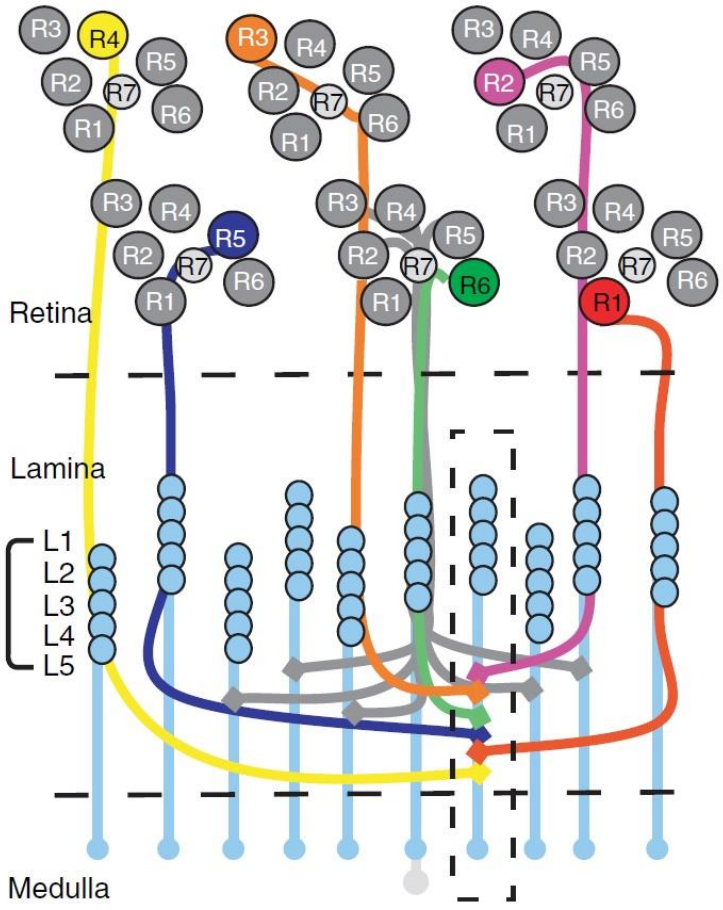

Figure 1-3. Wiring diagram of the retinotopic mapping in the fly lamina. Six outer photoreceptors R1-R6, belonging to six neighbouring ommatidia but pointing to the same direction, send their neural signal downstream to the same lamina column. Figure from (Morante and Desplan, 2005).

Fly eye is of the neural superposition type (Borst, 2009). That is, neural signals of eight photoreceptors belonging to seven neighbouring ommatidia, which look at the same point in space, are pooled together at one neural cartridge in the next two neuropils: the lamina and medulla. While the six outer photoreceptors R1-R6 project their axon terminals to neural columns in the lamina (**Fig. 1-3**), R7 and R8 cells bypass this layer and make synaptic contacts with their corresponding medulla column (Kirschfeld, 1967, Morante and Desplan, 2005, Fischbach and Hiesinger, 2008). These exact wirings produce the neural substrate for the retinotopic mapping of fly early vision, where every lamina and medulla column (cartridge) represents a single point in space.

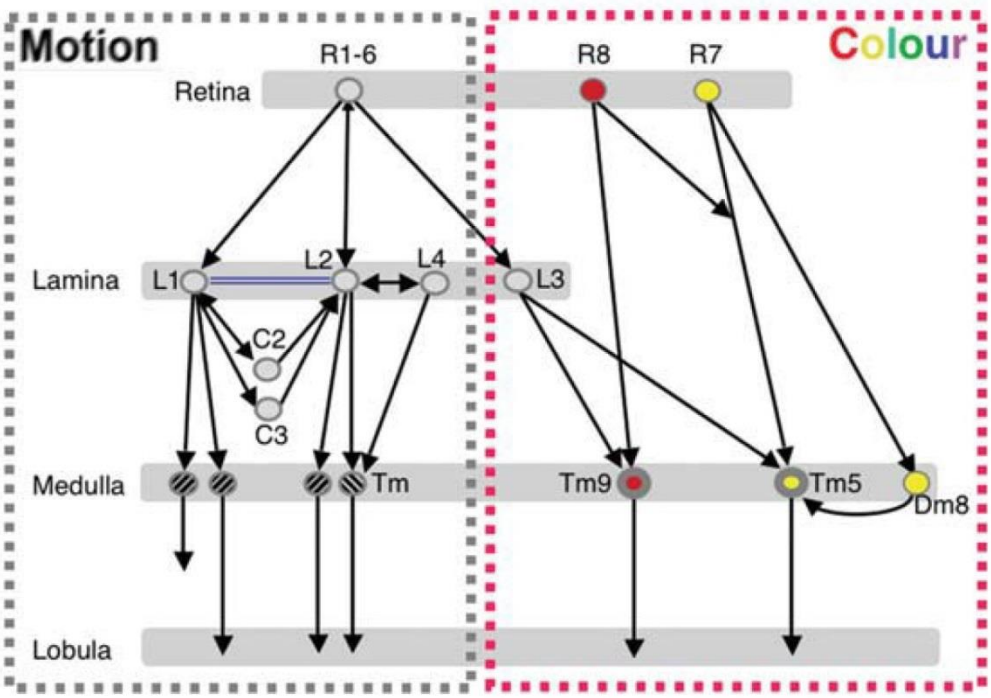

Figure 1-4. Simplified representation of neural pathways in the fly visual system, of which L1 and L2 pathways are thought to be most important for motion perception. Figure from (Melnattur and Lee, 2011).

Direct inputs from R1-R6 photoreceptors are received by the Large Monopolar Cells (LMCs) L1, L2, L3 and the Amacrine Cell (AC) in the lamina (Shaw, 1984, Meinertzhagen and Sorra, 2001). Out of these, L1 and L2 are the largest cells, mediating major information pathways (**Fig. 1-4**), which respond to on and off moving edges, thus form the computational basis of the motion detector (Joesch et al., 2010, Clark et al., 2011). At intermediate contrast, the two pathways facilitate motion perception of opposite directions, back-to-front in L1 and front-to-back in L2 (Rister et al., 2007, Vogt and Desplan, 2007). Electron Microscopy (EM) works have

shown that L4 neurons play critical roles in the lateral connectivity of neighbouring neural cartridges (Strausfeld and Braitenberg, 1970, Strausfeld and Campos-Ortega, 1973). Reciprocal synapses were found between L2 and L4 cells located in the same and two adjacent columns. Downstream, each L2 cell and its three associated L4 cells project their axons to a common target, the Tm2 neuron in the Medulla, where inputs from neighbouring cartridges are believed to be integrated for processing of front-to-back motion (Takemura et al., 2011). Although L1 neurons receive input from same-cartridge L2s via both gap junctions and synapses, they are not directly connected to L4s and hence adjacent lamina columns.

Synaptic feedbacks to photoreceptor axons are provided only by neurons belonging to the L2/L4 circuits but not the L1 pathway (Meinertzhagen and Oneil, 1991, Rivera-Alba et al., 2011). Whilst same-cartridge connections are selectively from L2 to R1 and R2 and from L4 to R5, all photoreceptor R1-6 receive feedback signals from L4 of either or both neighbouring cartridges. Besides, there are strong synaptic connections from AC to R1, R2, R4 and R5 and glia cells are also synaptically connected to the network (**Table 1-1**) and may thus participate in visual information processing.

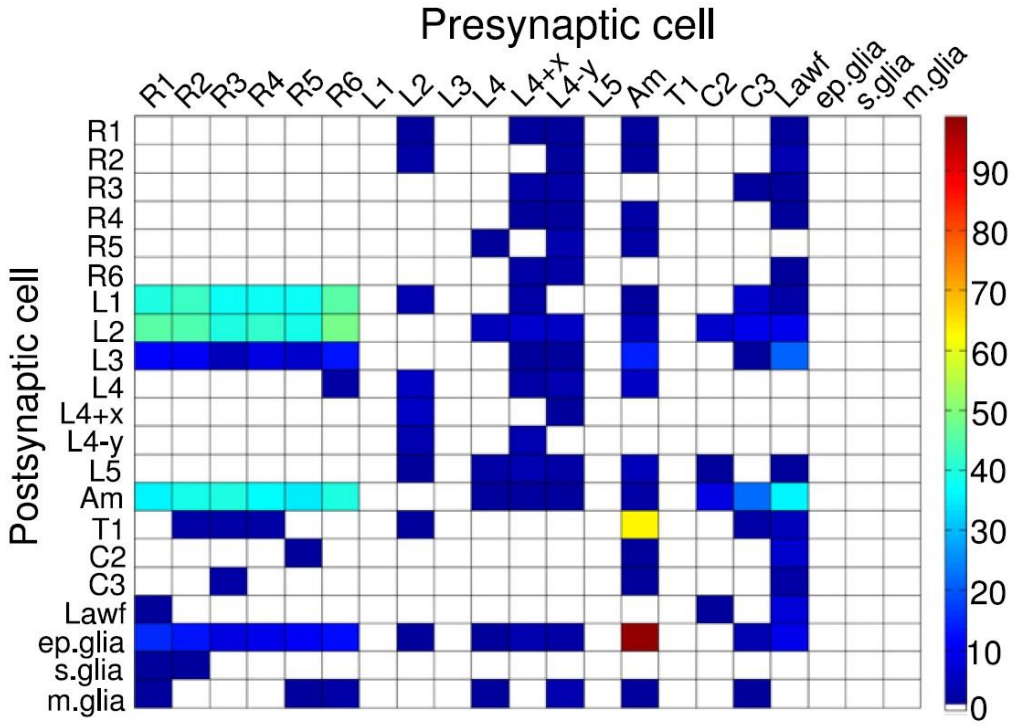

Table 1-1. Synaptic connectivity between neurons within a neural cartridge. Number of synapses are coded by colour as indicated by the column on the right. Table from (Rivera-Alba et al., 2011).

In both dim and bright conditions, receptive fields of fly photoreceptors measured physiologically at the level of somata are purely excitatory and predictable from optical and physical considerations (see section 1.3). In contrast, those of LMCs were found to be largely dependent on ambient light. While dark-adapted LMCs and photoreceptors exhibit very similar receptive fields, measurements on light-adapted LMCs reported centre-surround organisation, with the width and strength of the antagonistic surround vary according to ambient illumination (Dubs, 1982, Srinivasan et al., 1990). This complex structure of LMCs receptive field is attributable to the lateral interactions between neighbouring cartridges, most probable via L4 collateral branches.

The rich horizontal connectivity also suggests that temporal information might be compared laterally in the lamina, thus motion processing could happen as early as in this neuropil. However, signs of motion-sensitive response were only found by labelling with radioactive deoxyglucose in the bushy T-cells T4 and T5 of the next layers, the medulla and lobula, respectively (Bausenwein and Fischbach, 1992, Douglass and Strausfeld, 2003).

The lobula plate is a flat structure with four layers, each of them is thought to contain information of local motion belonging to a different direction (Eckert, 1982, Hengstenberg et al., 1982), which is processed by a class of large neurons, the lobula plate tangential cells (LPTCs) (Egelhaaf and Borst, 1993). The 60 LPTCs in each hemisphere of the blowfly brain play vital roles in the optomotor response circuit and are categorised into subgroups according to their directional preference, although local directional sensitivity varies within their large receptive field. Detailed descriptions of LPTCs can be found in the work by Borst and Haag (2002), Egelhaaf et al. (2002) and Borst and Haag (2007).

1.4 Response of fly photoreceptor to light stimuli

The process which converts light energy to photoreceptor electrical signals can be described by two functional blocks, as depicted in **Fig. 1-5A**.

The first block is implemented in the stack made from tens of thousands of photosensitive microvilli (from around 30,000 units in *Drosophila* to 90,000 units in *Calliphora*), known as a rhabdomere (**Fig. 1-5B**). In dark conditions, once a photon is absorbed by light-sensitive pigments in a microvillus, there is a very high probability that a G-protein coupled cascade is activated, generating discrete

quantum current fluctuations (quantum bumps). Molecular components and the sequence of events in this phototransduction cascade are systematically reviewed by (Hardie and Raghu, 2001, Hardie, 2001, Minke and Cook, 2002, Hardie and Postma, 2008) and (Katz and Minke, 2009). Quantum bumps produced by all microvilli are summed up to yield the macroscopic light-induced current (LICs).

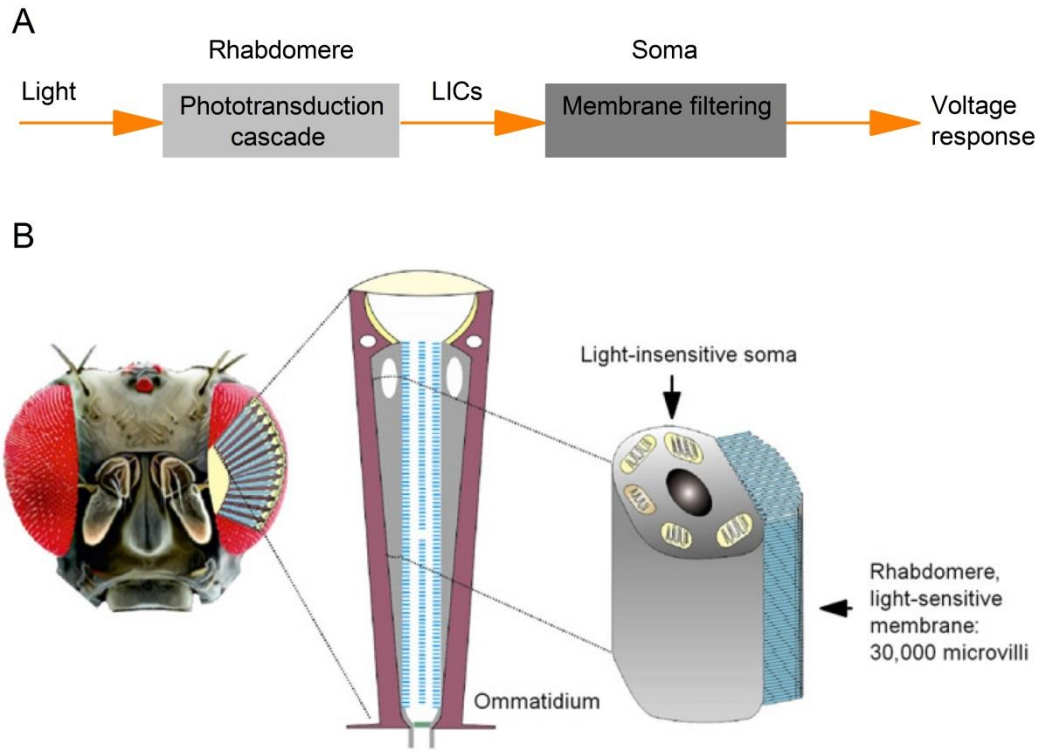

Figure 1-5. **(A)** Voltage response of fly photoreceptor is generated in a process which consists of two functional blocks. Firstly, light input is converted to macroscopic light-induced currents (LICs) by the phototransduction cascade, which happens in the photoreceptor rhabdomere. Secondly, LICs is filtered by the photo-insensitive membrane in photoreceptor soma to produce voltage response.
(B) Schematic structure of a photoreceptor. Figure from (Song et al., 2012).

In the second functional block, LIC is filtered by the light-insensitive membrane in the photoreceptor soma, resulting in the voltage response that drives synaptic transmissions to lamina interneurons. Thus, photoreceptor output is shaped not only by its phototransduction cascade, but also by electrical characteristics of its membrane. The main neural components which define filtering properties of *Drosophila* photoreceptor membrane were identified as voltage-sensitive K^+-channels, including *Shaker* and delayed rectifier channels (Hardie, 1991a, Niven et al., 2003, Niven et al., 2004). Besides, minor contributions to photoreceptor

response of other ion channels such as Na^+- and Cl^-- channels have also been described (Hardie and Raghu, 2001, Ugarte et al., 2005).

More recently, Zheng et al. (2006) showed that lamina feedback, via ligand-gated neurotransmitter channels, also remarkably influences photoreceptor output. Input from higher order interneurons probably acts as a dynamic gain controller, enriching photoreceptor response with high quality LMCs signals or reducing excitatory conductances according to the risk of saturation. Other important roles of network feedback in improving information coding during light adaptation were reported by Zheng et al. (2009) and Nikolaev et al. (2009).

1.5 Spatial resolution of the compound eye

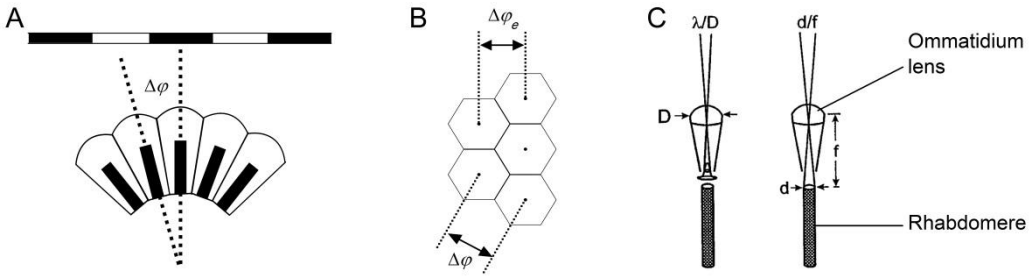

Figure 1-6. **(A)** The minimum angle that a compound eye can resolve is its interommatidial angle.
(B) The effective interommatidial angle of the fly eye with hexagonal layout, $\Delta\varphi_e$, is smaller than its actual interommatidial angle $\Delta\varphi$. Their geometrical relation is described by equation (1-1).
(C) Light diffraction at the ommatidum lens and the rhabdomere tip strongly affect optical quality of photoreceptor.
Figure redrawn from (Land, 1997).

Visual acuity is defined as the minimum angle that the eye can resolve. Since each ommatidium is a basic sampling unit, the upper limit of a compound eye's spatial resolution is set by the density of its ommatidial array (Snyder et al., 1977). Suppose a regular pattern of black and white stripes is presented to the fly. The maximum spatial frequency that the fly can resolve, ν_s, is achieved when one ommatidium points to a black stripe and its adjacent ommatidium "looks" at the next white stripe (**Fig. 1-6A**). Thus, the interommatidial angle $\Delta\varphi$ is the key parameter in determining ν_s (Snyder and Miller, 1977). For compound eyes with hexagonal layout, as in the

case of most flies, the effective interommatidial angle $\Delta\varphi_e$ (**Fig. 1-6B**) can be calculated by the following equation:

$$\Delta\varphi_e = \cos(30^\circ)\Delta\varphi = \frac{\sqrt{3}}{2}\Delta\varphi . \quad (1\text{-}1)$$

Thus, the upper limit of the fly eye's visual acuity is given by:

$$\nu_s = \frac{1}{2(\Delta\varphi_e)} = \frac{1}{\sqrt{3}(\Delta\varphi)} . \quad (1\text{-}2)$$

On the other hand, whether this limit is achieved or not depends on spatial performance of single sampling unit – a photoreceptor (Snyder, 1977). Several factors are considered in the sophisticated estimation of photoreceptor receptive field, which is quantified by its width at half-maximum, or acceptance angle $\Delta\rho$ (Warrant and Mcintyre, 1993).

Firstly, since the lens of ommatidium and rhabdomere of photoreceptor are very small, optical quality is strongly affected by the diffraction of light, of which airy pattern is a function of light wavelength λ, lens diameter D, rhabdomere diameter d and focal distance f (**Fig. 1-6C**). Theoretically, the blurring functions at ommatidium lens and rhabdomere tip are both Gaussian and therefore can be combined to yield a simple approximation of $\Delta\rho$ (Snyder, 1977):

$$\Delta\rho = \sqrt{\left(\frac{\lambda}{D}\right)^2 + \left(\frac{d}{f}\right)^2} . \quad (1\text{-}3)$$

However, this formula could not be safely applied in many cases, owing to the complication of waveguide theory in small-diameter structures. Hateren (1984) and Stavenga (2003a), (2003b) found that along the rhabdomere of fly photoreceptors, only a limited number of light patterns (modes) could be formed and that this number depends on incident angle of light, leading to smaller actual $\Delta\rho$ than what equation (1-3) implies.

In addition, another phenomenon to be taken into account is the spatial cross talk, in which a photon escapes the rhabdomere it first travels in and enters an adjacent rhabdomere (Warrant and McIntyre, 1991). Such effect is likely to happens when the

cross-talk index of the ommatidia/rhabdomere structure is less than three (Wijngaard and Stavenga, 1975). This was found to be indeed the case in *Drosophila* (Gonzalez-Bellido et al., 2011), hence resolution of their neural images might be lower than theoretically calculated.

Lastly, the pupil mechanism could further complicate the estimation of $\Delta\rho$. Inside each photoreceptor cell, there are tiny pigment granules that migrate toward its rhabdomere boundary upon light adaptation. These pigments absorb and scatter light that travels inside the rhabdomere, reducing light influx to be absorbed by photo-sensitive pigments (Kirschfeld and Franceschini, 1969a, Boschek, 1971, Roebroek and Stavenga, 1990). Consequently, pupil mechanism was found to have significant impacts on the angular and spectral sensitivity of photoreceptor (Stavenga, 2004a).

1.6 Theories of sensory processing

Sensory neurons are tasked to sample and encode the astronomical scale of environmental stimuli despite their information capacities are limited with narrow dynamic ranges and noisy signals. Thus, it has been hypothesised that there are conserved principles underlying the efficient coding of sensory messages. The common observation, from which theories of retinal processing were developed, is that intensities of pixels within a natural scene were highly correlated; hence a large portion of natural information is predictable. This led to the pioneering idea that one of the key strategies of early sensory coding is to remove redundancy (Attneave, 1954, Barlow, 1961).

Based on this principle, Srinivasan et al. (1982) introduced the “predictive coding”, which explained rather well the spatial and temporal inhibition found in voltage responses of the fly large monopolar cells. The proposed encoding scheme has two steps. Firstly, the “best linear prediction” of a photoreceptor response is computed from responses of its neighbouring photoreceptors and their spatial correlations. Secondly, only the difference between actual and predicted photoreceptor responses is encoded by interneurons. Such a scheme was shown to help increase sensitivity of neural images whilst reducing the risk of saturating LMCs. Moreover, the dependence of LMCs receptive field on ambient light was also theoretically reproduced. In bright conditions, since the correlation between data sampled at different points in space is high, voltage response of a photoreceptor could be predicted accurately from outputs of other cells within its close vicinity.

Consequently, the estimated antagonistic surround in the receptive field of light-adapted LMCs was strong but narrow. On the other hand, in dim, intensity of a single pixel could not be reliably estimated from its immediate neighbouring but a wider area. The resulting lateral inhibition was therefore weaker and more diffuse.

Another theory was later developed by van Hateren (1992c), who hypothesised that the aim of early sensory processing is to maximise the rate of information it sends downstream. For each specific type of stimuli, this alternative strategy allows the computation of a unique sensory system's transfer function, of which outcome reduces redundancy in bright condition (high signal-to-noise (SNR) stimuli) but increases redundancy in dim (low SNR). The argument was that in situations where photon shot noise is relatively large compared to signal contents, redundancy helps to increase reliability and thus is desirable (Kretzmer, 1954). The theory was then applied to the statistic structure of natural images to estimate the transfer function of fly early vision and simulate response of LMCs to light flashes with high accuracy (Van Hateren, 1992b).

The discrepancy of the two theories is in dim condition, where predictive coding theory only implies the reduction and diffusion of lateral inhibitions while theory for maximising sensory information suggests that signals from neighbouring sampling units should be pooled together, rather than being subtracted from each other. Nevertheless, both theories result in similar trends of sensory system properties: when ambient light changes from dim to bright (stimuli SNRs become higher), characteristics of sensory processing would shift from low-pass to band-pass.

Chapter 2: Ca^{2+}-activated K^{+}-channels reduce network excitability, increasing adaptability and survival for transmitting and perceiving sensory information

2.1 Introduction

Calcium-activated potassium channels are widely expressed in both the visual system and CNS and play important roles in cell physiology, such as mediating neuronal excitability and neurotransmitter release. Based on their kinetics, pharmacological and biophysical properties, these channels can be divided into two main types: the small- (SK: 2-20 pS) and large-conductance (BK: 200-400 pS) channels. The BK channel is both Ca^{2+}- and voltage-dependent, while SK channels are solely Ca^{2+}-activated (Sah, 1996, Faber and Sah, 2003, Stocker, 2004, Salkoff, 2006). At synapses, SK channels form negative feedback loops with Ca^{2+} sources and are therefore essential regulators of synaptic transmission (Faber et al., 2005, Ngo-Anh et al., 2005). The functional role of BK channels in synaptic activities is less well understood, with various effects of blocking BK channels on neurotransmitter release have been reported (Xu and Slaughter, 2005).

Although Ca^{2+}-activated K^{+}-channels – through regulation of synaptic transmission between retinal neurons – seem to have conserved roles in early vertebrate (Shatz, 1990, Wang et al., 1999, Klocker et al., 2001, Pelucchi et al., 2008, Clark et al., 2009, Grimes et al., 2009) and invertebrate vision (Abou Tayoun et al., 2011), it has been difficult to work out how these channels advance *in vivo* circuit functions and what are their evolutionary benefits. This is because of homeostatic processes that regulate electrical activity in neurons, in part, make communication in circuits surprisingly fault-tolerant against perturbations (LeMasson et al., 1993, Marder and Goaillard, 2006). Thus, the physical consequences of altering K^{+}-channel densities and those of homeostatic compensation are interconnected. Because *Drosophila* has single *SK* (*dSK*) and *BK* (*dSlo*) genes, electrophysiologically accessible photoreceptors and interneurons (Juusola and Hardie, 2001b, Zheng et al., 2006) with stereotypical connectivity (Meinertzhagen and Oneil, 1991, Rivera-Alba et al., 2011), and readily quantifiable optomotor behaviour (Blondeau and Heisenberg,

1982), it provides an excellent model system to characterize how Ca^{2+}-activated K^+-channels affect circuit functions and capacity to see. Here, we study to what extend intrinsic perturbations of missing one or both of these K^+-channels can be neutralized by homeostatic processes trying to sustain normal network functions, and what is the price of this compensation. Our results quantify the benefits of Ca^{2+}-activated K^+-channels in improving robustness, economics and adaptability of neural communication and visual perception.

2.2 Materials and Methods

2.2.1 Fly Stocks

The *dSK*$^-$ and *UAS-dSKDN* alleles were prepared as described earlier (Abou Tayoun et al., 2011). *Df7753* or *Df(1)Exel6290* line was obtained from Bloomington *Drosophila* stock center. *dSlo4* null allele (Atkinson et al., 1991) was a generous gift from Nigel Atkinson's lab. The *dSK*$^-$, *dSlo4* and *dSK*$^-$;;*dSlo4* lines were all outcrossed to a *w1118* background for the extracellular recording and eye morphology experiments. For intracellular recordings, these lines were outcrossed to Canton-S background.

2.2.2 Intracellular recordings

We prepared 3-7 days old (adult) female flies, reared in 12:12 h dark:light-cycle for *in vivo* experiments. A fly was fixed in a conical fly-holder with beeswax, and a small hole (6-10 ommatidia) for the recording microelectrode entrance was cut in its dorsal cornea and Vaseline-sealed to protect the eye (Juusola and Hardie, 2001a, Zheng et al., 2006). Sharp quartz and borosilicate microelectrodes (Sutter Instruments), having 120–200 MΩ resistance, were used for intracellular recordings from R1-R6 photoreceptors and large monopolar cells (LMCs). These recordings were performed separately; with the electrodes filled either with 3 M KCl solution for photoreceptor or 3 M potassium acetate with 0.5 mMKCl for LMC recordings, to maintain chloride battery. A reference electrode, filled with fly ringer, was gently pushed through ocelli ~100 µm into the head, where temperature was kept at 19 ± 1°C by a feedback-controlled Peltier device (Juusola and Hardie, 2001b). Only stable high quality recordings were included in this study. In darkness, photoreceptors' resting potentials were <−50 mV and maximum responses to saturating bright pulses >40 mV (wild-type Canton-S, all mutants); the

corresponding LMC recordings showed resting potentials <−30 mV and 10-24 mV maximum response amplitudes (wild-type Canton-S and all mutants). Different LMC subtypes were not identified, but most recordings were likely from L1 and L2 as they occupy the largest volume. It is unlikely, but not impossible, that we occasionally also recorded from other neurons or glia, which receive histaminergic inputs from photoreceptors (Shaw, 1984, Zheng et al., 2006, Zheng et al., 2009, Rivera-Alba et al., 2011). Nonetheless, because the selected recordings shared similar hyperpolarizing characteristics, all LMC data were analysed together.

Light stimulation was delivered to the studied cells at centre of its receptive field with a high-intensity green LED (Marl Optosource, with peak emission at 525 nm), through a fiber optic bundle, fixed on a rotatable Cardan arm, subtending 5° as seen by the fly. Its intensity was controlled by neutral density filters (Kodak Wratten) (Juusola and Hardie, 2001a); the results are shown for dim (6,000 photons/s), medium (6×10^5 photons/s) and bright luminance (6×10^6 photons/s); or log -3, log -1 and log 0, respectively.

Voltage responses were amplified in current-clamp mode using 15 kHz switching rate (SEC-10L single-electrode amplifier; NPI Electronic, Germany). The stimuli and responses were low-pass filtered at 500 Hz (KemoVBF8), and sampled at 1 or 10 kHz. The data were often re-sampled/processed off-line at 1-2 kHz for the analysis. Stimulus generation and data acquisition were performed by custom-written Matlab (MathWorks, Natick, MA) programs: BIOSYST (Juusola and Hardie, 2001a, Juusola and de Polavieja, 2003), with an interface package for National Instruments (Austin, TX) boards (MATDAQ; H. P. C. Robinson, 1997–2005).

2.2.3 Data Analysis

The signal was the average of consecutive 1,000 ms long voltage responses to a repeated light intensity time series, selected from the naturalistic stimulus (NS) library (Van Hateren, 1997), and its power spectrum was calculated using Matlab's Fast Fourier Transform (FFT) algorithm. First 10-20 responses were omitted because of their adaptive trends, and only approximately steady-state adapted responses were analysed. The noise was the difference between individual responses and the signal, and its power spectra were calculated from the corresponding traces (Juusola et al., 1994). Thus, n trials (with n = 40–90), gave one signal trace and n noise traces. Both signal and noise data were chunked into 50% overlapping stretches and windowed with a Blackman-Harris-term window,

each giving seven 250-point-long samples. This gave 280–630 spectral samples for the noise and seven spectral samples for the signal, which were averaged, respectively, to improve the estimates.

A triple extrapolation method (Juusola and de Polavieja, 2003) was used to estimate the rate of information transfer of steady-state-adapted photoreceptor voltage responses to naturalistic stimulus. This method, unlike SNR analysis, requires no assumptions about the signal and noise distributions or their additivity (Juusola and de Polavieja, 2003). Voltage responses were digitized by sectioning them into time intervals, *T*, that were subdivided into smaller intervals *t* = 1 ms. (Only dim luminance data was down-sampled to 125 Hz, giving *t* = 8 ms, which better represented their slow dynamics). In the final step, the estimates for the entropy rate, R_S, and noise entropy rate, R_N, were then extrapolated from the values of the experimentally obtained entropies to their successive limits, as in (Juusola and de Polavieja, 2003):

$$R = R_S - R_N = \lim_{T\to\infty} \frac{1}{T} \lim_{v\to\infty} \lim_{size\to\infty} \left(H_S^{T,v,size} - H_N^{T,v,size} \right), \qquad (2\text{-}1)$$

where *T* is the length of the 'words', *v* the number of voltage levels (in digitized amplitude resolution) and the *size* of the data file. The difference between the entropy and noise entropy rates is the rate of information transfer, *R* (Shannon, 1948, Juusola and de Polavieja, 2003). See (Juusola and de Polavieja, 2003) for further details.

2.2.4 Behavioural experiments and analysis

In the flight simulator experiments, we used 3-7 days old (adult) female flies, reared in 12:12 h dark:light cycle. A fly tethered from the classic torque-meter (Tang and Guo, 2001), which fixed its head in a rigid position and orientation, was lowered by a manipulator in the centre of a black-white cylinder (spectral full-width: 380-900 nm). A flying fly saw a continuous (360^o) stripe-scene. After viewing the still scene for one second, it was spun to the counter-clockwise by a linear stepping motor for two seconds, stopped for two seconds, before rotating to clock-wise for two seconds, and stopped again for a second. This eight-second stimulus was repeated 10 times and each trial, together with the fly's yaw torque responses, was sampled at 1 kHz and stored for later analysis (Wardill et al., 2012). Flies followed the scene rotations, generating yaw torque responses (optomotor responses to right and left), the

strength of which is thought to reflect the strength of their motion perception (Gotz, 1964). Stimulus parameters for the moving stripe scenes were: azimuth ±360°; elevation ±45 °; wavelength, 14 °; contrast, 1.0, as seen by the fly. For the slow scene rotation, the velocity was 45 °/s and for the fast rotation, 180 °/s;

Calculation of "optomotor index"

Optomotor index, *O*, was designed to provide a simple metric of how well flies intended to follow rotating stimuli. It was computed from a fly's yaw torque response by a simple function, comprising two steps (1-2):

(1) Quantifying the maximum changes in yaw torque within 0.5s from the stimulus onset. In the experimental protocol, the rotating field changes its direction four times: (i) start anti-clockwise at t = 1s, (ii) stop anti-clockwise at t = 3s, (iii) start clockwise at t = 5 s and (iv) stop clockwise at t = 7 s. Thus, there were four elements, $E_{1\text{-}4}$, computed in this step:

$$E_1 = -A(1) + max(A(1 \text{ to } 1.5 \text{ s})) \quad (2\text{-}2)$$

$$E_2 = A(3) - min(A(3 \text{ to } 3.5 \text{ s})) \quad (2\text{-}3)$$

$$E_3 = A(5) - min(A(5 \text{ to } 5.5 \text{ s})) \quad (2\text{-}4)$$

$$E_4 = -A(7) + max(A(7 \text{ to } 7.5 \text{ s})), \quad (2\text{-}5)$$

where $A(t)$ denotes the immediate magnitude of torque response at time, t, seconds. Torque responses to anti-clockwise field rotation were considered positive (+).

(2) Computing optomotor index from the four quantified elements. Because in typical wild-type behaviour, responses evoked by the start of the field rotation are significantly larger than those evoked by the stop of the rotation, E_2 and E_4 were weighted by 0.25 in the final formula:

$$O = E_1 + 0.25 \times E_2 + E_3 + 0.25 \times E_4 \quad (2\text{-}6)$$

2.3 Results

2.3.1 Mutant photoreceptors produce faster voltage responses to light

To examine the contribution of Ca^{2+}-activated K^+-channels to R1-R6 photoreceptor output, we performed *in vivo* intracellular recordings (**Fig. 2-1A**) from their somata in the retina (**Fig. 2-1B**) of *dSlo4*, *dSK*$^-$ and *dSK*$^-$;;*dSlo4* mutants and wild-type flies. In all the mutants, photoreceptors responded to light flashes of increasing intensity with graded depolarizations (**Fig. 2-1C**), having wild-type-like or smaller amplitudes (**Fig. 2-1D**) but each with faster (**Fig. 2-1E**) and/or briefer (**Fig. 2-1F**) waveforms that peaked and decayed to their respective resting potentials before wild-type responses. *dSK*$^-$ photoreceptors had the fastest rising responses, followed by *dSlo4*, while responses of *dSK*$^-$;;*dSlo4* were the briefest.

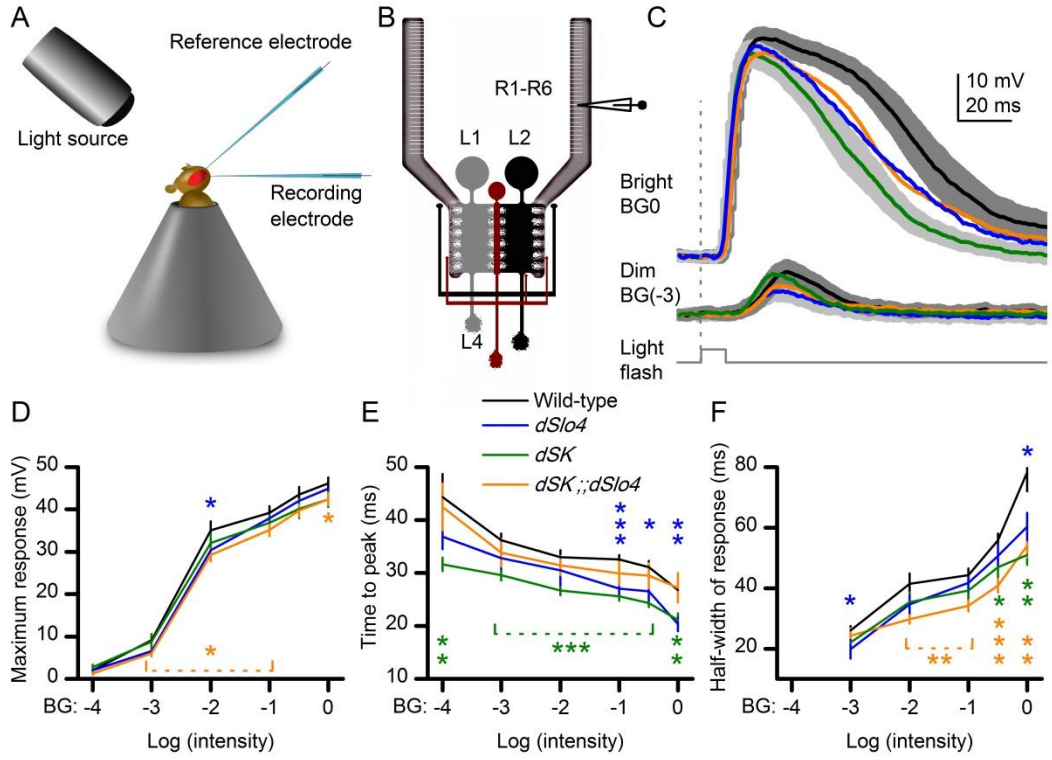

Figure 2-1. Voltage responses of R1-R6 photoreceptors to brief light flashes are accelerated in Ca^{2+}-activated K^+-channel mutants

(A) *In vivo* recordings from R1-6 photoreceptors.

(B) Photoreceptor axon terminals are connected to the lamina network; feedback from L2/AC and L4 to photoreceptors terminal highlighted.

(C) Voltage responses of photoreceptors to bright and dim 10 ms light pulses. Mutant photoreceptor generated depolarizing responses that peaked and decayed before wild-type (black).
(D) Average responses of the mutants to were typically less than wild-type, and those of *dSK⁻;dSlo4* significantly different ($0.02 < p < 0.04$, t-test; n = 9).
(E) Responses in *dSlo4* ($5.0\times10^{-4} < p < 0.02$, BG0-2; n = 10) and *dSK⁻* ($2.0\times10^{-5} < p < 0.01$; n = 7) peaked significantly sooner than wild-type, but not in *dSK⁻;;dSlo4* photoreceptors ($p > 0.14$; n = 10).
(F) Responses of the mutant photoreceptors were briefer than wild-type: *dSlo4* ($0.02 < p < 0.05$, BG0,4; n = 10); *dSK⁻* ($0.001 < p < 0.003$, BG0,1; n = 7); *dSK⁻;;dSlo4* ($1.0\times10^{-4} < p < 0.004$, BG0-3; n = 9). **C-F**: mean ± SEM, one-tailed t-test.

2.3.2 Faster responses are not due to intrinsic compensation in somatic membrane properties

We first asked whether these accelerated responses resulted from increased somatic conductances, which would reduce membrane input resistance, R_m, and thus its time constants ($\tau = R_m \cdot C$; C is constant membrane capacitance), accelerating signal conduction. Missing SK-channels in *dSK⁻* photoreceptors could be compensated for example by up-regulating dSlo-channel expression, for which these cells carry a normal gene; and the same could happen *vice versa* in *dSlo4* photoreceptors. Alternatively, the mutant photoreceptors could have increased K^+ or Cl^- leak-conductances (Niven et al., 2003, Vahasoyrinki et al., 2006). While such intrinsic homeostatic mechanisms could increase response speed, this would also lower their resting potential by reducing depolarizing Ca^{2+}-load and/or increasing hyperpolarizing K^+/Cl^--loads.

To test these hypotheses, I measured *in vivo* somatic electrical membrane properties of dark-adapted mutant and wild-type photoreceptors (**Fig. 2-2A**), using single-electrode current-clamp. I found that the mutant photoreceptors charged rather wild-type-like voltage responses to injected current pulses (**Fig. 2-2B**). Depolarization to positive currents showed normal outward rectification (arrows), presumably by activation of voltage-depended K^+-channels on their membranes (Hardie, 1991a, Hardie et al., 1991, Juusola and Hardie, 2001a, Vahasoyrinki et al., 2006), while hyperpolarization to negative currents was effectively passive. The input resistances of *dSlo4* and *dSK⁻*;;*dSlo4* photoreceptors, as determined by small hyperpolarizing responses to -0.04 nA current steps, were within the lower wild-type

bound (~200 MΩ; *cf.* Juusola and Hardie, 2001a; Niven et al., 2003). But the mean input resistance of *dSK*$^-$ photoreceptors was yet lower (~140 MΩ, p = 0.03; *cf.* Abou Tayoun et al., 2012) (**Fig. 2-2C**). Most crucially, however, the resting potentials of *dSK*$^-$ and *dSlo4* photoreceptors, instead of being more hyperpolarized, were more depolarized than wild-type: ~10 mV (p = 0.046) and ~5 mV (p = 5.0×10^{-4}), respectively, while *dSK*$^-$;;*dSlo4* photoreceptors were within the upper wild-type bound (**Fig. 2-2D**). Together, these results suggest that light-induced voltage responses of mutant photoreceptors (**Fig. 2-1E-F**) were not accelerated by compensatory expression of Ca^{2+}-activated K^+- or leak-channels at the photoreceptor somata but require other/further mechanisms.

2.3.3 Faster responses are not due to modified phototransduction or somatic K^+-conductances

Our collaborators Ahmad Abou Tayoun and Patrick Dolph at Dartmouth College then prepared eyes of dark-reared flies for light-microscopy and inspected whether the mutations caused developmental defects in photoreceptor morphology. The retinal sections of mutant flies showed no obvious differences to the wild-type, consisting of highly ordered ommatidia with normal looking photoreceptors and intact rhabdomeres (**Fig. S2-1**). Nonetheless, this did not exclude the possibility that deletion of dSlo, dSK, or both, could influence the compartmentalization and function of phototransduction cascade in the microvilli (Song et al., 2012), and so modifying sampling, amplification or integration of light-induced currents (LIC).

Therefore, other co-investigators of this project, Roger Hardie and Brian Chu, also compared elementary LICs to single photons (quantum bumps) and macroscopic LICs to light flashes (**Fig. S2-2A-G**) from the mutant and wild-type photoreceptors, using whole-cell recordings in dissociated ommatidia (Hardie, 1991b). In this preparation, axon terminals are severed so that dissociated photoreceptors lack any synaptic feedback from the lamina network. They found that quantum bumps and macroscopic LICs to brighter intensities were essentially identical in mutant and wild-type photoreceptors, sharing the same dynamics (**Fig. S2-2A-G**). Thus, deletion of dSlo, dSK or both neither affected photoreceptor morphology nor phototransduction machinery, suggesting that these cells were equally capable in sampling light information; see (Song et al., 2012). Furthermore, K^+ conductances in dissociated mutant photoreceptors showed normal slow delayed rectifier current (I_{KS} or *Shab*) and a slightly reduced A-current (I_A or *Shaker*) (**Fig. S2-2H-I**). The

decrease in the I_A current together with dSlo and/or dSK current removal should, all things being equal, increase input resistance and membrane time constant, leading to slower voltage responses. Yet, the *in vivo* data demonstrated the opposite: mutant photoreceptors had faster voltage responses and no significant increase in input resistance (**Fig. 2-1** and **2-2**, respectively). Hence, these results imply that the mutant photoreceptors' faster voltage responses and higher resting potentials must permeate from conductance changes in their axon terminals and/or the lamina network (Shaw, 1984, Zheng et al., 2006, Zheng et al., 2009, Abou Tayoun et al., 2011).

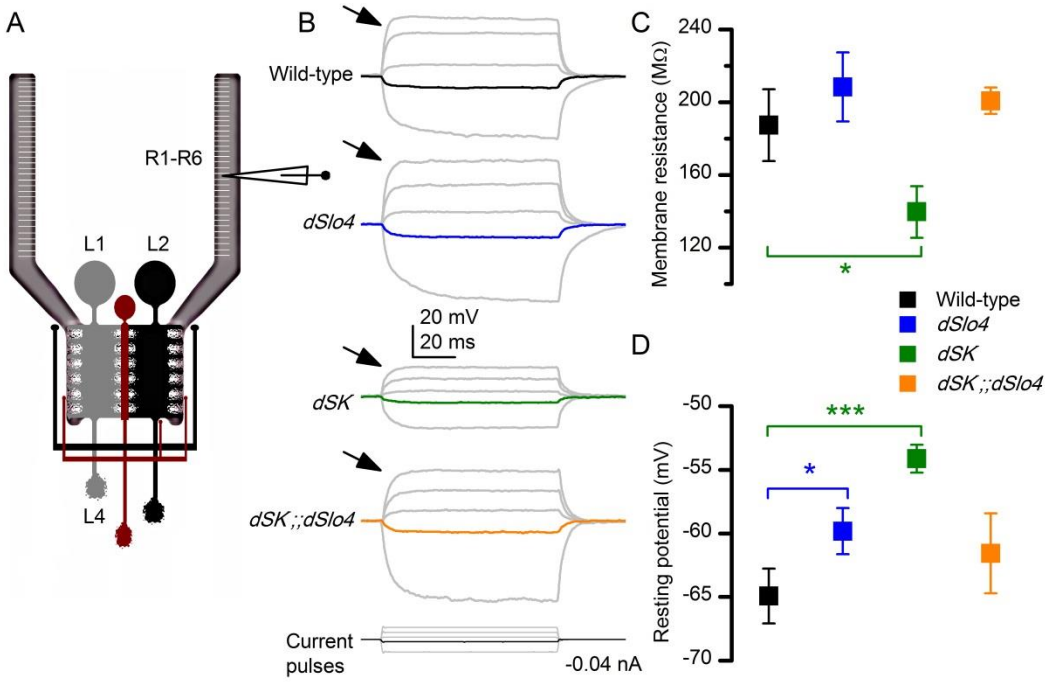

Figure 2-2. **R1-R6 photoreceptors in Ca^{2+}-activated K^+-channel mutants have more depolarized resting potentials in darkness but their electric membrane properties are wild-type like**

(B) Voltage responses of dark-adapted photoreceptors to intracellularly injected current pulses.

(C) Membrane input resistance of mutants and wild-type photoreceptors are similar (wild-type, n = 11; *dSlo4*, n = 12; *dSK⁻;;dSlo4*, n = 7), apart from *dSK⁻* ($p = 0.03$, n = 8).

(D) Photoreceptors' resting potentials are more depolarized in darkness in *dSlo4* (wild-type, n = 9; *dSlo4,* $p = 0.046$, n = 9) and in *dSK⁻* ($p = 5.0\times10^{-4}$, n = 11) than in wild-type. Photoreceptors in *dSK⁻;;dSlo4* had resting potentials within the upper wild-type range ($p = 0.198$, n = 7). **C-D**: mean ± SEM, one-tailed t-test.

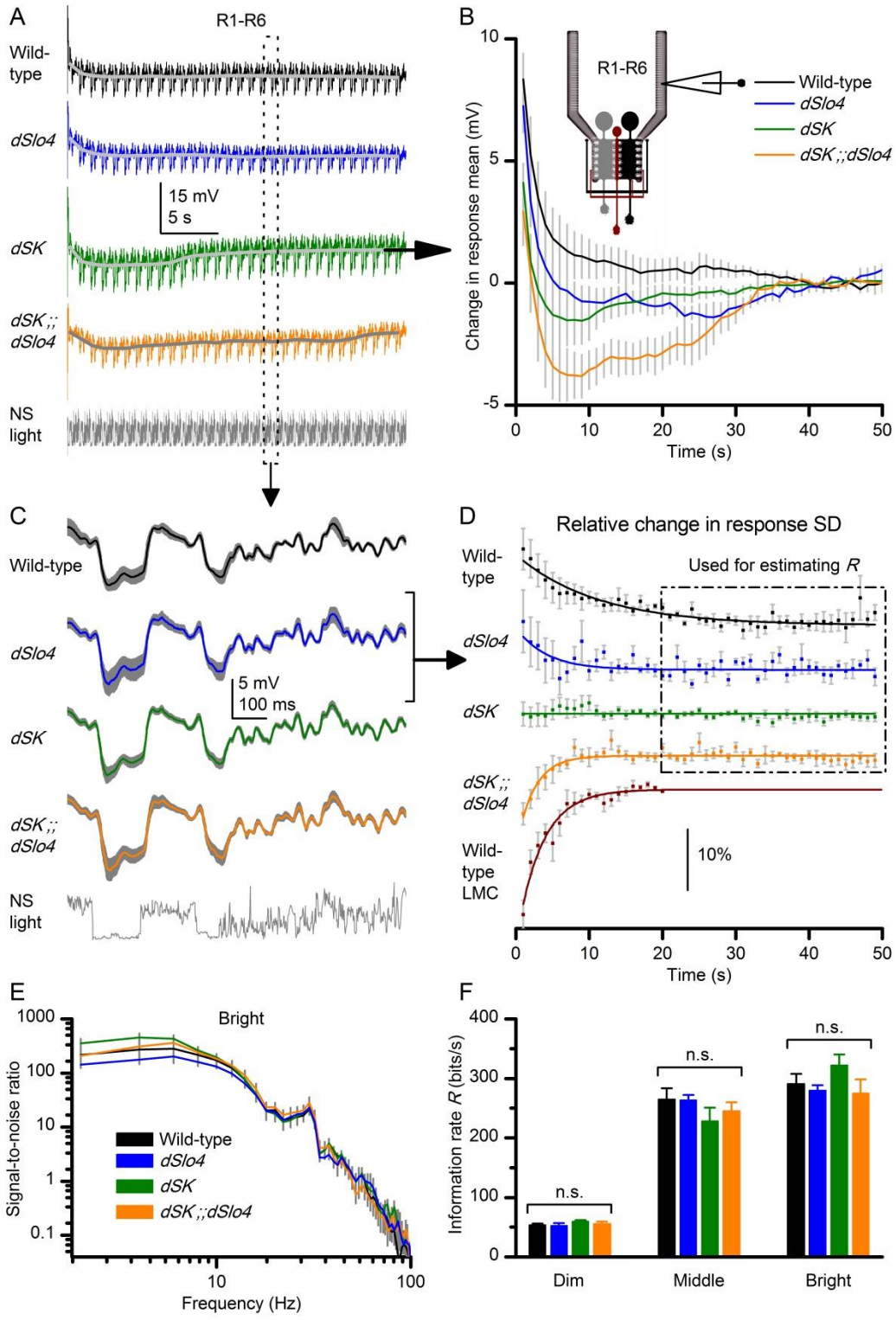

Figure 2-3. Adaptation properties and information transfer rates of R1-R6 photoreceptors in mutants and wild-type

(A) Intracellular voltage responses to a continuously repeated 1-second-long bright naturalistic light intensity time series.

(B) Change in the mean of 1-second-long response (± SEM) over 50 seconds of stimulation. Mean wild-type photoreceptor output decreased,

settling to steady-state level after 15~20 seconds (n = 6). Adaptation trend in mean *dSlo4* photoreceptor output showed slow fluctuations and an undershoot (n = 8). Mean *dSK*$^{-}$ photoreceptor output undershot earlier and then settled at 15~20 seconds (n = 7). Mean *dSK*$^{-}$*;;dSlo4* photoreceptor output had a large undershoot and settled to a relative steady-state in 30~35 seconds (n = 6).

(C) Mean waveforms ± SEM of steady-state adapted 1-second-long voltage responses.

(D) Relative change in photoreceptor output range, measured as Standard Deviation (SD), in 1-second-long voltage responses over 50 seconds of stimulation (mean ± SEM). Wild-type and *dSlo4* photoreceptors desensitized during repeated stimulation, following simple exponential time constants. Wild-type photoreceptor output range contracted from 114% to 100% in about 26 seconds ($\tau_{\text{Wild-type}}$ = 11.2 ± 1.9 s); *dSlo4* from 110% in about 10 seconds (τ_{dSlo4} = 4.2 ± 2.6 s). Output range of *dSK*$^{-}$ photoreceptors showed a small sensitizing trend and adapted to steady size in about 10 seconds. Output range of *dSK*$^{-}$*;;dSlo4* photoreceptors expanded from 87% to 100% in about 6 seconds ($\tau_{\text{dSK}^{-};;\text{dSlo4}}$ = 2.4 ± 0.5s), following the adaptive trends of wild-type LMC output (dark red).

(**E**) Photoreceptors' signal-to-noise ratios, measured from their steady-state adapted outputs to repeated naturalistic stimulation, are similar in the mutant and wild-type files.

(**F**) Information transfer rates to dim, moderately intense (middle) and bright naturalistic stimulation are similar in the mutant and wild-type photoreceptors (mean ± SEM; n = 3-7).

2.3.4 Mutations affect network adaptation but not photoreceptors' mean information transfer

In the adult *Drosophila* brain, dSlo and dSK share similar expression patterns, with higher expression in the lamina and medulla neuropils, together with a weaker expression in the retina (Becker et al., 1995, Abou Tayoun et al., 2011). BK channel is also known to contribute to regulating activity-dependent neurotransmitter release and thus synaptic gain control in the mammalian retina (Xu and Slaughter, 2005, Grimes et al., 2009).

We, therefore, examined the contributions of these channels to rescaling of photoreceptor output during dark-to-light stimulation, or presynaptic network adaptation, for synaptic signal transfer (Nikolaev et al., 2009, Zheng et al., 2009). We recorded voltage responses in *dSlo4*, *dSK*$^{-}$, *dSK*$^{-}$;;*dSlo4* and wild-type

photoreceptors to a repeated 1-s-long bright naturalistic intensity series (van Hateren, 1997) and found strikingly each of them adapting differently (**Fig. 2-3A**). Whilst the mean response of wild-type photoreceptors decreased approximately exponentially to a relative steady-state in 15-20 seconds (**Fig. 2-3B**), those of the mutants decreased more rapidly and then undershot, but each with unique dynamics. Correspondingly, the dynamic output range of wild-type and mutant photoreceptors (**Fig. 2-3C**), as measured by response SD during stimulation, adapted over time differently (**Fig. 2-3D**). Network adaptation in double-mutant photoreceptors, which lacked both dSK and dSlo channels, was most severely compromised with its output range changing remarkably similar to that of post-synaptic wild-type LMC-interneurons (Zheng et al., 2009), suggesting that its range was increased gradually by synaptic feedbacks from LMCs. These results indicate that absence of one or both Ca^{2+}-activated K^{+}-channel types leads to specific adaptive regimes, which are different for each mutant photoreceptor and thus likely reflect unique costs and limitations to compensate the missing K^{+}-channels by the network rebalancing its synaptic loads. For example, feedback in *dSlo4* network is weaker, or closer to wild-type, than in *dSK*$^{-}$, possibly because dSlo, like other BK channels, are less Ca^{2+}-sensitive (Sah, 1996). Thus, missing dSlo channels would require less compensation in repolarizing synaptic terminals during activity than missing SK channels.

Although homeostatic mechanisms likely increase synaptic inputs to the mutant photoreceptor terminals (in the lamina), their effect is marginal on the photoreceptors' signal-to-noise ratio (**Fig. 2-3E**) at the level of retina. This is because a fly photoreceptor's rate of information transfer depends primarily on its photon-absorption rate changes, set by the number of microvilli (individual sampling units) in its rhabdomere and the speed and refractoriness of their phototransduction reactions (Song et al., 2012). Nonetheless, information transfer can decrease when the mutated channels add noise (Niven et al., 2003); or increase when the photoreceptor receives extra information synaptically from other photoreceptors in the network (Shaw, 1984, Zheng et al., 2006, Wardill et al., 2012). In contrast, changes in membrane filtering will affect signal and noise equally, and thus cannot change information transfer rate; data processing theorem (Shannon, 1948, Juusola and de Polavieja, 2003). Theoretically, therefore, after initial network adaptation *dSK*$^{-}$, *dSlo4* and *dSK*$^{-}$;;*dSlo4* photoreceptors, which all have normal rhabdomeres and LIC dynamics (**Fig. S2-1** and **S2-2**), should show wild-type-like information transfer rates. Experimentally, this is indeed what we found (**Fig. 2-3F**).

2.3.5 Double mutant LMCs show the fastest post-synaptic responses

To explore how the absence of dSlo and/or dSK affects post-synaptic voltage responses to light flashes, we performed intracellular recordings in the mutant and wild-type lamina (**Fig. 2-4A**) from large monopolar cells (LMCs), which receive direct histaminergic inputs from R1-R6 photoreceptor terminals. LMCs convey information to different medulla layers, initiating on- and off-motion pathways (Joesch et al., 2010), but along the way they generate feedbacks through a complex web of synapses and gap-junctions (Shaw, 1984, Rivera-Alba et al., 2011) that participate in regulating R1-R6 photoreceptor output gain in the lamina (Zheng et al., 2006, Nikolaev et al., 2009, Zheng et al., 2009). Using perfused inside-out patches, it has also been shown that blowfly LMCs express two types of Ca^{2+}-activated K^{+}-channels (Hardie and Weckström, 1990).

We found that, overall, mutant LMCs generated smaller responses to light pulses than their wild-type counterparts (**Fig. 2-4B**). However, their dynamics were somewhat dispaired from presynaptic somatic recordings, indicating unique local adaptations at the level of terminals and synapses. Whilst presynaptically *dSlo4* and *dSK*$^{-}$ R1-R6s evoked faster responses than wild-type (**Fig. 2-1D-E**), postsynaptically their LMCs responded with wild-type-like or only slightly faster time-courses (**Fig. 2-4C**). Similarly, despite double-mutant R1-R6s evoking slower rising responses than those of single-mutants, double-mutant (*dSK*$^{-}$*;;dSlo4*) LMCs responded with the fastest dynamics, systematically peaking before the responses of single-mutants or wild-type over a broad intensity range. The different pre- and postsynaptic response dynamics in the single- and double-mutants are consistent with the hypothesis of the lamina gain control being an emergent feature of both local and global gain changes. These would homeostatically adapt the network into distinctive regimes, different from the wild-type.

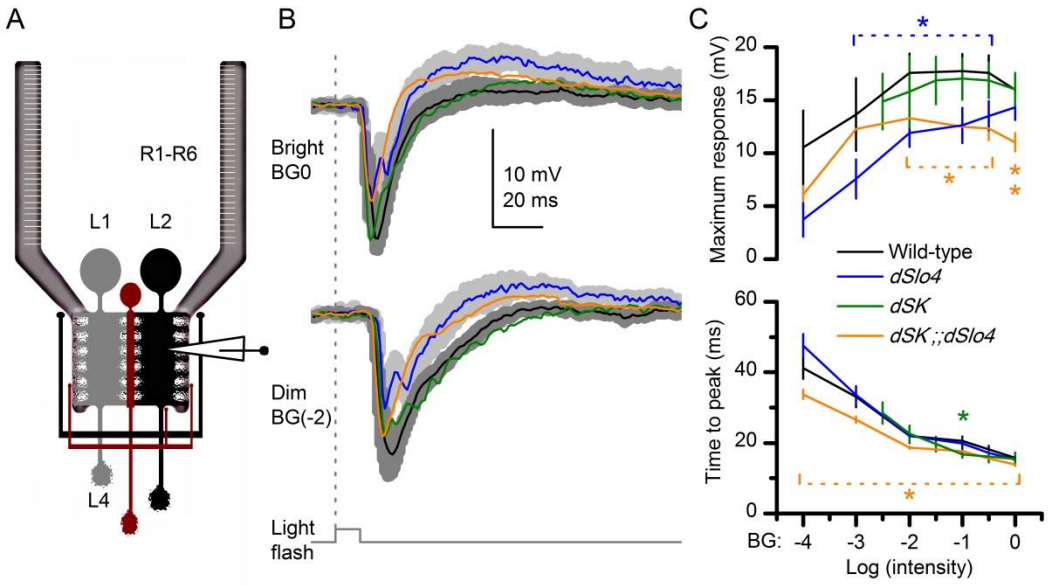

Figure 2-4. **Voltage responses of Large Monopolar Cells (LMCs) to light flashes are the briefest in the double mutant**

(A) Intracellular recordings were carried out from LMCs *in vivo*; the schematic highlights synaptic feedbacks from L2/AC and L4 to photoreceptors terminals.

(B) Voltage responses of the mutant and wild-type LMCs to bright and dim 10 ms light pulses.

(C) LMCs of *dSlo4* and *dSK⁻;;dSlo4* mutants generated smaller responses than wild-type over broad intensity ranges (*dSlo4*: 0.01< p <0.04, BG1-4, n = 5; *dSK⁻;;dSlo4*: 0.004 < p < 0.05, BG0-3, n = 8); mean ± SEM.

(D) *dSlo4* and *dSK⁻* LMCs had mostly similar response time-to-peak to that of wild-type, besides to the 2nd brightest pulse, which evoked faster responses from *dSK⁻* LMCs (p = 0.02). In contrast, responses of *dSK⁻;;dSlo4* LMCs were the fastest (p < 0.04) over the tested intensity range; mean ± SEM, one-tailed t-test.

2.3.6 Single-mutants undergo light-dependent retinal degeneration

The activity of SK and Slo channels can provide sustained neuroprotective functions during ischemia-induced excitotoxicity and neuronal cell death (Gribkoff et al., 2001, Allen et al., 2011). During brain ischemia, the reduced energy source disrupts neuronal electrochemical gradient leading to elevated intracellular Ca^{2+} and hyperexcitability, ultimately causing excitotoxic cell death (Dirnagl et al., 1999). Here, SK and Slo channels are thought to act as 'emergency brakes' by limiting Ca^{2+}-influx from different sources and blunting the biochemical cascade leading to

ischemia-induced cell death. Both *dSK⁻* and *dSlo4* photoreceptors have faster dynamics and are more depolarized (**Fig. 2-1, 2-2** and **2-3**), presumably because of increased synaptic activity at the lamina network. This excessive activity in the mutant photoreceptors, relative to wild-type, might be cytotoxic and lead to light-dependent neuronal cell death, similar to that seen in ischemic conditions.

To test this hypothesis, Ahmad Abou Tayoun and Patrick Dolph raised mutants and wild-type flies in light for ten days and, as controls, similar flies in the dark for the same duration. Afterwards, fly eyes were fixed, sectioned and their morphology examined for signs of degeneration. Dark-reared wild-type eyes were normal with highly organized ommatidia and intact rhabdomeres, while light-reared wild-type eyes showed some signs of vacuolization but still maintained a regular array of intact ommatidia (**Fig. S2-1**). Conversely, although dark-reared mutant eyes were indistinguishable from wild-type, light-rearing induced signs of retinal degeneration, including vacuolization, highly disorganized ommatidia, and diminished rhabdomeres. Degeneration was the severest in *dSK⁻* and *dSlo4* eyes, in which photoreceptors also have the most depolarized resting potentials (see **Fig. 2-2D**), indicating excessive synaptic inputs from the network. Unsurprisingly, double-mutant (*dSK⁻;;dSlo4*) eyes with lower resting potentials seemed wild-type-like. These findings suggest that, under continuous light exposure, the observed retinal degeneration is not due to the absence of either channel *per se* but rather indirectly results from the accompanying increase in network activity.

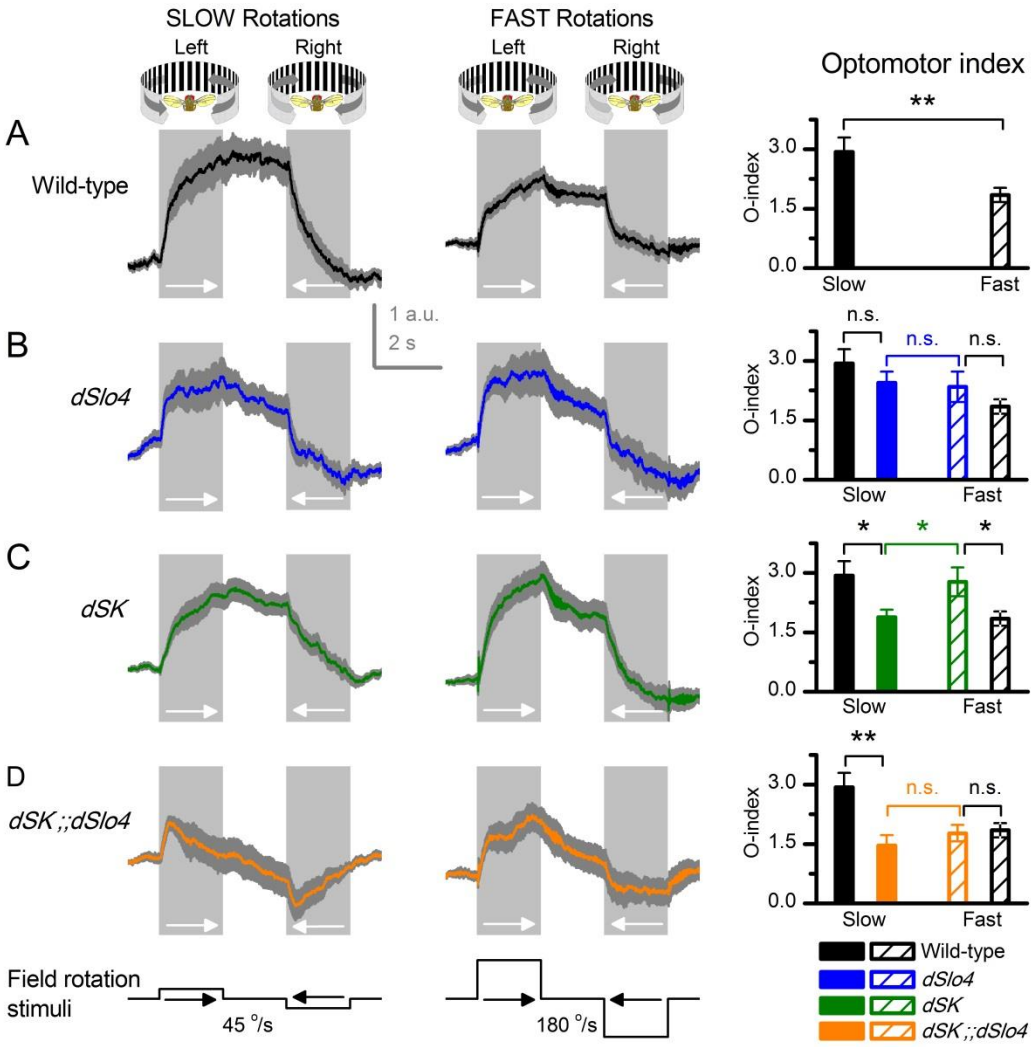

Figure 2-5. **Optomotor responses of Ca^{2+}-activated K^+-channel mutants are stronger or equal to fast field rotation while wild-type flies prefer slow rotation**

(A) Wild-type flies generate stronger torque (optomotor) responses to slow- (45 °/s) than to fast-rotating (180 °/s) brightly-lit black-and-while stripe-field (n = 10, p = 0.009).

(B) *dSlo4* mutants generate equally strong responses to the slow and fast stimuli (n = 10, p = 0.4).

(C) *dSK*$^-$ mutants generate stronger responses to the fast than to the slow stimuli (n_{slow} = 11, n_{fast} = 12, p = 0.02); their responses to slow stimulation are also weaker than those of wild-type (p = 0.01); *dSK*$^-$ responses to fast stimulation are stronger than those of wild-type (p = 0.018).

(D) *dSK*$^-$*;;dSlo4* mutants generate equally strong responses to the slow and fast stimuli (n = 10, p = 0.18), but their output is the most transient-like, adapting clearly faster than the other flies to both stimuli. Their responses to slow stimulation are also weaker than those of wild-type (p = 0.0024).

Optomotor index (right) quantifies how well the torque responses followed the stimuli; mean ± SEM. These results correspond well with the mutant and wild-type LMC outputs (*cf.* Fig.2-4).

2.3.7 Motion perception partly reflects mutation-induced adaptive changes in early vision

To investigate whether and how the distinctive mutation-dependent adaptive regimes in early vision influence the mutants' and wild-type flies' motion perception, I tested their optomotor behaviour in a classic *Drosophila* flight simulator (**Fig. 2-5**). Presumably to prevent visual images from slipping on their retinae, tethered flying flies attempt to follow field rotations, generating yaw torque (optomotor) responses, the waveforms of which indicate the strength and dynamics of their motion perception (Gotz, 1964, Wardill et al., 2012). I measured optomotor responses to brightly-lit slow (**Fig. 2-5 – left column**) and fast (**Fig. 2-5 – middle column**) field (black-and-white stripes) rotations, and computed the "optomotor index" (**Fig. 2-5 – right column**) to quantify how well individual flies perceived these stimuli (see Materials and Methods).

I first verified the classic result (Gotz, 1964, Blondeau and Heisenberg, 1982) of wild-type flies generating significantly stronger responses to slow than to fast field rotations (**Fig. 2-5A**). In striking contrast, however, all the mutants generated equally strong or stronger responses to fast than to slow rotations (**Fig. 2-5B-D**), indicating that they instead perceived better, or preferred, higher contrast frequencies over lower ones. *dSlo4* responded equally to fast and slow stimuli (**Fig. 2-5B**), suggesting that the rate of change (phase information) in LMC output (time-to-peak: *dSlo4* = wild-type) rather than its maximum amplitude (*dSlo4* < wild-type) (**Fig. 2-4C**) is more important for motion perception. Likewise, the accelerated LMC output dynamics of *dSK⁻* (**Fig. 2-4C**) compared well with its stronger responses to the faster field rotations (**Fig. 2-5C**). Lastly, similar to its quickest and most phasic LMC output (**Fig. 2-4C**), optomotor responses of the double mutant (*dSK⁻;;dSlo4*) were the most transient (**Fig. 2-5D**), adapting rapidly to clockwise and counter-clockwise changes in stimulation rotation. These results show that mutation-induced specific adaptive regimes in early vision lead to motion perception, which deviate from wild-type and is different in different mutants.

2.4 Discussion

Our results suggest that dSlo and dSK reduce excitability and increase neural adaptability and survival for transmitting information at the lamina network, ultimately improving visual perception in changing light conditions. Both single- and double-mutant photoreceptors showed accelerated responses and more depolarized resting potentials. Such changes likely emerged from homeostatic rebalancing of synaptic feed-forward and feedback signalling between photoreceptor axon terminals and the rest of the lamina network. However, this compensation was unique for each mutation and manifested itself as distinctive but suboptimal adaptive regimes, which accelerated LMC outputs, compromising the mutants' motion perception of slowly rotating scenes.

2.4.1 Ca^{2+}-activated K^+ channels reduce costs of adaptation and increase its range

Adaptability is critical for animal fitness. In sampling and transmission of sensory signals, it reduces communication errors, such as noise and saturation, by continuously adjusting new responses by memories of past stimuli, e.g. (Song et al., 2012). To ensure reliable perception of visual objects in changing conditions, retinal adaptation exploits visual world similarities and differences (van Hateren, 1992c) and employs costly codes (de Polavieja, 2002) through multiple layers of feedbacks. This gives emergence for *homeostatic* network gain regulation, in which photoreceptor adaptation is mediated both by intrinsic (Juusola and Hardie, 2001a, Song et al., 2012) and synaptic feedbacks (Zheng et al., 2006, Zheng et al., 2009, Nikolaev et al., 2009). Here, absence of dSK and/or dSlo left the phototransduction cascade intact and affected only marginally intrinsic membrane conductances of the photoreceptor somata; see also (Abou Tayoun et al., 2011). Therefore, the observed defects in photoreceptor adaptability, including undershoots, response fluctuations and altered dynamic ranges during repetitive stimulation, are attributable to synaptic inputs; presumably, reflecting homeostatic changes in bidirectional signalling between photoreceptors and lamina neurons.

Consistent with this hypothesis, we also found that the mutant photoreceptors' resting potentials and response speed differed from wild-type (Zheng et al., 2006, Abou Tayoun et al., 2011). Markedly, if these changes were directly caused by the absence of Ca^{2+}-activated K^+-channels, double-mutant (*dSK⁻;;dSlo4*)

photoreceptors, which lack both the channels, should be the most depolarized. But instead they were hyperpolarized close to wild-type resting potentials, suggesting reduced synaptic excitation and/or increased inhibition. Conversely, single-mutant photoreceptors were more depolarized and prone to degenerate under continuous stimulation with their outputs oscillating occasionally, suggesting that these cells received more excitation from the network than double-mutant photoreceptors.

The primary effects of mutations can be difficult to separate from the secondary effects of homeostatic compensation (Marder and Goaillard, 2006). Nonetheless, the overall consistency of our findings suggest that many differences in *in vivo* response properties of the mutant photoreceptors and LMCs result from homeostatic gain regulation, whereupon differently balanced excitatory and inhibitory loads in the lamina network generate heterogenetic adaptive regimes; see also (Abbott and LeMasson, 1993, LeMasson et al., 1993). In the double-mutant, the least depolarized photoreceptors and the fastest LMC output imply that the network gain was particularly challenging to regulate, providing the most compromised adaptability and motion perception range. In the single-mutants, adaptability of early vision was better, compensated by enhanced network excitation that caused lesser trade-offs in motion perception. But this came with the cost of reduced photoreceptor survival. Thus, Ca^{2+}-activated K^{+}-channels serve well local and global communication, improving neural economics and adaptability. Locally, they help to reduce calcium load and repolarize membrane potentials in synaptic terminals. Globally, they reduce the overall network excitability and the cost of transmitting information, while increasing the range of neural adaptation and visual perception.

Chapter 3: Comparative study on photoreceptor light-induced responses in wild-type *Drosophila* and the Histidine Decarboxylase-deficient mutant

3.1 Introduction

For long, anatomical studies have demonstrated the abundant presence of synaptic feedback in invertebrate eyes as well as vertebrate outer retinas, highlighting their essential roles in parallel processing of early vision (Sterling, 1983, Meinertzhagen and Oneil, 1991, Meinertzhagen and Sorra, 2001, Wassle, 2004, Rivera-Alba et al., 2011). In the spatial domain, feedback from horizontal cells to cones and rods facilitate photoreceptor lateral inhibitions, shaping the antagonistic centre-surround receptive field and thus enhance visual representation of local contrast (Thoreson et al., 2008, Jackman et al., 2011). Chromatically, negative feedback to cones is proposed to be the underlying mechanism of colour constancy and colour opponency in non-mammalian vertebrates (Burkhardt, 1993, Thoreson and Mangel, 2012). In the temporal domain, however, their contributions to dynamics and coding of retinal neurons are less well understood, partly because of experimental difficulty in acquiring long-lasting neural signals from living vertebrate retina.

On the other hand, the visual system of the fruit fly *Drosophila* offers great opportunities to advance our knowledge of synaptic feedback, with their photoreceptors and interneurons are accessible for *in vivo* electrophysiological recordings of high quality. Although synaptic connections in the photoreceptor-lamina network have been fully reconstructed from electron-micrograph (EM) studies, a simplified wiring diagram, which only includes connections between photoreceptors and key interneurons, is often considered (Zheng et al., 2006, Joesch et al., 2010, Abou Tayoun et al., 2011). In such model, photoreceptors make downstream synaptic contacts with large monopolar cells L1-L3 (LMCs) and amacrine cells (ACs), while majority of feedbacks, either directly or indirectly, are from L4, L2 and ACs onto photoreceptors terminals. Moreover, histamine is identified as the main, if not the sole, neurotransmitter in the inhibitory feed-forward pathway (Hardie, 1987, Hardie, 1989, Gengs et al., 2002) and excitatory feedback is

known to be transmitted by acetylcholine and glutamate (Sinakevitch and Strausfeld, 2004, Kolodziejczyk et al., 2008, Raghu and Borst, 2011).

Importantly, synaptic transmissions in both pathways are modifiable by using genetics tools, thus enabling the study of this highly interconnected network. Pioneering research has shown that feedback from interneurons dynamically adjust photoreceptor outputs, preventing them from being saturated and improving their signal quality with enriched modulations (Zheng et al., 2006). Furthermore, studies on synaptic mutants found that feed-forward and feedback are tightly coupled, as defection in one pathway leads to detrimental alteration in the other and consequently results in faulty network adaptation in the photoreceptor-interneurons circuit (Zheng et al., 2009, Nikolaev et al., 2009).

Histidine decarboxylase, the enzyme which facilitates histamine synthesis, is coded by the single *hdc* gene in the *Drosophila* genome (Burg et al., 1993, Melzig et al., 1996, Melzig et al., 1998). Since nervous system of the null allele hdc^{JK910} lacks histamine, their photoreceptors are unable to communicate synaptically with LMCs and ACs. In addition, *in vitro* properties of hdc^{JK910} photoreceptors were not noticeably different from wild-type, according to preliminary data, and their feedback pathway is intact. Other than visual system, histamine defection in hdc^{JK910} also affects mechanoreceptors and ~42 neurons in the Centre Nervous System (CNS), which are outside the scope of my research. Here, to further investigate functional roles of interneurons feedback, I examined hdc^{JK910} photoreceptors in darkness and under light stimulation. I found that blocking feed-forward pathway (**Fig. 3-1A**) causes excitatory feedback to be tonic and enhanced, which in turn lifts dark-adapted hdc^{JK910} photoreceptors to an artificially depolarized resting potential. Under extremely bright and/or prolonged light stimulation, photoreceptors of hdc^{JK910} mutant exhibited contracted responses and narrower operational ranges than those of wild-type. In addition, despite having normal adapting trends during dark-light transitions, their responses to naturalistic stimuli showed reduced signal power spectra. While possible alterations in hdc^{JK910} phototransduction cascade cannot be ruled out, I speculate that weakened responses of mutant photoreceptors are due to the lack of interneuron modulations via feedback signals. Together with previous studies, my findings here emphasise important roles of interneurons feedback as gain controller and signal regulator of photoreceptor output.

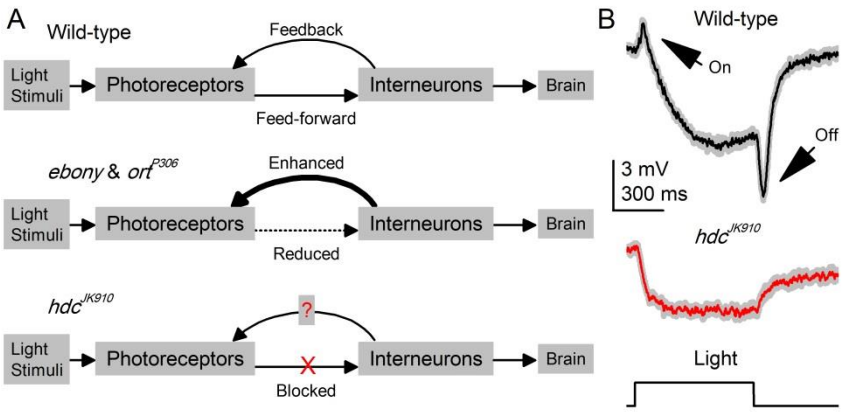

Figure 3-1. **(A)** Graphical representation of photoreceptor-lamina circuit in wild-type and mutants. Reduced feed-forward synaptic transmissions in *ebony and ort*^{P306} lead to enhanced excitatory feedback from interneurons to their photoreceptors (Zheng et al., 2006). In *hdc*^{JK910}, the feed-forward pathway is completely blocked.

(B) Electroretinogram measured from retina surface of wild-type and *hdc*^{JK910}. Mutant ERGs had smaller back ground and did not show the transients found in wild-type (arrows). Mean ± SEM

3.2 Materials and methods

3.2.1 Fly stocks

hdc^{JK910} flies were from Erich Buchner's lab (Julius-Maximilians-Universität, Würzburg, Germany). As part of stocks maintenance procedures, wild-type and mutant flies were regularly checked by their clearly distinguishable Electroretinograms (ERG – see below). Flies were reared in 12:12 h dark:light cycle and kept at room temperature (20-22 °C). Only female flies of 3 to 7 day-old (adults) were used for *in vivo* electrophysiology.

3.2.2 *in vivo* electrophysiology

Intracellular recordings from photoreceptors were performed as described in Chapter 2.

Electroretinograms. Flies were fixed onto a conical fly holder using bee wax and were stimulated by 700 ms light pulses of the brightest intensity (estimated to be ~6 × 10^6 photons/s, based on the calibration data in (Juusola and Hardie, 2001a)). The same green LED mounted on a Cardan arm as in *intracellular recordings* were used. Both recording and reference electrodes were filled with fly ringer, of which

ingredients are described in (Joesch et al., 2008). Before being placed on retina's surface, the tip of the recording electrode was cut so that its contact area is approximately of the size of one ommatidium. The electrical circuit was closed by driving the reference electrode through one of the three ocelli. Recorded signals were low-pass filtered at 500 Hz and amplified as detailed in *intracellular recordings* procedures.

Typical ERG potential recorded from retina surface of wild-type *Drosophila* comprises two main components: a background and transients coincide with changes in light stimuli (Heisenbe.M, 1971). The background potential is attributed to photoreceptor output and has the inverse waveform of photoreceptor intracellular responses, while on- and off-transients are believed to originate from the lamina. *hdc*^{JK910} ERGs did not show any transients, reflecting their blind interneurons, and had smaller background than wild-type ERG, suggesting that their photoreceptors produced smaller intracellular responses to this light stimulus (**Fig. 3-1B**).

Current-clamp. Electric membrane properties of dark-adapted photoreceptors were investigated by injecting current steps of ±0.04 nA, ±0.13 nA, ±0.21 nA and ±0.3 nA. Membrane input resistance, R_m, was calculated by the most hyperpolarized voltage (U) evoked by a -0.04 nA current step (I) according to Ohm's law:

$$R_m = \frac{U}{I}. \tag{3-1}$$

As shown in previous publications (Vahasoyrinki et al., 2006, Zheng et al., 2006, Abou Tayoun et al., 2011), outcomes of this measurement vary depending on the type of electrode used, room temperature, the experimentalist and other unaccounted factors. To ensure fair comparisons between photoreceptors of wild-type and the *hdc* mutant, I carried out all of these experiments within one week time, under controlled temperature (19 ± 1 ºC), using the same borosilicate electrode type and alternately for the two genotypes.

3.2.3 Data analysis

Signal power, noise power, signal-to-noise ratio (SNR) and Information transfer rate were calculated as described in Chapter 2.

Shannon Information Transfer Rate. To cross-check our extrapolation method, I also estimated information transfer rate, R, based on signal-to-noise ratio of photoreceptor responses by using Shannon's formula:

$$R = \int_0^\infty (\log_2[\mathrm{SNR}(f)+1])df\ , \tag{3-2}$$

where $\mathrm{SNR}(f)$ is the signal-to-noise ratio computed for each frequency.

Since data sampling rate of 1 kHz was used for every NS experiment, this estimation did not integrate information rate for frequencies from 0 to infinite, but from 2 Hz to 500 Hz instead. However, the limited bandwidth would not considerably affect estimation results because high frequency components have *SNR* << 1 and therefore contain mostly noise.

Finite data can be used to estimate information transfer rate using Shannon method with the following assumptions: (i) input stimulus is Gaussian, (ii) response is linear and (iii) noise is Gaussian and additive (Shannon, 1948). Thus, estimation accuracy of this method could be affected as these assumptions were not satisfied in photoreceptor responses to naturalistic stimuli (van Hateren and Snippe, 2001, Juusola and de Polavieja, 2003).

Although the Juusola and De Polavieja method is not based on assumptions of response and noise statistics, errors could occur in its triple extrapolation to the infinite limit of three finite parameters: data length, time interval and digitized voltage level.

Nevertheless, both methods, each of which is based on different principles and has different limitations, produced similar estimations and consistent relative comparisons (**Fig. 3-6F** and **Fig. S3-1**).

Relative variation, $\boldsymbol{RV}$, was used to approximate the extent of cell-to-cell variations. For measurements or parameters computed from responses of photoreceptors belonging to each group (wild-type or the *hdc* mutant), relative variation is calculated as:

$$\boldsymbol{RV} = \frac{Standard\ Deviation}{Mean}. \tag{3-3}$$

Probability Density Functions (PDFs) were calculated for the first, second and fifteenth second of photoreceptor responses to Bright NS. Initially, the mean of each one-second-long response is removed. Then, histograms of their voltage outputs were created by using bin size (resolution) of 2mV. Finally, because each response has 1000 data point, *PDFs* were calculated by dividing the y-axis of histograms by 1000.

3.3 Results

3.3.1 Voltage responses of the *hdc* mutant R1-R6 photoreceptors to brief and long light pulses

To characterise properties of hdc^{JK910} mutant photoreceptors, I first recorded *in vivo* their intracellular somatic voltage responses to 10 ms light flashes of increasing intensities (**Fig. 3-2A-B**).

Photoreceptors of the *hdc* mutant responded to brief light impulses with graded depolarization (**Fig. 3-2C**) of similar rise-times (**Fig. 3-2D**) to those of wild-type over most tested light intensities. The exceptions were in experiments using the second-brightest flash, where responses of hdc^{JK910} photoreceptors peaked ~3 ms earlier. Interestingly, average responses of mutant photoreceptors to light impulses of Mid to Bright intensities consistently decayed to resting potential more slowly than their wild-type counterparts (**Fig. 3-2C**). Although this characteristic was prevalent, the difference in responses half-width of wild-type and mutant photoreceptors reached statistical significance in only one set of experiments (**Fig. 3-2E**). The reason is that the slower decays typically became more evident when membrane voltage dropped to values lower than the half-maximum.

In addition, response amplitude of hdc^{JK910} photoreceptors were wild-type like but ~3.4 mV smaller when stimulated by the brightest flashes (**Fig. 3-2F**), suggesting earlier light saturation.

In respect to a previous study of mutants with reduced synaptic transmission from photoreceptors to the lamina circuit (Zheng et al., 2006), these findings here are somewhat surprising. Photoreceptors of both ort^{P306} and *ebony* mutants, which has defective histamine receptor in LMCs (Gengs et al., 2002) and faulty histamine recycling process (Hotta and Benzer, 1969), respectively, exhibited boosted output. Presumably due to increased excitatory feedback from their interneurons (**Fig. 3-1A**), voltage responses to 10ms light flash, measured from photoreceptors of these synaptic mutants, were larger and peaked and decayed ~40% faster than those of wild-type.

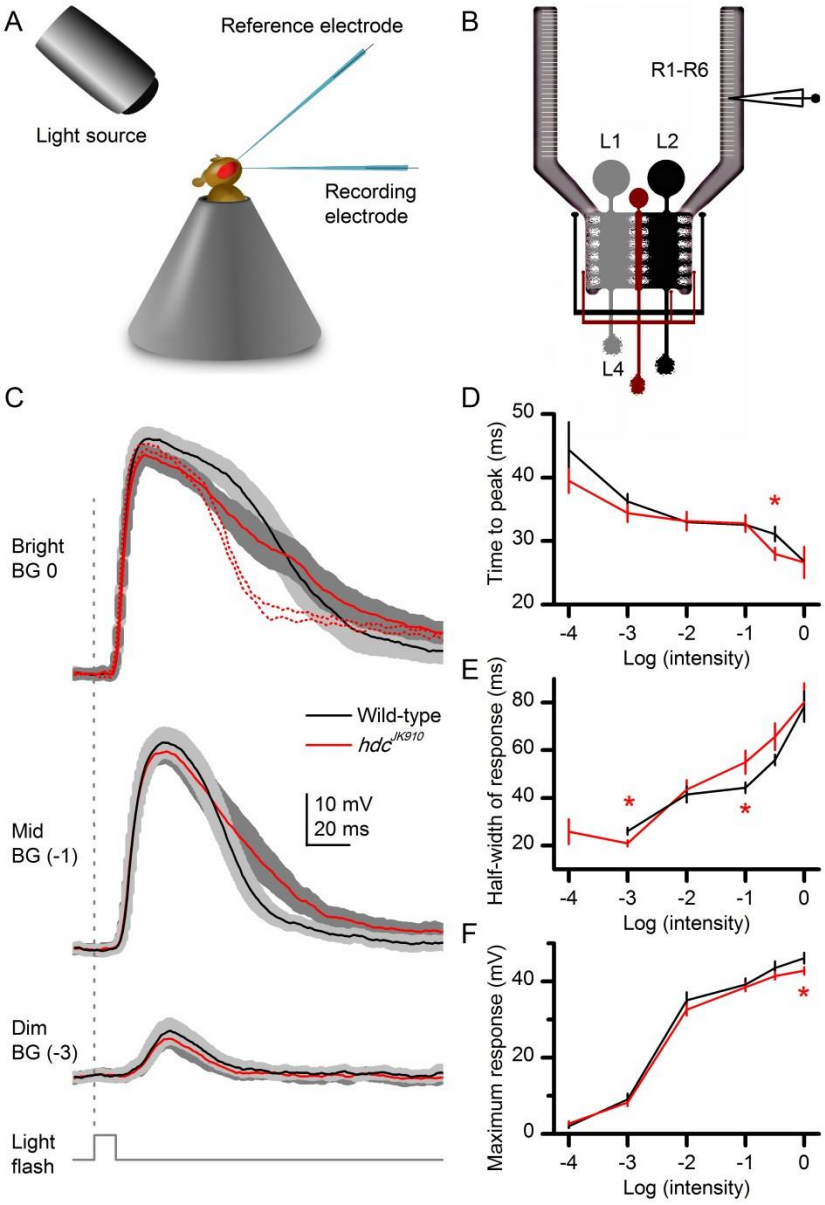

Figure 3-2. ***hdc*^{JK910} mutant R1-R6 photoreceptors responded to brief light flashes with similar speed and amplitude to that of wild-type, but recovered more slowly**

(A) *In vivo* recording from R1-R6 photoreceptors.

(B) Synaptic connections between photoreceptor axon terminals and the lamina network include feed-forward and feedback from L2/AC and L4. In the *hdc* mutant, feed-forward transmission pathways are cut off.

(C) Voltage responses of photoreceptors to Bright, Mid and Dim 10ms light pulses. Mutant photoreceptors (red) took longer time than wild-type (black) to re-polarize. Some photoreceptors of *hdc*^{JK910} at the frontal part of the eye (red dot) showed particularly fast responses.

(D) Response time-to-peak of mutant and wild-type photoreceptors were typically similar, except in the second-brightest test where responses of

mutant photoreceptors peaked earlier ($ttp_{wild\text{-}type}$ = 31.11 ± 1.15 s, ttp_{hdc} = 28 ± 0.98 s, p = 0.02, t-test).

(E) Average response of mutant photoreceptors were lengthier than that of wild-type in experiments using brighter flashes, with those of third-brightest flash tests reach significant level (p = 0.03, t-test)

(F) Average response amplitude of *hdc*^{JK910} photoreceptor were wild-type like except in the brightest flash tests, where mutant photoreceptor produced smaller responses ($Max_{wild\text{-}type}$ = 46.16 ± 1.42 mV, Max_{hdc} = 42.79 ± 0.97 mV, p = 0.035, t-test).

C-F: Mean ± SEM; one-tailed t-test; $n_{wild\text{-}type}$ = 9, n_{hdc} = 8.

Interestingly, two *hdc*^{JK910} photoreceptors in the frontal part of the eye (**Fig. 3-2C** – red dotted lines) were found to display remarkably faster kinetics than the average. Since responses of two other photoreceptors in the same fly, which located closer to the central of the eye, were within the average ranges, it is possible that the *Drosophila* eye also develop an acute zone similar to what has been reported in blowfly *Calliphora* (Hardie, 1979, Burton et al., 2001) and hoverfly *Eristalis* (Straw et al., 2006). Further morphological and physiological studies are required to verify the existence of such an area where photoreceptors have higher temporal and spatial resolutions.

Next, in order to compare wild-type and *hdc*^{JK910} photoreceptors' ability to maintain response under prolonged light stimuli, I recorded their intracellular voltage response to one-second-long light pulses of Dim (-3 log unit), Mid (-1 log unit) and Bright intensities. Typical waveform of wild-type response comprises a first peak and a flat plateau. Initially, all microvilli of a photoreceptor are available to produce their elementary bumps, of which summation constitutes the first peak. Following that, fewer microvilli are available to be activated due to their refractory period, which last about 100-200 ms. Hence, depending on intensity of light pulse thus how many microvilli have been used in the previous phase, the plateau's amplitude could be significantly smaller than the first peak (Song et al., 2012). For that reason, wild-type photoreceptors showed large initial peaks in responses to Mid and Bright but not to Dim light pulses. Moreover, microvilli's refractory periods become longer under brighter light stimulation, leading to smaller plateau evoked by Bright light pulse than those under Mid intensity. Mutant photoreceptors exhibited wild-type like waveforms (**Fig. 3-3A**) but consistently with smaller peak (**Fig. 3-3B**) and/or plateau amplitudes (**Fig. 3-3C**).

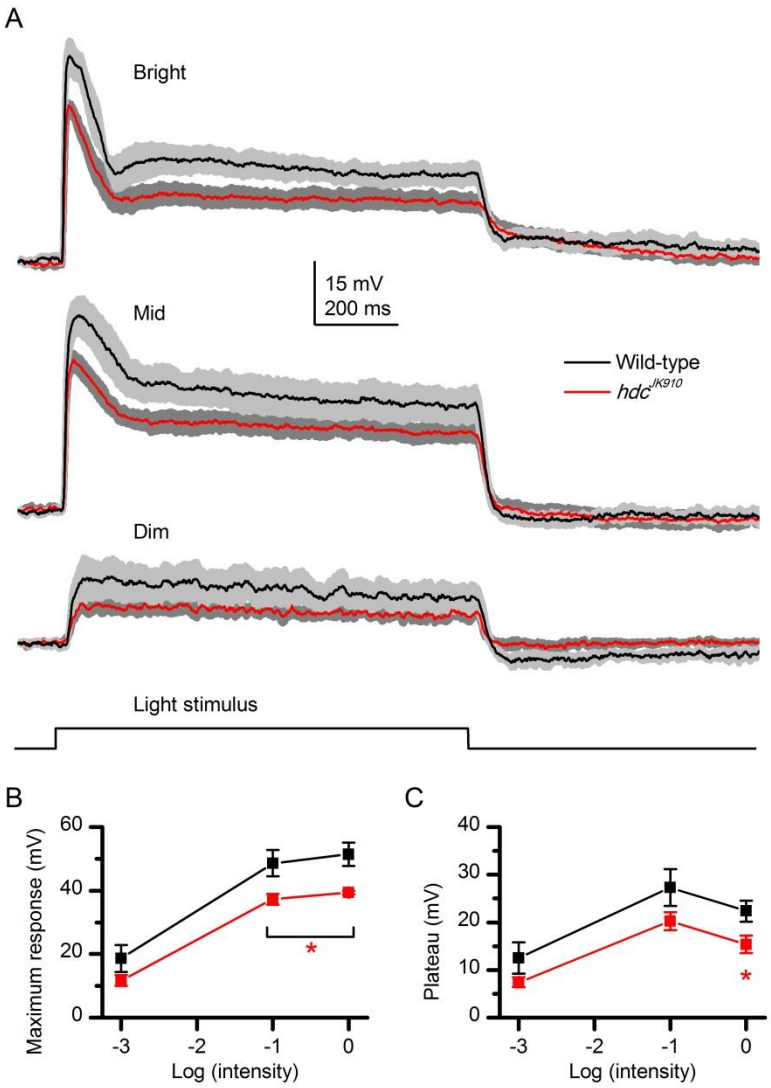

Figure 3-3. **Responses to one-second-long light pulse of wild-type and the *hdc* mutant photoreceptors.**

(A) on average, *hdc*^{JK910} photoreceptors produced smaller responses to long light pulses of all tested intensity levels.

(B) The difference in maximum amplitude reached statistical significance in experiments using light pulses of Bright and Mid intensity.

Dim: $Max_{wild\text{-}type}$ = 18.62 ± 4.28 mV, Max_{hdc} = 11.74 ± 1.69 mV, p = 0.1, t-test

Mid: $Max_{wild\text{-}type}$ = 48.6 ± 4.14 mV, Max_{hdc} = 37.23 ± 1.7 mV, p = 0.02, t-test

Bright: $Max_{wild\text{-}type}$ = 51.35 ± 3.64 mV, Max_{hdc} = 39.35 ± 0.57 mV, p = 0.01, t-test.

(C) Their plateau voltage differed significantly only in experiments with Bright light pulses.

Dim: $P_{wild\text{-}type}$ = 12.51 ± 3.29 mV, P_{hdc} = 7.44 ± 1.04 mV, p = 0.1, t-test.

Mid: $P_{wild\text{-}type}$ = 27.28 ± 3.86 mV, P_{hdc} = 20.24 ± 1.87 mV, p = 0.07, t-test.

Bright: $P_{wild\text{-}type}$ = 22.36 ± 2.23 mV, P_{hdc} = 15.37 ± 1.82 mV, p = 0.02, t-test.

A-C: $n_{wild\text{-}type}$ = 5, n_{hdc} = 5; Mean ± SEM, one-tailed t-test.

3.3.2 *hdc* mutation affects electrical properties of dark-adapted photoreceptors somatic membrane

Photoreceptor output is the outcome of a sophisticated convolution of three components: light-induced currents (LICs), light-insensitive membrane conductances and feedback from interneurons. Therefore, in order to explain the differences between response characteristics of wild-type and mutant photoreceptors, it is essential to compare those componential properties in isolation. Phototransduction cascade and *in vitro* membrane properties could be tested by performing whole-cell patch-clamp recordings on dissociated photoreceptors (Hardie, 1991b), which do not receive feedback input from neural network. Our collaborator Roger Hardie has preliminarily carried out such experiments on *hdc*^{JK910} mutant. His unpublished data indicate that firstly, macroscopic LICs evoked by 10ms flash measured from photoreceptors of *hdc*^{JK910} mutant take slightly longer to recover than those of wild-type and secondly, *in vitro* somatic K^+ conductances of *hdc*^{JK910} photoreceptors are normal.

On the other hand, since *hdc*^{JK910} interneurons do not receive synaptic information from photoreceptors, their feedback signal is expected to be independent of light stimuli. Thus, two questions arise here are how this tonic feedback signal affects photoreceptors *in vivo* membrane conductance and how together these three components constitute *hdc*^{JK910} photoreceptor output.

To discover the impacts of feedback signals from interneurons when feed-forward synaptic pathways are blocked and without the interference of LICs, I investigated *in vivo* membrane properties of dark-adapted photoreceptors by using single-electrode current-clamp technique. Voltage responses to negative and positive injected current steps were indistinguishable in somata of wild-type and *hdc*^{JK910} mutant photoreceptors (**Fig. 3-4A**). Also, their membrane input resistances, R_m, which were calculated from hyperpolarizing responses to small negative current step (-0.04 nA) to prevent the activation of voltage-gated K^+ channels (Hardie, 1991a), were in the same range (**Fig. 3-4B**). Perhaps surprisingly, resting potentials of mutant photoreceptors, selected from ones which had stable responses for 20 minutes or over, were ~6 mV more depolarized than their wild-type counterparts (**Fig. 3-4C**). Compared to wild-type, *hdc*^{JK910} photoreceptors possibly receive more depolarizing conductances from feedback input, however other intrinsic compensatory mechanisms, such as down-regulation of K^+ channels, possibly restore their membrane resistance to wild-type level. These findings strongly suggest that the

disrupted interneurons feedbacks caused by blocking feed-forward synaptic transmissions alter the dynamic equilibrium of ion channels in photoreceptor cell membrane.

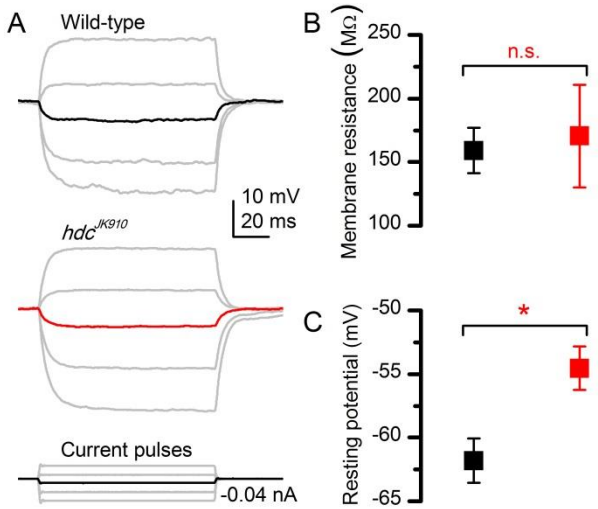

Figure 3-4. **R1-R6 photoreceptors of the *hdc* mutant had wild-type like electric membrane properties but more depolarized resting potential in darkness**

(A) Voltage response of dark-adapted wild-type and mutant photoreceptors when current pulses were injected intracellularly.

(B) Membrane resistance of mutant photoreceptors were wild-type like ($R_{m\ \text{wild-type}}$ = 159 ± 17.8 MΩ, $R_{m\ \text{hdc}}$ = 170.5 ± 40.4 MΩ, p = 0.4, t-test, $n_{\text{wild-type}}$ = 4, n_{hdc} = 4).

(C) In darkness, resting potential of mutant photoreceptors were significantly higher than that of wild-type ($V_{\text{wild-type}}$ = -61.8 ± 1.74 mV, V_{hdc} = -54.5 ± 1.7 mV, p = 0.011, t-test, $n_{\text{wild-type}}$ = 5, n_{hdc} = 4).

B-C: Mean ± SEM, one-tailed t-test.

In addition, my data here, combined with Hardie's preliminary work, are consistent with photoreceptor response kinetics observed in experiment using 10 ms light impulses (**Fig. 3-2C**): convolution of *hdc*^{JK910} LICs which recover more slowly and their membrane filtering with normal input resistance would yield responses with wild-type like rising and slower decaying phases.

3.3.3 Photoreceptors of the *hdc* mutant exhibited normal adaptation trends during dark-to-light stimuli

Modulations from the lamina network are known to have important contributions in improving photoreceptor adaptability during naturalistic light stimulation. This was demonstrated by our work described in Chapter 2 as well as previous studies (Abou Tayoun et al., 2011): despite having normal *in vitro* properties, photoreceptors of mutants with altered lamina network and thus abnormal feedback signals due to the missing of Ca^{2+}-activated K^+ channels showed remarkably defective *in vivo* dark-to-light adapting trends. To find out how concerted actions of the constant feedback from interneurons, the slightly lengthier LICs and intrinsic compensations affect adaptability of hdc^{JK910} photoreceptors, I recorded and analysed their intracellular voltage response to repeated one-second-long Naturalistic Stimuli (NS) at different light intensity levels (**Fig. 3-5A**).

Compared to wild-type photoreceptors, those of the *hdc* mutant exhibited well matching adaptation trends. **Fig. 3-5B** depicts the changes in mean of each one-second-long response (response mean – $\boldsymbol{RM}$) while the time series of NS light was repeated. $\boldsymbol{RM}$ hyperpolarized to steady state level in ~15-20 seconds in experiments using Bright and Mid intensity levels and stayed relatively unchanged in experiments with Dim NS intensity. Although average $\boldsymbol{RM}$ measured from hdc^{JK910} photoreceptors appeared to decay faster than those of wild-type for all three intensity levels, the differences of the two groups were not statistically significant. Likewise, their photoreceptor response output ranges, measured by Standard Deviation (SD) of response, changed in similar manners (**Fig. 3-5D**). Responses of mutant photoreceptors to Mid and Bright (data not shown for clarity) NS were consistently smaller than those of wild-type but decayed in parallel exponential curve, reaching steady-state ranges in comparable time scale. Furthermore, I found that probability density functions of wild-type and mutant photoreceptors, which indicate how their voltage ranges were utilized to represent light intensity modulations, adapted very similarly over time (**Fig. 3-5E-F**). None of the examined photoreceptors exhibited notable changes or flattening and widening of PDFs.

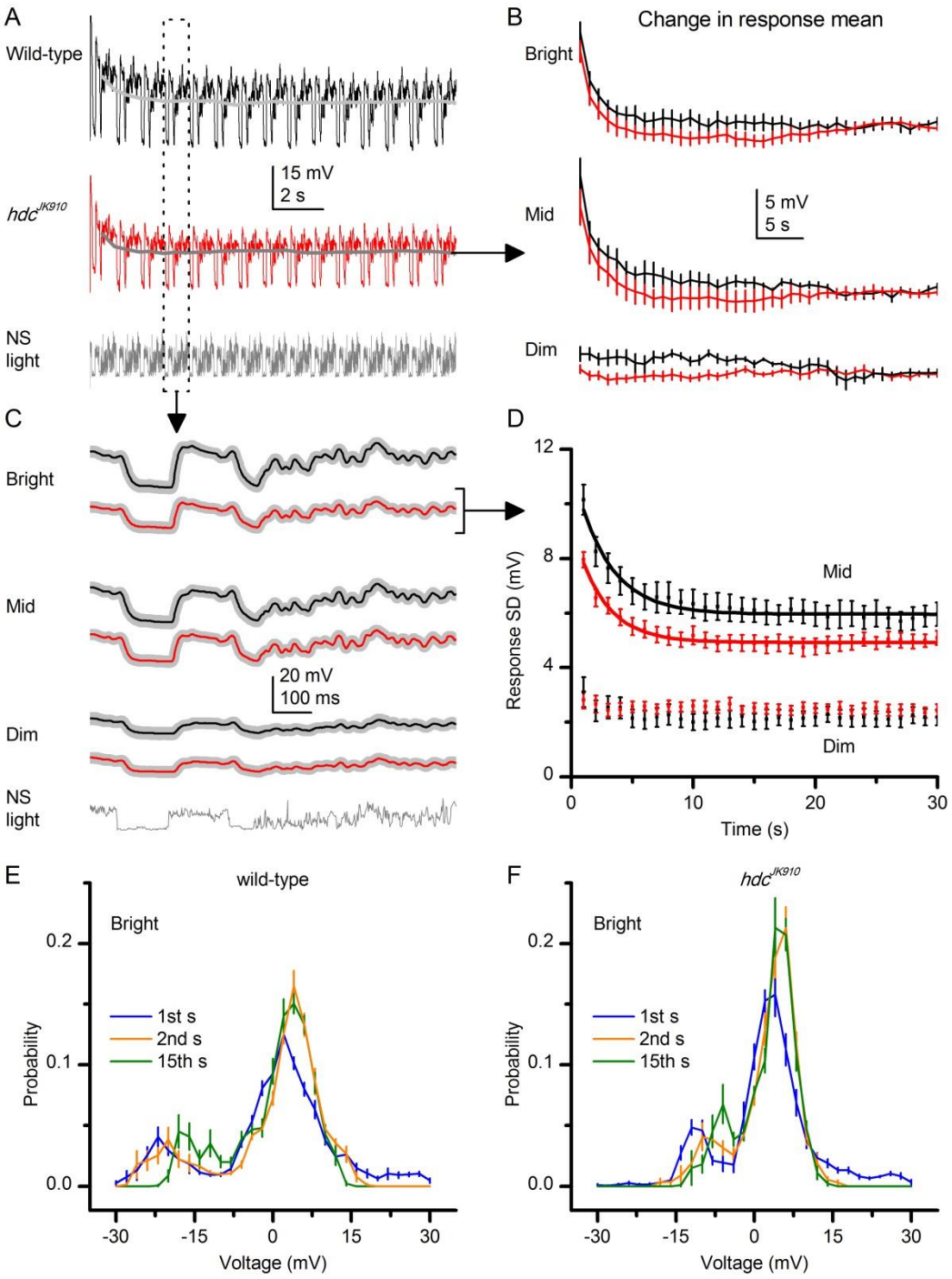

Figure 3-5. **R1-R6 photoreceptors of *hdc*^{JK910} mutant showed wild-type adaptation properties to prolonged naturalistic light stimulation**

(A) Voltage response of wild-type and mutant photoreceptor to repeated 1-second-long bright naturalistic light intensity time series.

(B) Change in the mean of 1-second-long response over 40 seconds of stimulation. Differences between wild-type and mutant mean of responses were not statistically significant.

(C) Average waveforms of steady-state adapted 1-second-long voltage responses.

(D) Change in response range (Standard Deviation of each 1-second-long response) over 30 seconds of stimulation. Data for Mid light intensities are fitted with exponential curve: $T_{wild\text{-}type}$ = 2.83 ± 0.06 s, T_{hdc} = 2.49 ± 0.07 s. Data for Bright condition were not shown for clarity.
(E) Probability Density Functions (PDFs) of wild-type photoreceptor output in the first, second and fifteenth second of Bright naturalistic stimulation.
(F) PDFs of *hdc*^{JK910} photoreceptor output in the first, second and fifteenth second of Bright naturalistic stimulation.
B-F: Mean ± SEM, $n_{wild\text{-}type}$ = 7, n_{hdc} = 8.

3.3.4 Responses of mutant photoreceptors contained similar noise spectra but carried less signal power than those of wild-type

The ultimate tasks of photoreceptors are to collect and encode information from natural environment. To obtain consistent estimates of how well different cells performed these tasks, I next discarded the first 10-20 one-second-long responses, which contain adapting changes, and compared coding performances of steady-state adapted responses from wild-type and *hdc*^{JK910} photoreceptors.

I found that response SD of the two groups were similar in experiments using Dim NS but *hdc*^{JK910} photoreceptors indeed produced significantly smaller response sizes in Mid and Bright conditions (**Fig. 3-6A**), as partly shown in the analysis of adaptation trends (**Fig. 3-5D-F**). Accordingly, average responses of mutant photoreceptors carried wild-type like signal power spectra in Dim conditions but significantly less power in Mid, at low frequencies, (**Fig. 3-6B**) and especially in Bright, over a broad frequency range (**Fig. 3-6C**). Furthermore, noise power spectra extracted from responses of wild-type and mutant photoreceptors were similar and stayed almost unaffected by different NS intensity levels (**Fig. 3-6D**). Together, these findings might imply considerable reductions in coding capacity of *hdc*^{JK910} photoreceptors. However, compared to wild-type photoreceptors, those of the *hdc* mutant surprisingly showed similar signal-to-noise ratios (SNR; **Fig. 3-6E**) over all three NS intensity levels and hence were able to encode comparable information rate R (**Fig. 3-6F**). To ensure that these statistically insignificant differences were not errors introduced by the extrapolation method for estimating rate of information (Juusola and de Polavieja, 2003), I also calculated photoreceptors coding capacity using the Shannon's estimation method (Shannon, 1948), which produced slightly

different R values (**Fig. S3-1**) but confirmed all the comparative relations shown in **Fig. 3-6F**.

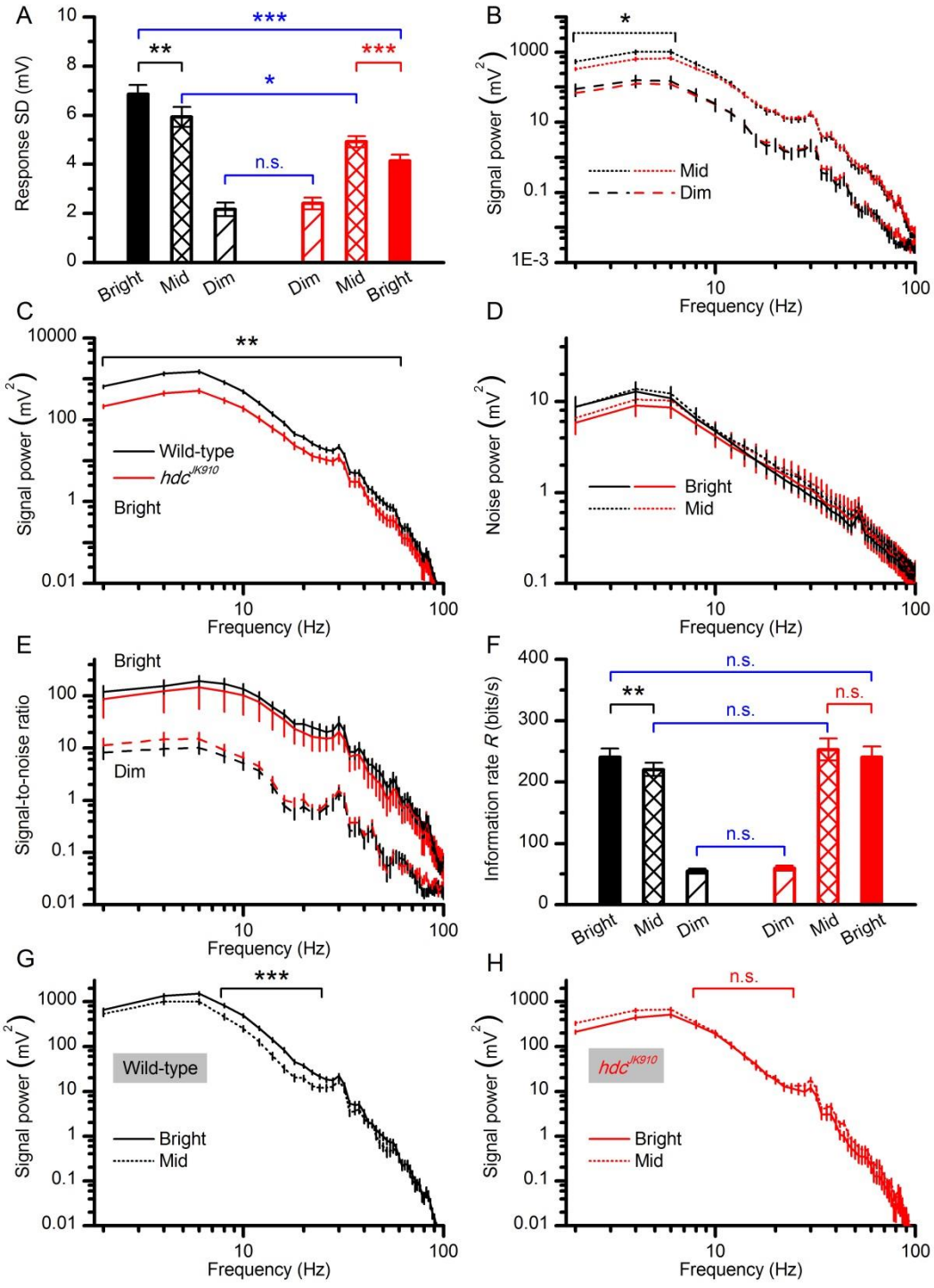

Figure 3-6. Analysis and information coding capacity of voltage responses measured from *hdc*^{JK910} mutant and wild-type photoreceptors over different NS light intensity ranges

(A) In Dim, wild-type and mutant photoreceptors showed similar response sizes ($SD_{wild\text{-}type}$ = 2.16 ± 0.27 mV, SD_{hdc} = 2.4 ± 0.23 mV, p = 0.26, t-test). In

Mid and Bright, output ranges of wild-type photoreceptors were significantly larger (Mid: $SD_{wild\text{-}type}$ = 5.93 ± 0.4 mV, SD_{hdc} = 4.92 ± 0.23 mV, p = 0.028, t-test; Bright: $SD_{wild\text{-}type}$ = 6.85 ± 0.37 mV, SD_{hdc} = 4.13 ± 0.27 mV, p = 4.0×10^{-5}, t-test).

Compared to response sizes in Mid condition, wild-type photoreceptors responded with larger voltage ranges in Bright (p = 0.007, one-tailed paired t-test) while mutant photoreceptors exhibited contracted voltage ranges (p = 3.0×10^{-4}, one-tailed paired t-test).

(B) In Dim, responses of wild-type and mutant photoreceptors carried similar signal power spectra. In Mid, wild-type signal carried more power only in low frequencies.

(C) In Bright, wild-type photoreceptors contained more signal power over a broad range of frequencies.

(D) Power spectra of noise measured in responses of wild-type and mutant photoreceptor were similar in all light intensity levels. Data in Dim condition were not shown for clarity.

(E) Signal-to-noise ratio of responses measured from wild-type and mutant photoreceptors were similar over all three light intensity levels. Data for Mid condition were not shown for clarity.

(F) Over three different light intensity ranges tested, information transfer rate measured in responses of wild-type and mutant photoreceptors were similar (Dim: $R_{\text{wild-type}}$ = 54.73 ± 3.67, R_{hdc} = 59.53 ± 4.23; Mid: $R_{\text{wild-type}}$ = 220.44 ± 10.75, R_{hdc} = 252.92 ± 17.86; Bright: $R_{\text{wild-type}}$ = 240.4 ± 14.62, R_{hdc} = 240.64 ± 17.41, all in bits/second, p>0.05, t-test).

Wild-type photoreceptors showed higher information transfer rate in Bright condition than in Mid (p = 0.004, one-tailed paired t-test) while mutant photoreceptors encode similar information rate in Mid and Bright (p = 0.07, one-tailed paired t-test).

(G) For frequencies from 8 to 24 Hz, responses of wild-type photoreceptors to Bright NS carried significantly more power than their resopnses to Mid intensities (p < 0.001, paired one-tailed t-test).

(H) Responses of *hdc*^{JK910} mutant photoreceptors to Bright and Mid naturalistic light intensities had similar power spectra (p > 0.05, paired one-tailed t-test).

A-H: Mean ± SEM, $n_{wild\text{-}type}$ = 7, n_{hdc} = 8.

These apparently contradictory results can be explained by considering the large cell-to-cell variations within each group. Average *relative variations* (computed as $\frac{SD}{Mean}$, see Materials and Methods), calculated for frequencies ≤ 40 Hz, of signal,

noise power and SNR from wild-type photoreceptor responses to Bright NS were 32%, 45% and 70% respectively. Corresponding values for responses of *hdc*^{JK910} photoreceptors were 53% (signal power), 78% (noise power) and 141% (SNR). Evidently, individual differences were intensified by the mathematical relationship SNR = $\frac{signal\ power}{noise\ power}$, resulting in remarkably larger *relative variation* in SNR than those in signal and noise power measurements. For that reason, the statistically significant difference in average signal power carried by mutant and wild-type photoreceptor responses was undermined, leading to insignificant difference in their SNRs and coding capacities.

3.3.5 Photoreceptors of the *hdc* mutant reached maximum coding capacity before their wild-type counterparts

Light intensity varies vastly in nature and could change by millions-fold from direct sun light to shadows. Therefore, photoreceptor ability to encode this huge luminance range is essential for insect as well as other animal survivability. To examine operational ranges of wild-type and *hdc*^{JK910} photoreceptors, I compared response of *the same* photoreceptor to Mid and Bright NS. These *paired comparisons* would minimise effects of cell-to-cell variations and highlight common changes in photoreceptor response when NS light intensity is changed by one log-unit.

From Mid to Bright condition, wild-type photoreceptors expanded their voltage output ranges by ~15% (**Fig. 3-6A**), leading to significant increase in signal power carried in frequencies from 8 to 24 Hz (**Fig. 3-6G**). As noise level stayed effectively unchanged (**Fig. 3-6D**, solid and dotted black lines), information transfer rate of all examined wild-type photoreceptors (n = 7), calculated by our triple extrapolation method, improved by ~10% on average (**Fig. 3-6F**). Larger increase (~25%) was observed in R values computed by using Shannon's estimation method (**Fig. S3-1**). Nonetheless, both estimation methods indicated that this trend of improvement in information transfer rate was significant with similar p-value of ~0.004. On the other hand, all photoreceptors of the *hdc* mutant (n = 8) showed the opposite trend with remarkably smaller response. However, their ~16% reduction in response size (**Fig. 3-6A**) only decreased signal power carried in low frequencies (**Fig. 3-6H**), which could contain only little information, hence did not result in significantly lower coding capacity (**Fig. 3-6F** and **Fig. S3-1**). Altogether, information transfer rate R of

hdc^{JK910} photoreceptors exhibited a slight reduction of ~5% on average, having only 2 out of 8 cells showed minor increases in their R values.

3.4 Discussions

3.4.1 Photoreceptors of *hdc*^{JK910} showed distinctive response characteristics

In this chapter, I had characterized response to short and prolonged light stimuli of *hdc*^{JK910} photoreceptors and their electrical membrane properties in darkness. My data support the hypothesis which was previously corroborated in (Zheng et al., 2006, Zheng et al., 2009, Nikolaev et al., 2009). In mutated flies where the histaminergic, feed-forward transmissions from photoreceptors are reduced, interneurons are more depolarized; thus release more excitatory neurotransmitter onto photoreceptor axon terminals. Not only did the enhanced synaptic feedback signals drive photoreceptors of *ort*^{P306} and *ebony* mutants to faster kinetics and larger responses, they also carried high SNR modulations from interneurons and therefore boosted photoreceptors to richer signal contents (Zheng et al., 2006). In *hdc*^{JK910} mutant, the completely blocked feed-forward pathways probably also lead to elevated LMCs and Amacrine cells. Hence, similar to those of *ort*^{P306} and *ebony*, *hdc*^{JK910} photoreceptors are likely to receive excessive excitatory feedback. This is indeed suggested by their more depolarized resting potentials than those of wild-type (**Fig. 3-4C**). However, since interneurons of the *hdc* mutant are effectively blind, their tonic feedback signals are not able to improve signal quality of photoreceptors. Additionally, other intrinsic mechanisms are likely to compensate for these extrinsic changes and thus convert *hdc*^{JK910} photoreceptors into a distinctive regime with unique response characteristics rather than mimicking or exaggerating those observed in *ort*^{P306} and *ebony* mutant. For instance, rebalancing of intrinsic ion channels restores their membrane input resistance to wild-type level both in darkness (**Fig. 3-4B**) and under brief light stimulation, as evidenced by the non-accelerated responses to 10ms light pulses (**Fig. 3-2E**).

3.4.2 *hdc*^{JK910} photoreceptors possibly function in narrower light intensity ranges

Compared to wild-type, *ort*^{P306} and *ebony* mutant, the most notable characteristics of *hdc*^{JK910} photoreceptors are their weakened responses to excessively bright and/or

prolonged light stimuli. They exhibited smaller responses to a brief light pulse of the brightest intensity (**Fig. 3-2F**) and to a long light pulse (**Fig. 3-3**) as well as contracted voltage ranges during Mid and Bright naturalistic light stimuli (**Fig. 3-6A**), leading to significantly lower signal power spectra (**Fig. 3-6B-C**). Moreover, photoreceptors of the *hdc* mutant displayed signs of declining operations when NS light intensity was increased from Mid to Bright. All hdc^{JK910} photoreceptors showed remarkably reduced response SD (**Fig. 3-6A**) and 6/8 cells had lower information rate in Bright condition (**Fig. 3-6F** and **Fig. S3-1**). Taken together, these results consistently suggest narrower functional range for histamine-mutant photoreceptors. With light stimuli of increasing intensities, their voltage response reached maximum amplitude and maximum coding capacity before those of wild-type. At least in theory, if intensity of light input continues to increase, hdc^{JK910} photoreceptors would be saturated and their information capacity might start to decline before those of wild-type photoreceptors.

3.4.3 Effects of tonic interneurons feedback on mutant photoreceptor outputs

Based on the data presented in this chapter, ones could not rule out other defections in hdc^{JK910} phototransduction cascade, which might greatly affect their light-induced response. Yet *in vitro* properties of mutant photoreceptors, according to Roger Hardie's unpublished work, could not explain their *in vivo* characteristics. For example, the slightly lengthier macroscopic LICs and wild-type like somatic membrane conductances found in dissociated hdc^{JK910} photoreceptors do not directly result in their contracted response to long light pulses and naturalistic stimuli.

Therefore, I speculate that the detrimental features of mutant photoreceptor outputs are largely attributable to the abnormal feedback signals from their interneurons. As demonstrated in (Zheng et al., 2006), feed-forward and feedback signals dynamically contribute to photoreceptors and interneurons outputs. When the chance of light saturation is low, the stronger synaptic transmissions in both pathways helped to amplify their response amplitudes. Moreover, since each lamina cartridge receives input from six different photoreceptors, which are aligned to the same direction in space and thus are stimulated by the same light input (Meinertzhagen and Oneil, 1991), signal-to-noise ratio of LMCs and ACs voltage responses should be higher than those of photoreceptors. In turn, the high quality

interneuron feedback helps to improve photoreceptor's signal quality. When depolarizing and hyperpolarizing outputs of photoreceptors and interneurons, respectively, are large, synaptic loads are reduced to prevent them from being saturated. Lacking these dynamic mechanisms, along with the artificially high resting potentials (**Fig. 3-4C**), could hypothetically lead to such weakened responses observed in photoreceptors of the *hdc* mutant.

Nevertheless, in order to fully elucidate the role of network feedback, a comprehensive examination of dissociated hdc^{JK910} photoreceptors incorporating conclusive data from whole-cell patch-clamp recordings, and biophysical modelling (Song et al., 2012) is required. Moreover, the absence of histamine in *Drosophila* visual system can be rescued by food supply or by a transgene expressing the histidine decarboxylase enzyme under heat-shock control (Melzig et al., 1998). Future study on "rescued" hdc^{JK910} mutants is recommended to consolidate the findings presented in this chapter.

Chapter 4: Receptive fields of wild-type and *hdc* mutant photoreceptors

4.1 Introduction

Insect eyes are small and size-constrained; presumably, owing to energy-saving and survival strategies (Laughlin et al., 1998, Land, 1999a, Niven et al., 2007). This puts their sensitivity/acuity trade-offs under intense evolutional pressure (Snyder et al., 1977, Nilsson, 1989, Laughlin, 1989, Warrant and McIntyre, 1992). While an increase of ommatidium size would improve photon capture, it would also result in fewer sampling units could be packed into an eye, lower resolution of neural images. In dim condition, where photon noise is relatively large compared to available information (signal), the task to enhance visual reliability and sensitivity is especially challenging. Since optical mechanisms, for instance the widening of photoreceptor receptive fields by pupil opening (Williams, 1982, Laughlin, 1992, Nilsson and Ro, 1994, Stavenga, 2004a), only slightly improve the amount of light collected by each ommatidium, insects' prevailing behaviour under low light intensities (Pick and Buchner, 1979, Warrant et al., 1996) suggested that other neural machineries could successfully overcome the shortfall of photon supply (Warrant, 1999). Sensitivity can be increased neurally at the cost of decreasing acuity by (i) tuning photoreceptors to higher voltage/intensity gain (Laughlin and Hardie, 1978, Matic and Laughlin, 1981), (ii) increasing photoreceptor integration time (temporal summation) (Skorupski and Chittka, 2010) and (iii) spatially summing information or reducing lateral inhibitions of neighbouring photoreceptors (Srinivasan et al., 1982, van Hateren, 1992c, Van Hateren, 1993a).

Whereas the former two neural mechanisms are known to take place already at the level of photoreceptors, the neural substrate for the latter one is less well understood. Electrical couplings by gap junctions in the retina were found only between photoreceptors which share the same optical axis (Ribi, 1978, Shaw, 1984, Van Hateren, 1986), hence these do not support neural pooling of spatial information. Occurrence of such summation was found in the directionally-selective movement-detecting (DSMD) neurons of the fly lobula plate (Srinivasan and Dvorak, 1980) but it might originate as early as in the Large Monopolar Cells (LMCs), in which intracellular response to narrow (point source) and wide-field light stimuli were shown to match well theoretical predictions of spatiotemporal summation (Dubs et

al., 1981, van Hateren, 1992a, Van Hateren, 1992b). This hypothesis is further supported by anatomical examinations using Golgi-electron microscopy technique, which have revealed intensive lateral synaptic connections between adjacent lamina cartridges in the nocturnal bee *Megalopta genalis* (Greiner et al., 2005). A question that arises here is *whether this summation is synaptically fed back to photoreceptors, contributing to their outputs*. The tight coupling between feed-forward and feedback pathways in the photoreceptor-lamina circuit is known to have crucial roles in maintaining robust adaptation and temporal coding efficiency (Zheng et al., 2006, Zheng et al., 2009, Nikolaev et al., 2009). Similar top-down regulation of spatial information might be functionally beneficial.

Several studies have provided preliminary data to answer this question. Dubs et al. (1981) recorded quantum bump in photoreceptors of the fly *Musca domestica* at light intensity as low as the behavioural threshold and found that small-amplitude events were not caused by the impaled cell but by single photon captures in its neighbouring cells. In addition, receptive fields of dark-adapted fly photoreceptors were reported to have wider flanks than expected (Dubs, 1982).

Here to further elucidate this problem, I took advantage of the genetics tools available in *Drosophila* and compared photoreceptors of wild-type and the *hdc* mutant. Synaptic transmissions from hdc^{JK910} photoreceptors were blocked, making their interneurons effectively blind (see Chapter 3). Therefore feedback from mutant LMCs would not contain any lateral interactions, either spatial inhibitory or excitatory. I found that receptive fields of dark-adapted mutant photoreceptors were on average 10.9% narrower than those of wild-type, while no significant difference was detected between light-adapted cells of the two groups. Moreover, I report the effect of stimuli history on photoreceptor receptive fields and retinal movements in the *Drosophila* eye. My data strongly suggest the hypothesis that in dim conditions, spatial information is pooled in the lamina and fed-back to photoreceptors. However, specific anatomical and physiological studies are further recommended in order to draw a conclusion.

4.2 Materials and methods

Maintenance of fly stocks and procedures of *in vivo* electrophysiological recordings were as described in Chapter 2 and Chapter 3.

4.2.1 Measurement and calculation of photoreceptors Receptive Field

Receptive field of a photoreceptor is assessed by measuring amplitude V_n of its intracellular response to light flash of intensity I_n at varying angular positions α_n. From all V_n, I_n, and α_n values generated by a complete scan, the width of the receptive field can be computed by three methods as comparatively reviewed below.

4.2.1.1 Method 1

In this method, V_n is clamped to a constant value by using a closed-loop system to accordingly vary I_n for different light source position (Smakman et al., 1984, Smakman and Stavenga, 1987). Sensitivity to each position, S_n, is then defined by:

$$S_n = \frac{I_0}{I_n}, \tag{4-1}$$

where I_0 is the intensity required from a point source at the centre of the receptive field. The definition of sensitivity can be equivalently expressed as a light source at an off-axis position is required to be $\frac{1}{S_n}$ fold brighter than an axial one in order to stimulate flash responses of the same amplitude.

After corresponding S_n was computed for every α_n, the sensitivity-angle relation is fitted by a Gaussian function. The width at half-maximum of this Gaussian curve is termed *acceptance angle* and is the common parameter for quantifying the width of receptive field.

4.2.1.2 Method 2

Method 2, in which I_n is the same for light flash at every angular position, is the most widely used (Wilson, 1975, Horridge et al., 1976, Hardie, 1979, Mimura, 1981, Gonzalez-Bellido et al., 2011). Initially, the $V/\log(I)$ relation of the impaled photoreceptor is determined by using a light source at the centre of the receptive field and a system of neutral density filters. V_n elicited by light source at each off-axis angle α_n is then substituted into this $V/\log(I)$ function to estimate I_a, the

intensity of light that was effectively absorbed by photo-sensitive pigments. Angular sensitivity, S_n, is given by the following equation:

$$S_n = \frac{I_a}{I_n}. \tag{4-2}$$

Gaussian fitting and calculation of acceptance angle are as previously described in Method 1.

This method is based on the same principle with Method 1, which is to assess the light intensity necessary to elicit a criterion response (Warrant and Nilsson, 2006). When the lighting point with intensity I_0 is exactly on the optical axis of the cell, sensitivity is the highest with response amplitude V_0. In order to evoked $V_n = V_0$ by a light source located at an angular position α_n, it is required that the effective intensity I_a to equal I_0. Given the angular sensitivity formula:

$$S_n = \frac{I_a}{I_n} = \frac{I_0}{I_n}, \tag{4-3}$$

the necessary intensity I_n would be $\frac{1}{S_n}$ fold brighter than I_0.

Though Method 2 does not require a closed-loop system and therefore is less experimentally challenging, its estimation of effective intensity I_a has some drawbacks. Not only does the use of $V/\log(I)$ function introduce a likely source of errors, its underlying assumption that the Voltage/Effective Intensity relation is independent of light source position neglects possible direct and indirect lateral interactions between neighbouring photoreceptors.

Nonetheless, the outcomes of both methods are theoretically independent of the phototransduction cascade and intensity of testing flashes, hence enabling the measurements of photoreceptor receptive fields by electro-physiological recordings to be compared with those derived from optical, morphological and waveguide theories.

4.2.1.3 Method 3

Similar to Method 2, photoreceptors are stimulated by light impulses of the same intensity at different angular positions around their optical axes. Amplitude V_n of response to a light flash coming from angle α_n is then normalised to the maximum response evoked by an on-axis light source, V_0. Receptive field is determined by the Gaussian fitting of the relation between ratios $\frac{V_n}{V_0}$ and incident angle α_n, which yields wider width at half-maximum ($\Delta\rho$ values) than the acceptance angles estimated by using Method 1 and Method 2 (Washizu et al., 1964, Burkhardt, 1977).

In this chapter, I chose Method 3 to interpret photoreceptor receptive fields from intracellular recordings despite its disadvantages: results would depend on flash intensity and would not be comparable to other approaches as well as previous studies in *Drosophila*. The main rationale is that this method reflect "how well flies see" the most directly and reliably, without taking any assumptions of lateral interactions between photoreceptors and/or feedback from LMCs. Moreover, limitations of the method should not compromise the objectives of this chapter, which are to compare photoreceptor receptive fields of different genotypes and report the effect of different ambient conditions and stimuli history. Experimentally, it was also not feasible to facilitate our equipment with either a closed-loop system (as in Method 1) or neutral density filters for characterising $V/\log(I)$ function (as in Method 2).

4.2.2 The 25-point array and LEDs pads

Receptive fields of photoreceptors were scanned by using an array of 25 lighting points, mounted on a Cardan arm (**Fig. 4-1**). Each point subtends an angle of 1.71º as seen by the fly and is the ending of a light guide cable, of which other end collects light input from a LEDs box. The system is controlled by 2 channels, both with voltage inputs ranging from 0 V to 10 V. Channel 0 selects a point to be tuned and Channel 1 linearly defines its intensity.

Fig. 4-2A depicts typical spectral density delivered by the 25-point array with a narrow peak at 450 nm (P1) and a broader peak at of 570 nm (P2). Peak intensity and wavelength from each point were precisely measured by using a Hamamatsu photometry and are detailed in **Table 4-1**. Given that voltage responses of fly photoreceptors show notable changes only when intensity of light input changes by

several folds, as demonstrated by the sigmoid shape of the $V / \log(I)$ relationship (Matic and Laughlin, 1981), it can be assumed that all 25 points of the array, except point No.22, provide relatively uniform light stimuli. Standard light pulses, containing 2×10^6 photons/second at P1 and 3×10^6 photons/second at P2, were produced by setting Channel 1 to an input value of 2 V.

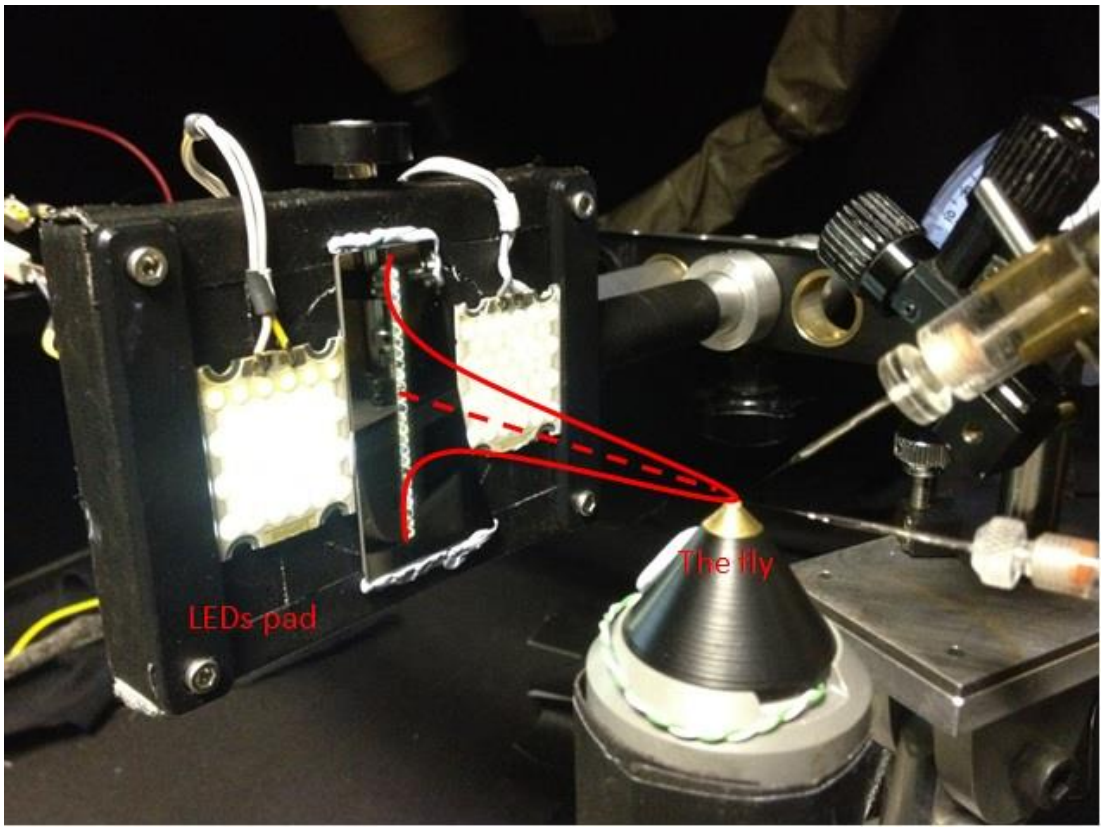

Figure 4-1. The receptive field of a *Drosophila* photoreceptor (illustrated as a red Gaussian shape) is assessed by measuring its intracellular voltage response to successive light impulses from 25 lighting points. In light-adapting experiments, two Lamina pads, each of which has 39 LEDs, were placed at the outer half and outside the photoreceptor's receptive field to provide background light.

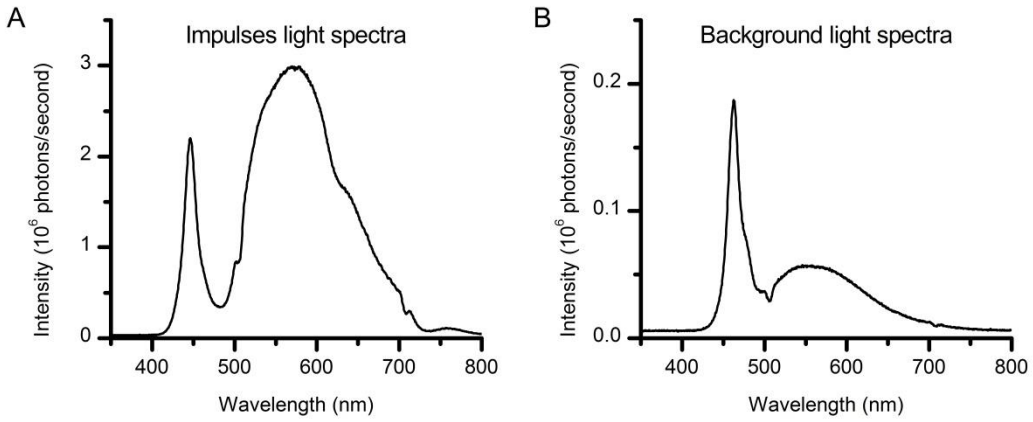

Figure 4-2. **(A)** Typical spectral density of impulses delivered by the 25-point array. **(B)** Spectral density of a single LED on the two Lamina pads, which were used to provide ambient light in light-adapting experiments.

Lighting point	Peak 1 wavelength (nm)	P1 intensity (10^6 photons per second)	P2 wavelength (nm)	P2 intensity (10^6 photons per second)
No.1	448	2.720	571	2.805
No.2	452	1.790	570	2.818
No.3	448	2.618	565	2.900
No.4	451	1.840	576	3.020
No.5	451	2.570	575	3.710
No.6	451	2.214	572	3.640
No.7	452	1.430	575	2.020
No.8	446	2.203	570	2.990
No.9	453	1.465	571	2.350
No.10	451	3.300	578	5.100
No.11	453	1.877	575	3.080
No.12	455	1.763	575	3.020
No.13	451	2.334	575	3.440
No.14	451	2.009	576	2.634
No.15	454	2.400	568	4.480
No.16	452	2.390	572	4.165
No.17	455	3.190	566	3.010
No.18	452	1.990	578	3.320
No.19	455	1.958	578	3.336
No.20	454	1.745	569	2.670
No.21	450	2.642	573	2.314
No.22	452	9.520	572	13.300
No.23	452	2.420	575	3.380
No.24	452	2.658	573	3.284
No.25	452	1.670	570	2.750

Table 4-1. Peak wavelengths and intensities of light flash delivered by each of the 25 lighting points.

Point No.22 was always four-fold brighter than the others. However, no attempt was made to correct its intensity because of three main reasons. Firstly, it locates at the periphery of the receptive field hence should not significantly affect measurements. Secondly, since this "error" occurred identically in every experiment, the unusual brightness of No.22 would not bias the comparative studies in this chapter. Lastly, having an exceptionally bright point was beneficial for other experiments, as will be discussed in Chapter 5.

Two Lamina pads, each of which has 39 identical LEDs, were used to provide ambient illumination in experiments where photoreceptors were required to be moderately light-adapted. These pads were located at the outer half and outside receptive field of the recorded cell (**Fig. 4-1**), thus a large portion of ambient light was projected to the neighbouring photoreceptors. But these light sources also much illuminated the whole recording chamber, revealing its spatial structure, provoking possible spatial effects of neural network. As shown in **Fig. 4-2B**, light emitted by a single LED peaked at 460 nm, delivering estimated ~2×10^5 photons/s.

4.2.3 Pseudo-random scan of receptive field

At the beginning of experiments, centre of photoreceptor receptive field was located by flashing only lighting point No.13 (the centre point of the array) and moving the array until maximum response amplitude was elicited. The photoreceptor was then adapted to background light level for 30 seconds – one minute before its receptive field was measured.

A complete scan of receptive field comprises light impulses from all 25 points, one after another in a pseudo-random order (**Fig. 4-3A**). Each impulse was 10 ms long and was followed by 490 ms of darkness (**Fig. 4-3B**). Although the resting period should approximately re-adapt photoreceptors to background light level, spatiotemporal adaptation might still affect their response. For instance, a flash near centre of the receptive field would light-adapt the cell more than one at the periphery, possibly causing response to the next flash to be artificially smaller. To further minimise such potential adaptation effect, the lighting order was randomised by using the command *randperm(25)* in MATLAB.

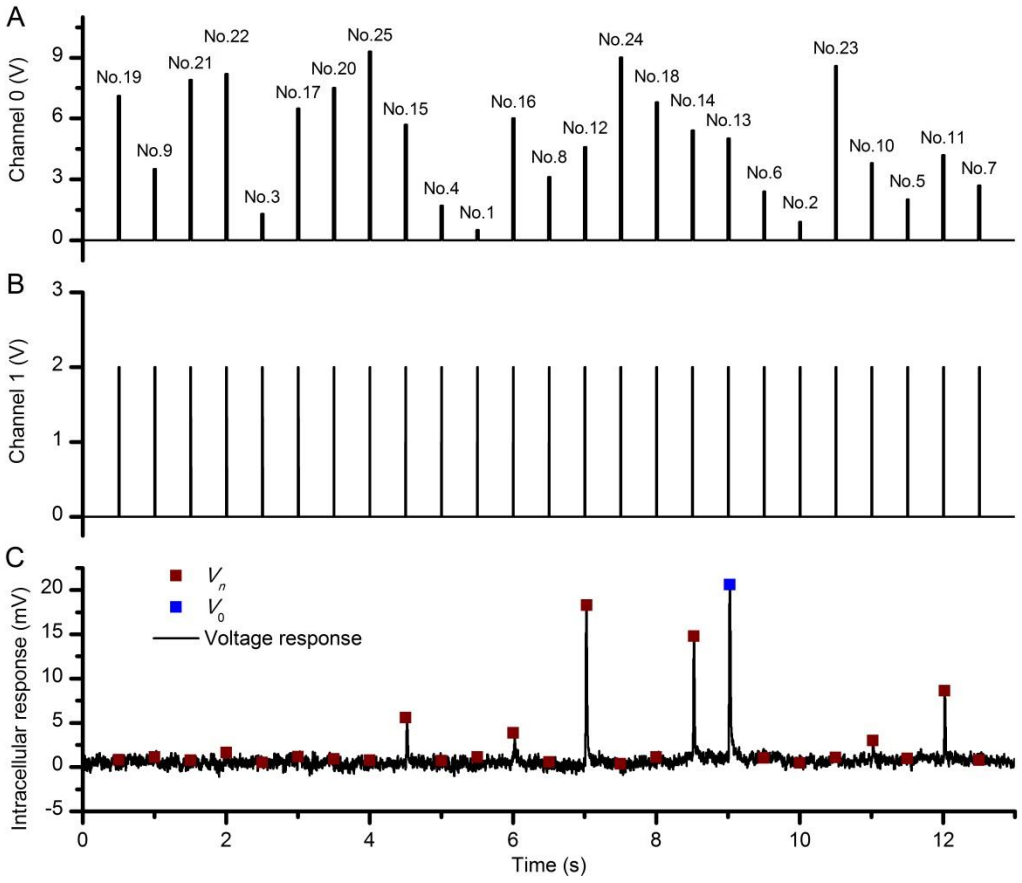

Figure 4-3. **(A)** Channel 0 input was used to select a lighting point to be tuned.
(B) Channel 1 input defined light intensity of the selected point. A standard light impulse was produced by a 2 V input, which lasted 10 ms.
(C) Intracellular voltage response of a photoreceptor to a complete receptive field scan. Amplitude V_n of each flash response was calculated by assessing local maxima. V_0 is the amplitude of the response to a flash at the centre of the receptive field (on-axis).

Input of Channel 0 was tuned only when Channel 1 was set at zero Volt, i.e. in the resting period when all lighting points were off, otherwise the transitions of Channel 0 input values would generate images of a running dot.

Intracellular responses of photoreceptors to 2-5 repetitions of pseudo-random scans were averaged (**Fig. 4-3C**) before the widths at half-maximum $\Delta\rho$ of receptive fields were determined (**Fig. 4-4**).

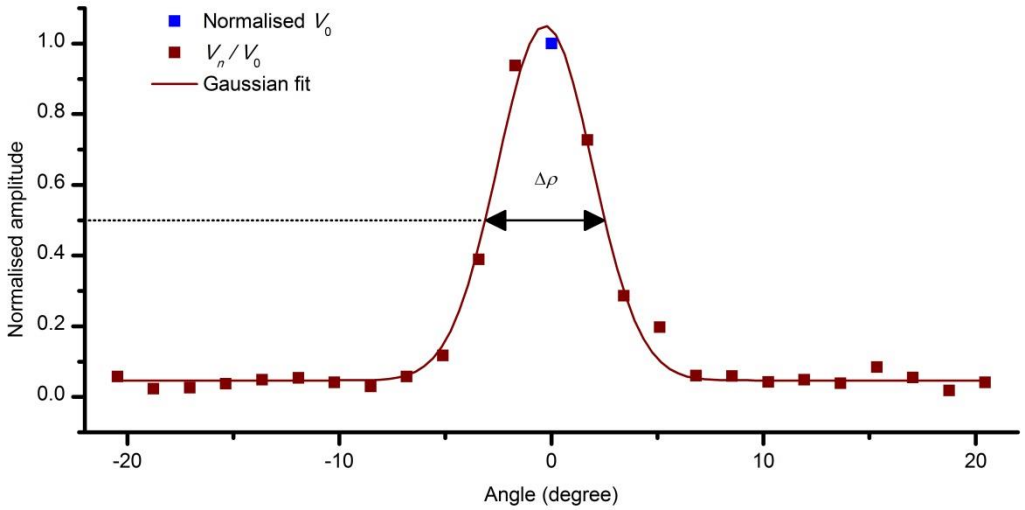

Figure 4-4. Flash response amplitudes V_n were initially normalised to V_0, the maximum response elicited by an on-axis lighting point. A Gaussian curve was then fitted to these normalised values, yielding an estimation of the receptive field. Width at half-maximum of this Gaussian function, $\Delta\rho$, is used for quantification.

4.2.4 White-noise stimuli

Light intensities of lighting point No.13 was controlled by setting Channel 0 input to 5 V and modulating Channel 1 input with a white-noise time series, which has mean value of 2.5 V and cut-off frequency of 200 Hz. Accordingly, the lighting point delivered 2.5×10^6 photons/second at P1 (450 nm) and 3.75×10^6 photons/second at P2 (570 nm) on average.

4.3 Results

4.3.1 Receptive field of dark-adapted photoreceptors

In every experiment, the first examination of the impaled photoreceptor was always to assess its dark-adapted receptive field. Half-maximum widths $\Delta\rho$ measured from 19 wild-type photoreceptors were 9.47 ± 1.57º (mean ± SD), ranging from 7º to 11.65º. Interestingly, receptive fields of 18 *hdc*^{JK910} photoreceptors were on average ~10.9% narrower, with mean, minimum and maximum values of 8.44 ± 1.36º, 6.18º and 11.5º, respectively. Moreover, the difference between receptive field widths of wild-type and mutant photoreceptors was statistically significant as indicated by one-tailed student test (p = 0.0198, **Fig. 4-5A**).

Amplitudes V_n of photoreceptor flash responses were directly used to estimate receptive fields, rather than being converted to angular sensitivities (see Materials and Methods). Therefore outcomes of $\Delta\rho$ measurements presented in this chapter were dependent on photoreceptor input/output (voltage/light intensity) characteristics as well as intensity of the testing flashes. To ensure that the comparison of $\Delta\rho$ values was unbiased, i.e. on-axis light sensitivity of photoreceptors belonging to the two groups were comparable, I also compared their maximum response amplitude V_0 and their $V_0 / \Delta\rho$ relations. As illustrated in **Fig. 4-5B**, V_0 measured from wild-type and mutant photoreceptors were indeed similar. Most recorded V_0 values were from 20 to 35 mV (**Fig. 4-5C-D**), the range in which *hdc*^{JK910} photoreceptors were shown to have wild-type like $V/\log(I)$ curves (see **Fig. 3-2F** in Chapter 3). Moreover, the linear correlations between V_0 and $\Delta\rho$, reflecting the trend of more sensitive photoreceptors (larger V_0) to have wider receptive fields (larger $\Delta\rho$), were weak in both wild-type and the *hdc* mutant (**Fig. 4-5C-D**). Together, these data demonstrated that the narrower $\Delta\rho$ found in dark-adapted *hdc*^{JK910} photoreceptors were neither caused by variation in their phototransduction cascades nor an artefact of this measurement method.

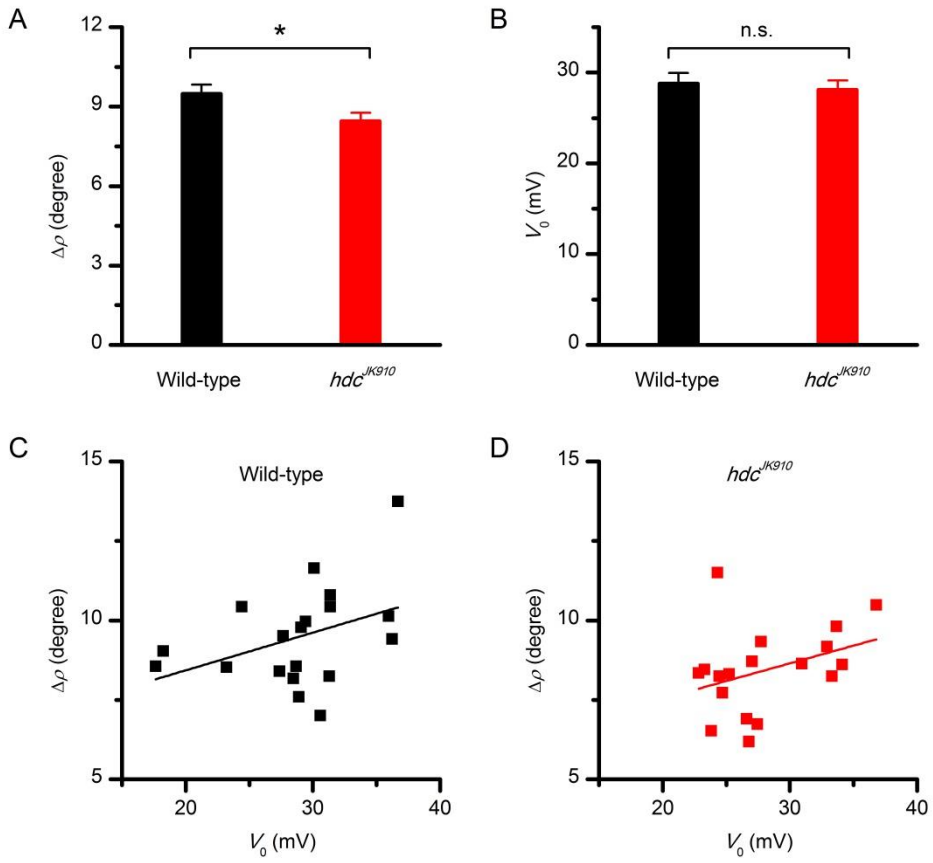

Figure 4-5. **(A)** Receptive fields of dark-adapted wild-type photoreceptors were significantly wider than those of *hdc*^{JK910} photoreceptors. $\Delta\rho_{\text{wild-type}}$ = 9.47 ± 0.36°; $\Delta\rho_{\text{hdc}}$ = 8.44 ± 0.32°; p = 0.0198, t-test.

(B) V_0, response amplitude evoked by a light impulse at the centre of the receptive field, measured from wild-type and mutant photoreceptors were in the same range. $V_{0\ \text{wild-type}}$ = 28.77 ± 1.19 mV; $V_{0\ \text{hdc}}$ = 28.11 ± 1.03 mV; p = 0.34, t-test.

(C) Linear correlation between $\Delta\rho$ and V_0 of dark-adapted wild-type photoreceptors. Adjusted R-squared = 0.1043.

(D) Liner correlation between $\Delta\rho$ and V_0 of dark-adapted *hdc*^{JK910} photoreceptors. Adjusted R-squared = 0.072.

A-D: $n_{\text{wild-type}}$ = 19; n_{hdc} = 18.

C-D: Mean ± SEM; one-tailed student test.

4.3.2 Receptive field of light-adapted photoreceptors

A photoreceptor's $\Delta\rho$ measured under the specified ambient illumination is expected to be smaller than its dark-adapted $\Delta\rho$ for four reasons. Firstly, its

$V/\log(I)$ function becomes steeper as the cell is light-adapted (Laughlin and Hardie, 1978, Matic and Laughlin, 1981, Eguchi and Horikoshi, 1984), hence the difference between I_0 and I_{a50}, the effective intensity that could evoke response amplitude $\frac{V_0}{2}$, will be reduced. Consequently this leads to smaller α_{50}, the corresponding angular position of I_{a50} and thus narrower $\Delta\rho$ reported by the chosen method. Secondly, because intensity of testing flashes were kept unchanged as against dark and light background, contrast of each flash would be lower than in dark-adapted experiments, further reducing the $\frac{I_0}{I_{a50}}$ ratio, α_{50} and $\Delta\rho$. Thirdly, light adaptation activates the closure of pupil pigments, reducing the amount of light from off-axis angles that can be absorbed by photo-sensitive pigments (Hardie, 1979, Smakman et al., 1984, Stavenga, 2004a, Stavenga, 2004b). Lastly, theoretical studies and preliminary experimental data have suggested that in dim condition, summing neural signals of neighbouring photoreceptors would help to enhance sensitivity whereas in bright condition, lateral inhibitory would be beneficial for increasing image resolution (Srinivasan et al., 1982, van Hateren, 1992c, Van Hateren, 1993b, Warrant, 1999, Klaus and Warrant, 2009). These potential effects of neural network might also contribute to the narrowing receptive fields of light-adapted photoreceptors.

Next, to quantify how moderate ambient light affect spatial performance of the fly eye, I analysed the six wild-type photoreceptors and eight *hdc*^{JK910} photoreceptors of which receptive fields were assessed in both dark- and light-adapted state.

In dark condition, $\Delta\rho$ of these wild-type and mutant photoreceptors were 9.65 ± 2.59° and 8.16 ± 1.74° (mean ± SD), respectively (**Fig. 4-6A**). This difference of 15.44% on average was not statistically significant probably because the n-numbers of both groups were not large enough.

Under ambient illumination, corresponding $\Delta\rho$ values were 7.7 ± 1.27º for wild-type photoreceptors and 6.98 ± 1.29º for their *hdc*^{JK910} counterparts. Switching from dark- to light-adapted states, receptive fields of wild-type photoreceptors narrowed down by 18.44 ± 8.58%, slightly more than those of mutants, which changed by 13.68 ± 9.53%. Nevertheless, none of these parameters were significantly different between the two photoreceptor groups.

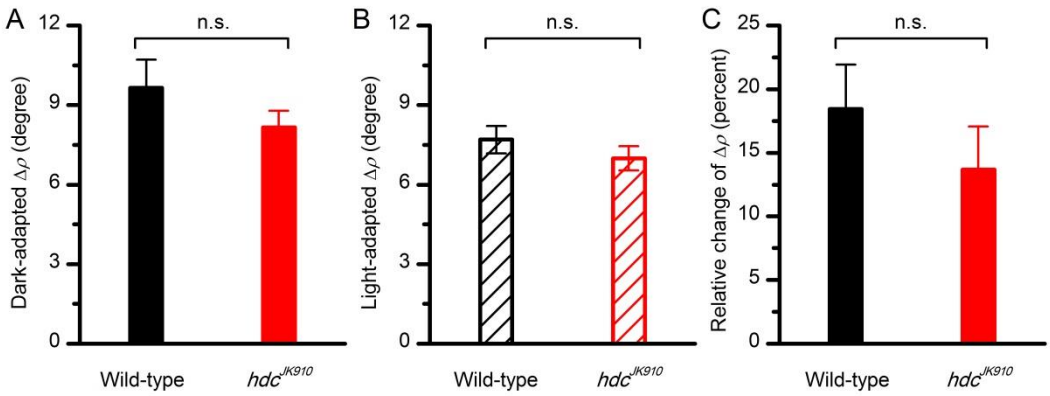

Figure 4-6. Wild-type and *hdc*^{JK910} photoreceptors, of which receptive fields were assessed in both dark- and light-adapted states, were compared. Their dark-adapted **(A)** and light-adapted $\Delta\rho$ values **(B)** as well as relative changes between the two adaptation states **(C)** were statistically similar.

Dark-adapted: $\Delta\rho_{\text{wild-type}}$ = 9.65 ± 1.06°; $\Delta\rho_{\text{hdc}}$ = 8.16 ± 0.62°; p = 0.129, t-test.

Light-adapted: $\Delta\rho_{\text{wild-type}}$ = 7.7 ± 0.52°; $\Delta\rho_{\text{hdc}}$ = 6.98 ± 0.46°; p = 0.161, t-test.

Relative changes, calculated as $C = \frac{\Delta\rho_{\text{Dark}} - \Delta\rho_{\text{Light}}}{\Delta\rho_{\text{Dark}}} \text{ x } 100\%$:

$C_{\text{wild-type}}$ = 18.44 ± 3.5%; C_{hdc} = 13.68 ± 3.37%, p = 0.174, t-test.

A-C: Mean ± SEM; one-tailed student test; $n_{\text{wild-type}}$ = 6; n_{hdc} = 8.

4.3.3 Effect of stimulation history on photoreceptor receptive fields

Other than ambient illumination which light-adapted photoreceptors, prolonged periods of light stimulation could also desensitise retinal cells, resulting in similar effects. Such consequences of stimulation history were recorded in five wild-type and six *hdc*^{JK910} photoreceptors. Receptive field of each cell was scanned twice in dark condition, with a one-minute period of white-noise stimuli in between (see Materials and Methods). The second scan was started within 10 s of ceasing white-noise light modulation.

As illustrated in **Fig. 4-7**, this specific stimulation history affected wild-type and mutant photoreceptors almost identically, narrowing their receptive field widths down by ~6.5% on average, which were quantitatively ~35-50% the effects caused by moderate light-adaptation. The differences between $\Delta\rho$ values of the two photoreceptor groups were virtually unchanged by white-noise stimulation and were

at the margin of statistical significance, with p-values corresponding to outcomes of first and second scans were 0.045 and 0.053, respectively.

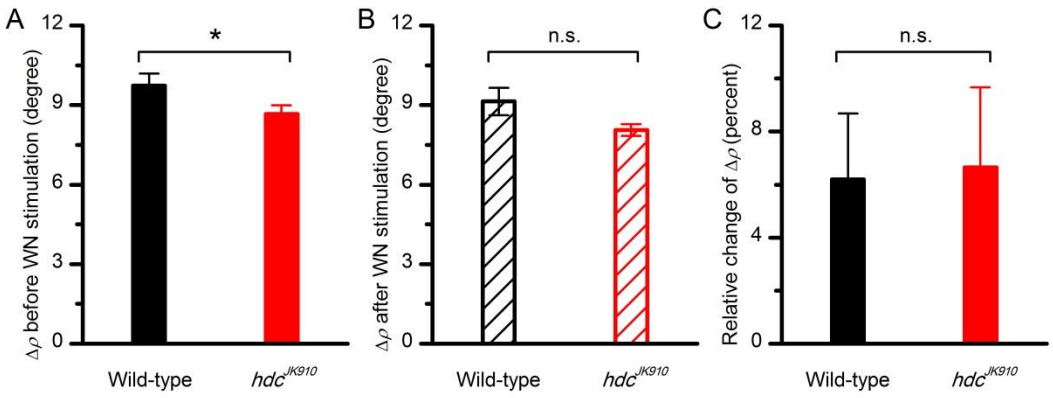

Figure 4-7. **(A)** Dark-adapted receptive fields' half-widths of the considered wild-type and *hdc*^{JK910} photoreceptors, measured before one-minute white-noise stimulation: $\Delta\rho_{\text{wild-type}}$ = 9.73 ± 0.45°; $\Delta\rho_{\text{hdc}}$ = 8.66 ± 0.32°; p = 0.045, t-test.

(B) $\Delta\rho$ of the same photoreceptors measured in dark condition within 10s of ceasing white-noise stimulation: $\Delta\rho_{\text{wild-type}}$ = 9.14 ± 0.52°; $\Delta\rho_{\text{hdc}}$ = 8.05 ± 0.22°; p = 0.053, t-test.

(C) Relative changes in $\Delta\rho$ of photoreceptors belonging to the two groups: $C_{\text{wild-type}}$ = 6.2 ± 2.48%; C_{hdc} = 6.65 ± 3.01%, p = 0.45, t-test.

A-C: Mean ± SEM; one-tailed student test; $n_{\text{wild-type}}$ = 5; n_{hdc} = 6.

4.3.4 Possible movements of the *Drosophila* retina

Despite the head and body of a fly were fixed onto the holding cone, its eye could still move and hence distort the on-going electrophysiological recordings (Kirschfeld and Franceschini, 1969b). Retinal movements have also been described in blowfly and treated by different methods, including cooling the fly, anaesthesia and fixing the slightly pulled out antennae (Smakman et al., 1984).

Here I reported that similar retinal movements could also occur in *Drosophila* preparations. **Figure 4-8** shows an example, in which optical axis of a photoreceptor appeared to move slightly. In the first scan, the centre of the receptive field, which was located by the largest flash response, corresponded to lighting point No.12. However, the second receptive field scan indicated that the cell's optical axis pointed toward lighting point No.10, reflecting an angular movement of ~3º. Around 50% of photoreceptors, in which receptive fields were scanned more than once

(8/18 wild-type and 8/16 mutant photoreceptors), displayed similar retina movements in the range of 1-3.5º. Moreover, movements occurred in both directions, suggesting that they were not caused by equipment errors, for instance the displacement of the Cardan arm, which held the lighting-point array, due to gravity.

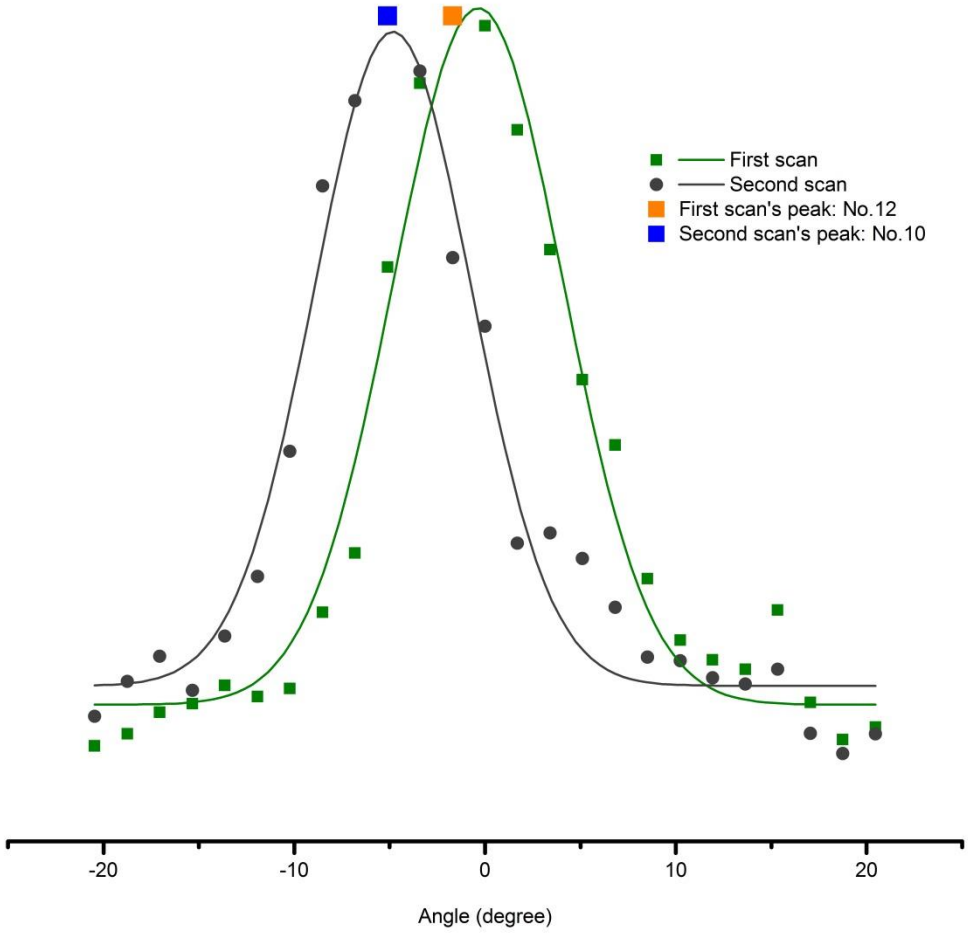

Figure 4-8. Example of retinal movements in the *Drosophila* eye. The first scan showed that the centre of the receptive field were closet to lighting point No.22 while in the second scan, the peak response was evoked by point No.10. The difference between optical axes indicated by the two scans was ~3º.

It has been reported that recordings from damaged photoreceptors usually resulted in extraordinarily wide acceptance angle, diminishing sensitivity (Wilson, 1975) or markedly asymmetrical receptive field due to artificial electrical coupling with neighbouring cells (Smakman and Stavenga, 1987). To ensure high quality for $\Delta\rho$ measurements presented in this study, I only considered data from photoreceptors

of which receptive fields were reasonably symmetrical and intracellular responses were stable and repeatable. Nonetheless, it is acknowledged that retinal movements in the *Drosophila* eye possibly affect accuracy of receptive field assessments.

4.4 Discussions

In this chapter, receptive field of wild-type and *hdc*^{JK910} photoreceptors were assessed and compared in dark- and moderately light-adapted states, and under the desensitisation effects caused by prolonged light stimulation. In the specifically tested settings, $\Delta\rho$ values belonging to the two groups were largely similar except those measured in dark-adapted state.

Responses of wild-type LMCs to light impulses produced depolarizing potentials in the extracellular space, which might be picked up by the electrode and hence artificially add a DC component to the measurement of V_n. In contrast, since *hdc*^{JK910} LMCs did not respond to light, this extra component was absent in recordings from their photoreceptors. At the first glance, one may attribute the narrower receptive field measured from mutant photoreceptors to this possible contamination of intracellular recordings (Hardie et al., 1981). However, this possibility can be ruled out as the bases of Gaussian curves were fitted to flanks amplitudes rather than to absolute zero (**Fig. 4-4**), therefore any extra DC component would not affect estimations of $\Delta\rho$ values.

Instead, $\Delta\rho$ of dark-adapted photoreceptors were the most reliable data amongst those presented in this study, with the largest number of samples ($n_{wild\text{-}type}$ = 19, n_{hdc} = 18) and strong consistency in measurement procedure. In every case, assessment of receptive field in dark-adapted stated were strictly the first examination once the impaled cells were located, thus eliminating any potential effects of down-grading recording quality or variation in stimulation history.

The dominating factors that determine photoreceptor receptive field are optical, waveguide properties and, particularly for the chosen measurement method, phototransduction characteristics (Stavenga, 2003a, Stavenga, 2003b, Land, 1997, Snyder, 1977). As in the case of blowflies, Smakman et al. (1984) showed that the main peak of receptive field shape can be well described only by using physical considerations and waveguide theories. Given the *hdc* mutant's seemingly normal rhabdomere optics, as appeared under light microscopy, and their wild-type like photoreceptor voltage/intensity relations (see Chapter 3), it is conceivably expected

that $\Delta\rho$ values measured from *hdc*^{JK910} photoreceptors would be close to those of wild-type. Indeed, the difference of 10.9% between receptive field widths of dark-adapted wild-type and mutant photoreceptors was slight and marginal, compared to cell-to-cell variation within each genotype population, where the maximum values were 66% and 88% wider than the minimum values, respectively. Also, its statistical significance was not consistently detectable when only a sub-set of samples was taken into consideration, as in sections 4.3.2 and 4.3.3 of this chapter.

Alongside with previous studies by Dubs et al. (1981) and Dubs (1982), my findings presented in this chapter suggest that under dim light intensity, lateral excitation might occur rather early in the insect visual system. Summation of spatial information is possibly implemented by interneurons and fed back to photoreceptors. However, in order to exhaustively prove or disprove this hypothesis, anatomical studies are required to investigate any possible developmental defection of *hdc*^{JK910} retina. For example, a slight decrease in rhabdomere size would also lead to narrower photoreceptor receptive field.

From the available data, the effects of ambient illumination on $\Delta\rho$ of wild-type and *hdc*^{JK910} photoreceptors were very similar, despite wild-type receptive field appeared to be slightly more affected. Further experiments to increase the n-number are necessary to either consolidate this finding or identify any marginal difference. Moreover, comparing photoreceptor receptive fields under brighter ambient light, which might reveal important adaptation features of spatial coding, is recommended for future research.

Chapter 5: Neural images of moving objects in fly retina

5.1 Introduction

Voltage response of a single photoreceptor reveals important aspects of retinal image processing that improve a fly's ability to detect small objects in fast chasing flights or against cluttered background (Burton and Laughlin, 2003, Brinkworth et al., 2008). Indeed, in an ideal case where an object uniformly moves across an array of photoreceptors, each cell would produce identical response but displaced in time by Δ*t*, which is the time needed for the object to travel between receptive field centres of two adjacent cells (Srinivasan and Bernard, 1975). Therefore, response of the whole array, i.e. neural representation of the moving object, would be a travelling pattern with the mirrored waveform of and can be extrapolated from response of single sampling unit. Here, I apply this principle to simplify questions about retinal images of moving objects to aspects of single photoreceptor response, hence further investigate characteristics of spatiotemporal coding in the fly compound eye.

The first problem to be considered in this chapter is the compensation of neural latency in motion perception, which is related to the flash-lag effects observed in human (Krekelberg and Lappe, 2001, Nijhawan, 2002). Due to the inevitable delay of phototransduction, almost every animal encounters this same problem and flies are not exceptions. For instance, intracellular voltage of a dark-adapted *Drosophila* photoreceptor typically peaks 25-40 ms later than the stimulating light flash (**Fig. 3-2D**, Chapter 3; at 19 ºC). Given that *Drosophila* turning speed (yaw rotation) could be as fast as 1000 º/s (Fry et al., 2003), such delay must have been corrected by visual processing, otherwise neural images of surrounding environment would have lagged behind their actual positions by more than 25º, making fast behaviour infeasible. Physiological studies have shown that these compensations take place rather early in vertebrate visual systems. As in the tiger salamander and rabbit retina, firing rates of their ganglion cell lagged behind flashing but not moving bars (Berry et al., 1999). Whether similar neural computation happens in insect early vision is unknown. By monitoring voltage response of *Calliphora*, wild-type *Drosophila* and the mutant hdc^{JK910} photoreceptors while point objects travelled pass their visual fields, I found that neural latency is not compensated in the fly retina.

Photoreceptor responses to moving objects exhibited similar lagging time as responses elicited by light flashes.

Secondly, I examine whether response to motion in the fly retina displays directional preference, as might be suggested by previous studies. Anatomically, while each of the Large Monopolar Cells L1 and L2 mediate a major neural pathway in the lamina, L2 cells appeared to have much richer connectivity. Only L2 was found to project synaptic feedback to photoreceptors and have reciprocal connections with L4, which in turn is connected to L4s of neighbouring neural cartridges (Braitenberg and Debbage, 1974) and provide further direct/indirect feedback to photoreceptors. Moreover, every L2, but not L1 cell, is connected to two L4 cells belonging to adjacent cartridges (Meinertzhagen and Oneil, 1991, Rivera-Alba et al., 2011). Although limited physiological evidence is available to illustrate specific functional roles of this circuit (Joesch et al., 2010), these connections imply (i) stronger lateral interactions in the L2 pathway and (ii) its stronger influence on photoreceptor output than that from the L1 pathway. Importantly, Rister et al. (2007) have shown that at intermediate contrast conditions, each of L1 and L2 pathways specifically facilitate the perception of back-to-front and front-to-back motions, respectively. Since the animal fly forward much more often than moving backward, front-to-back is the dominant direction of visual stimuli. Therefore, it would be beneficial to process front-to-back stimuli by such elaborately connected neural network, including feedback from L2 and L4 interneurons to photoreceptors. Consequently, this uneven anatomical structure might result in directional selectivity of photoreceptor function. However, in the present study, directional preference was not found in the fly retina. Neural images of moving objects of both directions displayed similar waveforms and identical characteristics.

Spatiotemporal resolution of the eye is determined by two componential characteristics: temporal dynamics and static spatial resolution (Srinivasan and Bernard, 1975, Hornstein et al., 2000). These characteristics are in turn influenced by photoreceptor dark/light adaptation state and probably network feedback, as shown in Chapter 3 and Chapter 4, where photoreceptors of wild-type *Drosophila* and hdc^{JK910} mutant were comparatively studied. The third objective of this chapter is to examine possible effects of top-down regulation on visual acuity of the *Drosophila* eye by assessing the effects of motion blur and the eye's ability to resolve two objects moving together at certain speed. My data showed that in dim condition, wild-type photoreceptor exhibited markedly blurrier images and lower resolvability (*D*-values) than that of hdc^{JK910} mutant, in which interneurons are blind

and thus could not feed spatial information back to photoreceptors. Interestingly, the difference between *D*-values of wild-type and mutant photoreceptors was significantly reduced under moderate ambient illumination. These findings further support the hypothesis that was discussed in Chapter 4 and many previous studies: in dim, summation of neural signal increases sensitivity by trading-off acuity, whereas neural image is sharpened in bright by making photoreceptors more independent and/or increasing lateral inhibitory.

Volterra series is one of the most well understood and widely used modelling approaches in neurophysiology (Marmarelis and McCann, 1973, Eckert and Bishop, 1975, Gemperlein and McCann, 1975, Juusola et al., 1995, Korenberg et al., 1998), yet its applications in *Drosophila* photoreceptor have been limited to the analysis of temporal dynamics (Juusola et al., 2003, Niven et al., 2004). In this study, I also explored the use of this method in simulating *Drosophila* photoreceptor response to spatial stimuli created by moving objects. While the models were not able to consistently produce exact predictions of voltage responses, the effects of motion blurring and the difference in visual acuity of wild-type and hdc^{JK910} eyes were simulated. The detailed specifications and simulation procedures reported here might be useful for future work on mathematical modelling of photoreceptor.

5.2 Materials and Methods

5.2.1 Fly stocks

Stocks of wild-type *Drosophila* and the *hdc* mutant were maintained as described in Chapter 3.

Blowflies *Calliphora vicina* were collected in nature, bred in laboratory environment and used within 7 days of capture.

5.2.2 Visual stimuli

The lighting point array and LEDs pads used for creating images of moving objects and providing ambient illumination, respectively, were as described in Chapter 4 (**Fig. 4-1**). In experiments using *Drosophila*, the 25-point array was placed 6.7 cm away from the fly, subtending an angle of 40.92°. For *Calliphora*, the corresponding parameters were 17 cm (distance) and 16.73° (viewing angle).

Images of one moving point-object were produced by briefly turning each lighting point on and off, one after another in an incremental (for front-to-back direction) or decremental order (for back-to-front direction). Accordingly, Channel 0 input was driven with increasing or decreasing "ramp" (**Fig. 5-2A**), while Channel 1 input was set to 2 V. The travelling time of object, or duration of the "ramp", was between 50 ms and 500 ms, resulting in object speeds within naturalistic range (Hateren and Schilstra, 1999, Schilstra and Hateren, 1999, Fry et al., 2003): from 80°/s to 820°/s for *Drosophila* and 33 °/s to 334 °/s for *Calliphora*.

The ability to resolve two moving point-objects of *Drosophila* photoreceptors were tested in dim and bright conditions. The two dots were separated by 6.8° (four dark points in between) and moved together at 409°/s (**Fig. 5-5A**).

Each stimulus was presented 8-10 times to the fly and the resulting photoreceptor responses were averaged before being analysed.

5.2.3 Determining and validating Volterra series model of *Drosophila* photoreceptor from experiments using Gaussian White-noise stimuli

The principal assumptions of Volterra series method are that the system has finite memory and is time-invariant (Schetzen, 1980). That is, (i) the relationship between output (photoreceptor voltage response) $y(t)$ and input (light stimuli) $u(t)$ is characterised by an unchanging impulse response and (ii) $y(t)$ depends only on current and past values of $u(t-\tau) \to u(t)$ with limited regression time τ. The continuous form of this input/output relationship is described by the following equation:

$$y(t) = k_0 + \int_0^T k_1(\tau)u(t-\tau)\,\mathrm{d}\,\tau + \int_0^T\int_0^T k_2 u(t-\tau_1)u(t-\tau_2)\,\mathrm{d}\,\tau_1\,\mathrm{d}\,\tau_2\,, \qquad (5\text{-}1)$$

where k_0, k_1 and k_2 are the zero-, first- and second-order time-invariant kernels which define the system's impulse response. T is the finite limit of system memory.

Note that the order of the model is not limited, as expressed only up to second-order in equation (5-1), but instead could be extended arbitrarily further. However, it has been well established that response of light-adapted fly photoreceptor could be approximated accurately by linear terms (Juusola et al., 1994, Juusola et al., 1995).

Therefore, the estimation of system output was simplified to a linear convolution of input with zero- and first-order kernels. Each measurement of photoreceptor voltage response and light stimuli could be fit into the discrete and simplified form of equation (5-1) as:

$$\begin{aligned} y(n) &= k_0 + k_1(0)u(n) + k_1(1)u(n-1) + \ldots + k_1(T)u(n-T) \\ y(n-1) &= k_0 + k_1(0)u(n-1) + k_1(1)u(n-2) + \ldots + k_1(T)u(n-1-T) \\ &\vdots \\ y(n-N) &= k_0 + k_1(0)u(n-N) + k_1(1)u(n-N-1) + \ldots + k_1(T)u(n-n-T) \end{aligned} \tag{5-2}$$

The group of equations (5-2), which approximates N values of photoreceptor output, was then re-arranged into matrix form:

$$\begin{pmatrix} y(n) \\ y(n-1) \\ \vdots \\ y(n-N) \end{pmatrix} = \begin{pmatrix} 1 & u(n) & u(n-1) & \cdots & u(n-T) \\ 1 & u(n-1) & u(n-2) & \cdots & u(n-1-T) \\ & & \vdots & & \\ 1 & u(n-N) & u(n-N-1) & \cdots & u(n-N-T) \end{pmatrix} \times \begin{pmatrix} k_0 \\ k_1(0) \\ k_1(1) \\ \vdots \\ k_1(T) \end{pmatrix} \tag{5-3}$$

Equivalently, equation (5-3) could be symbolised as:

$$Y = P\theta, \tag{5-4}$$

where vector Y contained a sequence of N output values, P was the regression matrix and was constructed from lagged input values, and elements of column θ were kernel values. The problem of determining Volterra series model of fly photoreceptor was hence broken down to designing input stimuli $u(t)$ and measuring values of output $y(t)$ to construct matrices P and Y of equation (5-4), and estimating θ.

$u(t)$ was selected as a Gaussian White-noise (GWN) series with a band-width of 200 Hz so that the whole frequency range of photoreceptor response dynamics was activated. Initially, the impaled photoreceptor was light-adapted to a background (the average brightness of the GWN stimuli) in 30 seconds – 1 minute. Input was then delivered from lighting point No.13 by setting Channel 0 to 5 V and modulating Channel 1 input by the GWN series around the mean value of 2.5V. Each time series was three-second long and was repeated 8-10 times before responses were averaged. The first 1.5s of recorded data was used to estimate kernel values.

Photoreceptor output $y(t)$ was sampled at 10 kHz, then pre-processed by removing mean value and data trend and down-sampling.

Once the matrices Y and P of equation (5-4) are constructed, there are several approaches to estimate θ with minimal error, such as the least squares regression by using Gram-Schmidt orthogonalisation (Korenberg et al., 1988, Korenberg and Paarmann, 1989) or Meixner functions (Asyali and Juusola, 2005). In this study, θ was approximated by the single value decomposition method (Golub and Reinsch, 1970, Lawson and Hanson, 1974), in which the factorisation of matrix P and the calculation of its Moore-Penrose pseudoinverse matrix, P^+, were carried out by the command *pinv(P)* in MATLAB. Such large-scale computation was not possible 20 years ago but nowadays could be implemented almost instantly by any computer with more than 4GB Random Access Memory (RAM). The linear least-squares estimation of θ, θ, was given by:

$$\theta = P^{+}Y\,. \tag{5-5}$$

Computed kernels and the second half of GWN stimuli were then substituted to equation (5-2) to yield model prediction of photoreceptor response and accuracy, or fitness F, of prediction was quantified by the complement of mean squared error:

$$F = 1 - MSE = 1 - \frac{\overline{(y' - y)^2}}{\overline{(y - \bar{y})^2}}\,, \tag{5-6}$$

where y were the actual data measured from photoreceptor voltage response and y' were the values simulated by the mathematical model.

5.2.4 Simulation of photoreceptor intracellular response to motion

After determining and testing Volterra model, the next step of the modelling procedures was to approximate light stimuli (input) delivered by point-objects moving pass the visual field of a photoreceptor. Since photoreceptor response was assumed to be linearly correlated to light input, the amplitudes of flash responses obtained from receptive field scan (see Chapter 4) were also considered linear measurements of effective intensity from each lighting point. Therefore, $u_m(t)$ created by one moving object was modelled as 25 intensity steps, in which

amplitudes were proportional to their corresponding flash responses (**Fig. 5-1**). The temporal width of each step was calculated according to object speed. $u'_m(t)$ of two moving objects was constructed from the superimposition of $u_m(t)$ and $u_m(t+\Delta)$, where Δ was calculated according to objects speed and their separation angle.

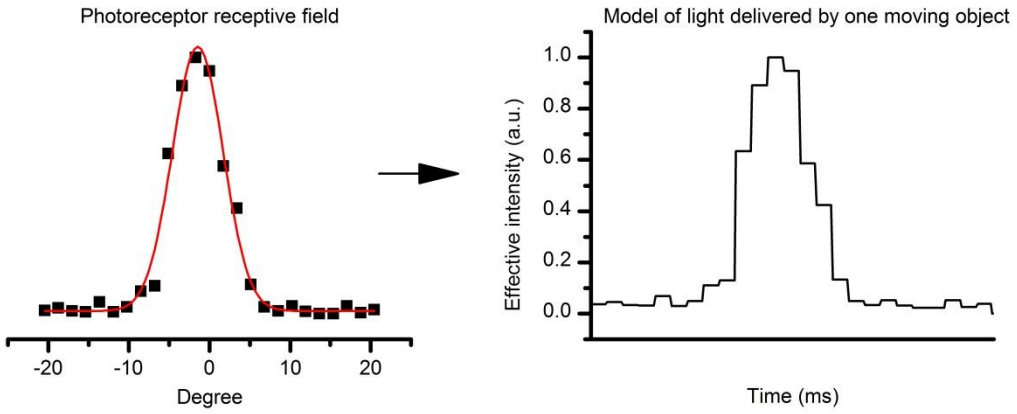

Figure 5-1. Effective light delivered to a photoreceptor by a moving object were estimated by a linear transformation of the cell's receptive field. The width of each intensity step was calculated accordingly to the object speed.

Lastly, voltage response of photoreceptor to motion was simulated by substituting input $u_m(t)$ or $u'_m(t)$ and kernels values to the zero- and first-order terms of equation (5-2).

5.3 Results

5.3.1 Retinal images in the fly eye lag behind actual positions of moving objects

Neural images in the fly retina, lamina and medulla are produced by retinotopic mapping, i.e. light coming from each point in space is sampled and processed by one neural cartridge (see Chapter 1). While a stationary object might be seen by several photoreceptors belonging to neighbouring ommatidia due to their overlapping receptive fields, the object position is perceived to be on the optical axis of the photoreceptor which itself and its corresponding lamina/medulla cartridge produce the largest/fastest intracellular responses. Thus, it is likely that position of a moving point-object is also associated with the peak of its neural image. Moreover, neural latency might be compensated at an early stage in the visual system so that

the peak of the travelling response wave would closely follow the object's actual position, as in the case of ganglion cells in vertebrate retina (Berry et al., 1999). At the level of single neuron, this "correction", if occurs, would be reflected by the coincidence of two events: (i) voltage response of the neuron peaks and (ii) the object travels pass the cell's centre of receptive field. Here to examine whether neural images of moving objects are compensated for latency at the fly retina, I measured photoreceptor intracellular responses while presenting the fly with a single point-object moving at different speeds.

Fig. 5-2B depicts typical response waveform of *Calliphora* photoreceptors to a moving point-object. Let x be the time needed for the object to travel through the 25-point array, t_1 be the moment when the object pass the cell's optical axis, i.e. the corresponding lighting-point is turned on, and t_2 be when intracellular response peaks. With varying x, and thus object speed, t_1 can be computed as:

$$t_1 = a \times x, \tag{5-7}$$

where the coefficient a is a constant. The aim was to align the 25-point array so that lighting point No.13 lie at the receptive field centre of the impaled photoreceptor, therefore in theory a is approximately 0.48. However, in fact, the lighting point No.13 might be off axis. For example, the centre of the cell's receptive field could lie in between No.13 and No.12, causing inaccuracy in the calculation of a, t_1 and lag time b, which is given by:

$$b = t_2 - t_1. \tag{5-8}$$

To overcome this ambiguity, I plotted t_2 against x, given that:

$$t_2 = t_1 + b = a \times x + b. \tag{5-9}$$

Fig. 5-2C illustrates an example of the relationship between t_2 and x obtained from a *Calliphora* photoreceptor. The two parameters fitted exceedingly well to a linear relationship (adjusted R-squared > 0.9999), in which coefficient a and lag time b were found as 0.486 and 14.62 ms, respectively. These data demonstrated that in this particular case, indeed lighting point No.13 was close to the centre of the cell's receptive field and that lag time b was virtually unchanged for different object

speeds. The on-axial position of lighting point No.13 was later confirmed by 11 receptive field scans, all of which indicated that response elicited by a light flash from No.13 was the largest (data not shown).

The same photoreceptor was also stimulated by repeating light flash, to which its voltage response displayed a time-to-peak of 15 ms. The minor difference between lag time of motion response and time-to-peak of flash response do not imply compensation of neural latency because of the essence of the two parameters. In case of moving object, photoreceptor was stimulated when the object entered its receptive field, causing its intracellular voltage to start depolarizing before the object reaching the cell's optical axis. Conversely, photoreceptor response to light impulse was only elicited after the rise of the stimulus, making time-to-peak slightly longer than lag time.

In the classic flash-lag psychological experiment, where a flashing bar and a uniformly illuminated one travelled together, the former was perceived to be trailing (Nijhawan, 1994, Brenner and Smeets, 2000). Thus, it is most probable that at some stage in the visual system, peak of voltage response caused by moving object would display shorter delay than those elicited by increase of light intensity. In the present study, the lighting point No.22 was four-fold brighter than the others, as discussed in Chapter 4, and somewhat played the role of the flashing bar, causing a "local peak" in voltage response of photoreceptors (**Fig. 5-2B**). Thus, to further examine neural latency at the fly retina, I next assessed the lag time b' corresponding to this peak of photoreceptor response. Given t_3 is the moment when No.22 was turned on, which can be calculated as:

$$t_3 = a' \times x\,, \tag{5-10}$$

and t_4 is the time of the local response peak (**Fig. 5-2B**), lag time is defined as their difference:

$$b' = t_4 - t_3\,. \tag{5-11}$$

The relationship between t_4 and x could also be described by linear fitting with almost zero residue (**Fig. 5-2D**), yielding a' and b' values of 0.83 and 13.29 ms, respectively.

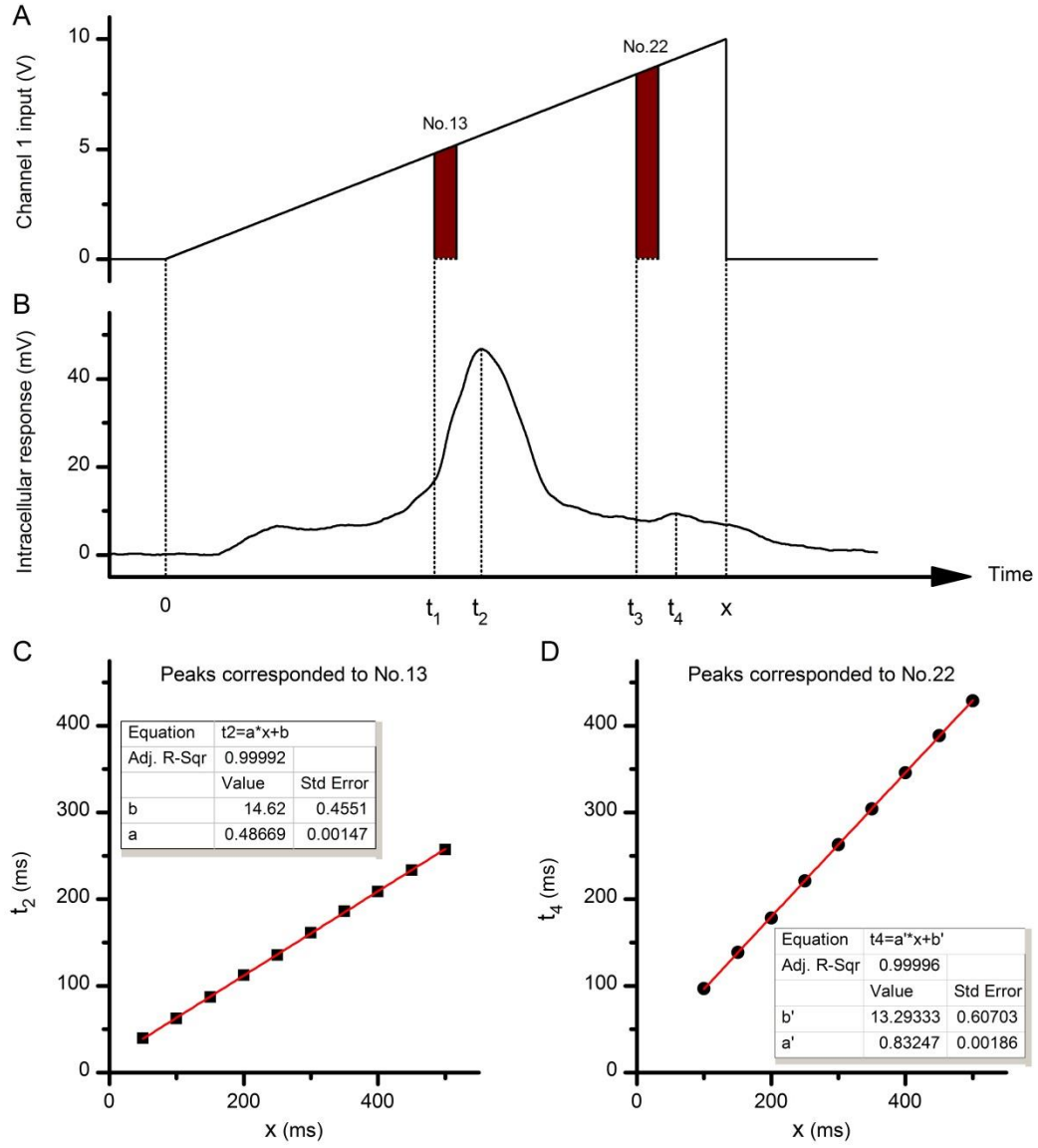

Figure 5-2. **(A)** Channel 1 input was driven by an incremental ramp to create an image of point-object moving from lighting point No.1 to No.25 (front-to-back). Similar decremental ramps were used to produce back-to-front motion.

(B) Intracellular responses of *Calliphora* photoreceptors to a moving point-object showed two response peaks: a large peak at t_2, which corresponded to the moment the object travelled pass the cell's optical axis at t_1, and a smaller peak at t_4 caused by the exceptional brightness of lighting point No.22, which was turn on at t_3. x was the object's travelling time.

(C) An example of the linear correlation between t_2 and x.

(D) An example of the linear correlation between t_4 and x.

These data illustrated that peaks of photoreceptor voltage responses, no matter caused by a point-object moving across the cell receptive field or an unexpected increase in light intensity, displayed lag time of identical characteristics. Both b and b' were independent of object speed and were comparable to the time-to-peak of flash response. These features were observed not only in this particular example but in all 7 *Calliphora* photoreceptors, without exception (**Table 5-1**).

Animal	Flash response time-to-peak (ms)	Peaks corresponded to centre of receptive field		Peaks corresponded to lighting point No.22	
		Lag-time b (ms)	Adj. R-Sqr	Lag-time b' (ms)	Adj. R-Sqr
Calliphora	14.85 ± 0.78	14.6 ± 0.64	0.99985 ± 0.00012	13.9 ± 3.59	0.99985 ± 0.00017
		n = 7		n = 5	

Table 5-1. Analysis of neural latency in response to motion of *Calliphora* photoreceptors (Mean ± SD).

Animal	Flash response time-to-peak (ms)	Front-to-back		Back-to-front	
		Lag-time b (ms)	Adj. R-Sqr	Lag-time b (ms)	Adj. R-Sqr
Wild-type *Drosophila*	23.81 ± 1.41	21.41 ± 4.5	0.99649 ± 0.0065	22.54 ± 4.15	0.99378 ± 0.007
		n = 12		n = 5	
hdc^{JK910}	24.4 ± 1.08	21.82 ± 1.36	0.9992 ± 0.0008	23.79 ± 5.72	0.9978 ± 0.003
		n = 3			

Table 5-2. Analysis of neural latency in response to motion of wild-type *Drosophila* and *hdc*^{JK910} photoreceptors (Mean ± SD).

Response of *Drosophila* photoreceptor did not clearly exhibit the "local peak" caused by lighting point No.22, owing to their slower temporal dynamics. Nevertheless, temporal position of "global peak", measured by t_2, of wild-type (n = 12) and *hdc*^{JK910} (n = 3) photoreceptors also consistently showed highly linear correlation to

x and comparable values of lag-time/time-to-peak (**Table 5-2**). Linear fittings of *Drosophila* data were not as error-free as in the case of *Calliphora* photoreceptors because lag time variations were slightly larger. However, no mathematical relation between lag time and object speed was found.

Altogether, my data demonstrated that fly photoreceptors utilise the same mechanism to sample intensity changes and motions. As neural latency is most likely compensated by the processing of higher order interneurons, neural images in the fly retina lag behind actual positions of moving objects.

5.3.2 Responses to motion of fly photoreceptor are not directionally selective

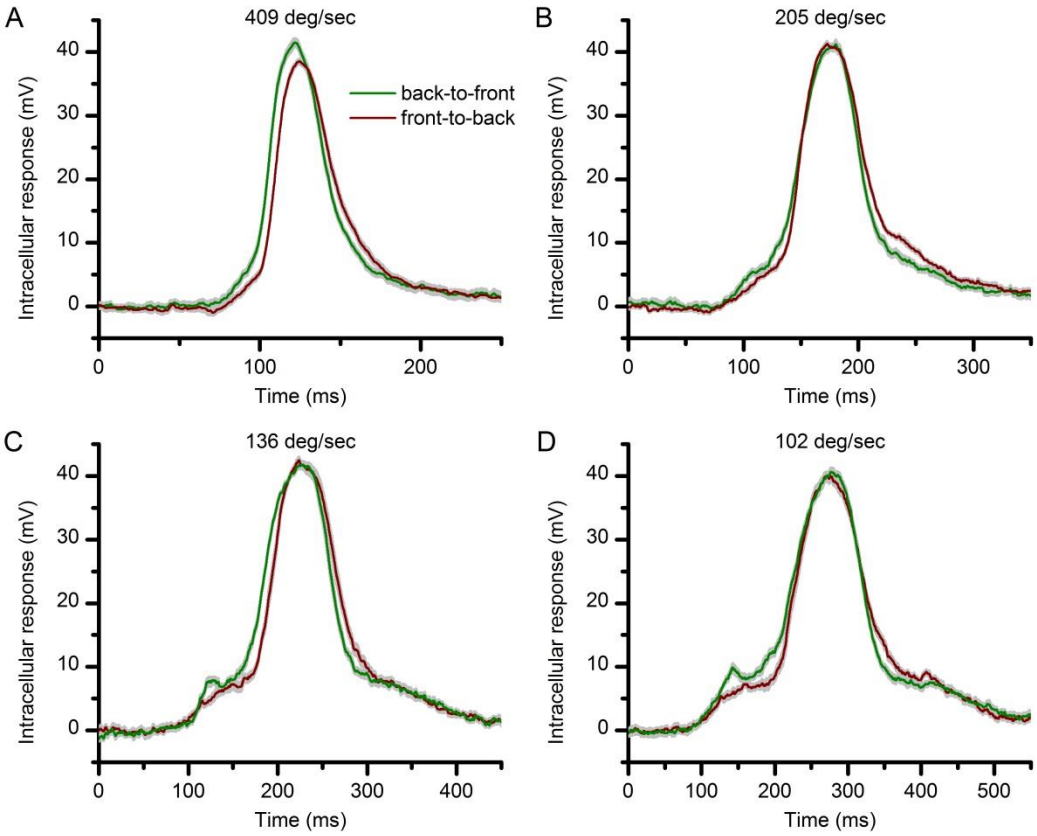

Figure 5-3. Examples of *Drosophila* photoreceptor responses to moving point-object of front-to-back and back-to-front directions (Mean ± SEM). No directional preference was found.
A-D: object speeds of 409 º/s, 205 º/s, 136 º/s and 102 º/s, respectively.

As summarised in **Table 5-2**, voltage response of *Drosophila* photoreceptor to motions of both front-to-back and back-to-front directions did not exhibit signs of

latency compensation. **Fig. 5-3** depicts typical photoreceptor response to object moving at different speeds, which shows great similarity between waveforms corresponding to the two directions. No further attempt was made to quantify minor differences, such as comparing response amplitude and temporal half-width, since such differences could be attributed to the varying intensity of the lighting point array, the off-axis position of the lighting point No.13 or the retinal movement as reported in Chapter 4 (**Fig. 4-8**). For instance, consider a photoreceptor of which optical axis points to lighting point No.14 or No.15. This would be indicated by coefficient a, obtained from responses to front-to-back motions, of values larger than 0.5. In this case, a point-object moving front-to-back (from No.1 to No.25) would give the cell slightly longer time to light-adapt before passing the cell's axis than one travelling in back-to-front direction. Consequently, intracellular response to front-to-back motion would exhibit smaller amplitude, shorter lag time and potentially narrower temporal width at half-maximum. These differences were observed in several recordings and were very slight but could be repeatable over the tested range of object speed.

In conclusion, the most prominent feature was the striking similarity between photoreceptor responses to motions of both directions. This was found in all somatic recordings of *Calliphora* and *Drosophila* photoreceptors, suggesting that there is no directional preference at the level of image sampling. Therefore, any directional preference suggested by anatomical studies can only emerge downstream at the level of network processing.

5.3.3 Possible influence of network feedback on visual acuity of the *Drosophila* compound eye

The comparative study in Chapter 3 found that, in some conditions, responses to light flashes of hdc^{JK910} photoreceptors rose faster but decayed slower than those of wild-type. On the other hand, in Chapter 4, photoreceptors of the *hdc* mutant were shown to have narrower static receptive field than their wild-type counterparts. While spatial characteristics of mutant photoreceptors imply sharper retinal images, their temporal dynamics could have mixed consequences. To further investigate how feedback regulation might affect the *Drosophila* eye, I examined two aspects of visual acuity in photoreceptors: the blurring effect of motion and the eye's ability to distinguish two moving point-objects.

Since a fast moving point-object stimulates several photoreceptors at the same time (**Fig. 5-4A**), it is not perceived as a single point but a streak, of which length is a function of object speed. This blurring effect of motion is quantified by the spatial half-width S of object's retinal image. Because spatial response in the retina has similar waveform with temporal response of a single photoreceptor (Srinivasan and Bernard, 1975, Juusola and French, 1997), S could be calculated as:

$$S = w \times T_h , \tag{5-12}$$

where w is the object speed and T_h is the temporal half-width of a single photoreceptor response.

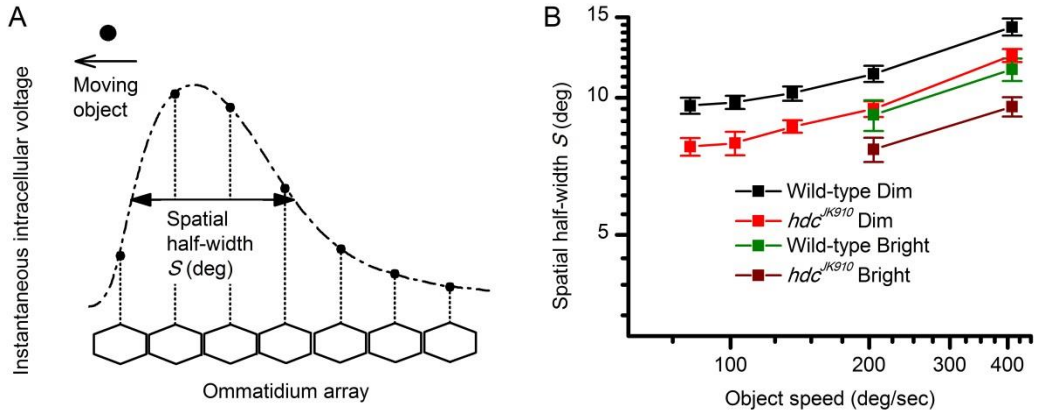

Figure 5-4. Blurring effect of motions on the *Drosophila* retinal images

(A) Spatial pattern of instantaneous voltage response at ommatidial array produced by a moving point-object (Figure redrawn from (Srinivasan and Bernard, 1975).

(B) Spatial half-width of retinal image as a function of object speed in Dim and Bright conditions. For all object speeds, S_{hdc} were significantly smaller than $S_{wild\text{-}type}$ ($p = 0.002$-0.02, t-test), except for object speed of 205°/s in Bright condition, where the statistical test yielded $p = 0.069$.

Mean ± SEM, $n_{wild\text{-}type} = 4$-15, $n_{hdc} = 3$-16, one-tailed student test.

Fig. 5-4B illustrates the relationship between object speed and image resolution in the retina of wild-type *Drosophila* and the *hdc* mutant. Data obtained from intracellular recordings were in good agreement with previous theoretical studies (Srinivasan and Bernard, 1975, Juusola and French, 1997), which predicted the existence of two distinct regions of image resolution. At low speed, visual acuity is mostly determined by the spatial receptive field of photoreceptor, while at high speed, effect of motion blurring increases rapidly to become the dominating factor.

The underlying trend suggests that the threshold dividing the two regions was approximately 100-120°/s. In both dim and moderately bright conditions, neural images encoded by mutant photoreceptors were 13%-19% sharper than those of wild-type. Besides, light-adaptation by illumination using the LEDs pads, as described in Chapter 4, narrowed the spatial half-width of retinal images by ~20% in both genotypes.

In the second type of experiments, images of two point-objects moving together at 409°/s were presented in the visual field of the fly (**Fig. 5-5A**). The ability of the eye to distinguish the objects could be assessed from whether voltage response of the impaled photoreceptors exhibit two clear peaks (**Fig. 5-5B**, solid line and **Fig. 5-5C**) or only one peak (**Fig. 5-5B**, dotted line). One-third of wild-type photoreceptors (six out of 18 cells), but only one out of 16 *hdc*^{JK910} photoreceptors, were unable to resolve the two objects. Interestingly, amongst those responses which displayed two separate peaks, the trailing peak was always larger than the leading one in wild-type responses (**Fig. 5-5B**, solid line), whereas all but one *hdc*^{JK910} photoreceptors had their leading peak as the larger (**Fig. 5-5C**).

Resolvability was further quantified by *D*-values:

$$D = \frac{d}{P}\%, \tag{5-13}$$

where P is the amplitude of the smaller peak and d is the depth of response dip between the two peaks (**Fig. 5-5C**). In darkness, *D*-values measured from mutant photoreceptors were, on average, more than double those of wild-type ($D_{\text{wild-type}}$ = 4.51 ± 2.33%, D_{hdc} = 10.5 ± 5.23%), demonstrating that *hdc*^{JK910} eye “sees” the two points more clearly than their wild-type counterpart (**Fig. 5-5D**). Under ambient illumination, while photoreceptors of both genotypes exhibited significant improvements in their image resolution ($D_{\text{wild-type}}$ = 9.81 ± 3.7%, D_{hdc} = 14.85 ± 6.95%), the difference between the two groups decreased and was at the margin of statistical significance (**Fig. 5-5E**; p = 0.058, t-test). Taking into account only cells in which *D*-values were measured in both dim and bright conditions, the enhancement of *D*-values when ambient light change was quantified by their relative change:

$$R_C = \frac{D_{\text{Bright}} - D_{\text{Dim}}}{D_{\text{Dim}}}\%. \tag{5-14}$$

On average, wild-type *D*-values improved by 262%, with a wide range from 43% to 604%. These changes appeared to be markedly larger than those observed in *hdc*^{JK910} photoreceptors, which varied from 4% to 89% and averaged as 31%. Yet, the difference between the two groups was not statistically significant because of the large individual variation (**Fig. 5-5F**).

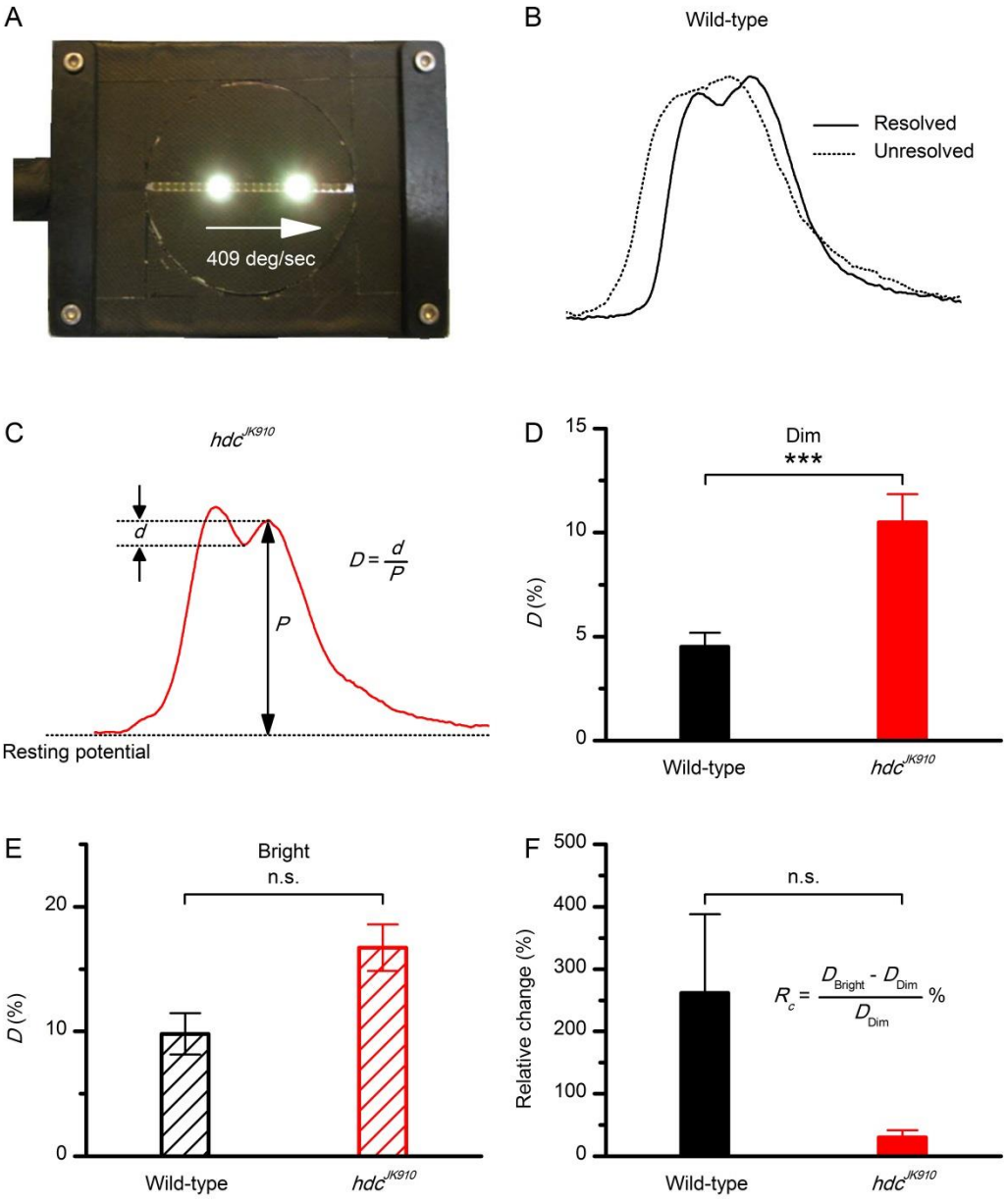

Figure 5-5. **(A)** Images of two point-objects moving together were presented in the visual field of flies. The objects were 6.8° apart and travelled at 409°/s in the front-to-back direction. For clarity, filter and the LEDs pads used for background illumination were not shown in this picture.

(B) In Dim, 6 out of 18 wild-type photoreceptors were unable to resolve the objects, showing the response waveform depicted by the dotted line, while

12 other distinguished the objects by showing the waveform as illustrated by the solid line, with the trailing peak was the larger. In Bright, 5 out of 6 examined wild-type photoreceptors produced resolved neural images.

(C) Response waveform of *hdc*^{JK910} photoreceptors exhibited two distinct peaks, with the leading one was the larger. In Dim, 15 out of 16 tested mutant photoreceptors were able to resolve the two objects and 14 of them displayed this waveform. In Bright, all of 8 recorded *hdc*^{JK910} photoreceptor responses resolved the objects. *D*-values were calculated from amplitude of the smaller peak and the dip in between (see Materials and Methods).

(D) In, Dim, *D*-values of *hdc*^{JK910} photoreceptor responses were significantly larger than their wild-type counterpart. $D_{\text{wild-type}}$ = 4.51 ± 0.67%, D_{hdc} = 10.5 ± 1.35%, p = 4×10^{-4}, t-test, $n_{\text{wild-type}}$ = 12, n_{hdc} = 15.

(E) In Bright, the difference of *D*-values of the two photoreceptor groups was at the margin of statistical significance. $D_{\text{wild-type}}$ = 9.81 ± 1.65%, D_{hdc} = 16.71 ± 1.86%, p = 0.058, t-test, $n_{\text{wild-type}}$ = 5, n_{hdc} = 8.

(F) Changing from Dim to Bright condition, *D*-values of wild-type photoreceptors appeared to exhibit larger changes than those of mutant photoreceptors. However, the difference was not statistically significant due to the large cell-to-cell variation. $R_{C\ \text{wild-type}}$ = 262 ± 126%, $R_{C\ \text{hdc}}$ = 31 ± 11%, p = 0.08, $n_{\text{wild-type}}$ = 4, n_{hdc} = 7.

D-F: Mean ± SEM, one-tailed student test.

Together, outcomes of the two experiment types consistently demonstrated that resolutions of retinal images in the *hdc* mutant's eye were better than those of wild-type in both dim and moderately bright conditions. However, when ambient light intensity changed, wild-type retina seemed to exhibit stronger improvements. One possible explanation is that these large relative changes were caused by adjustment of network feedback, of which one of main functions might be to fine-tune the balance of sensitivity and acuity. In bright condition where visual sensitivity is naturally high, resolution of neural image could be enhanced by reducing coupling of photoreceptors and/or increasing lateral inhibition in bright.

5.3.4 Modelling of *Drosophila* photoreceptor responses to Gaussian White-noise (GWN) stimuli by the Volterra series method

Volterra kernels of each photoreceptor model were computed from the first half (1.5 second) of GWN data, before the other half of recorded light stimuli and voltage response were used to validate the model. Since accuracy of output simulation

depends on factors such as input statistics and specifications of the model computation, the system identification process was optimised by selecting suitable parameters.

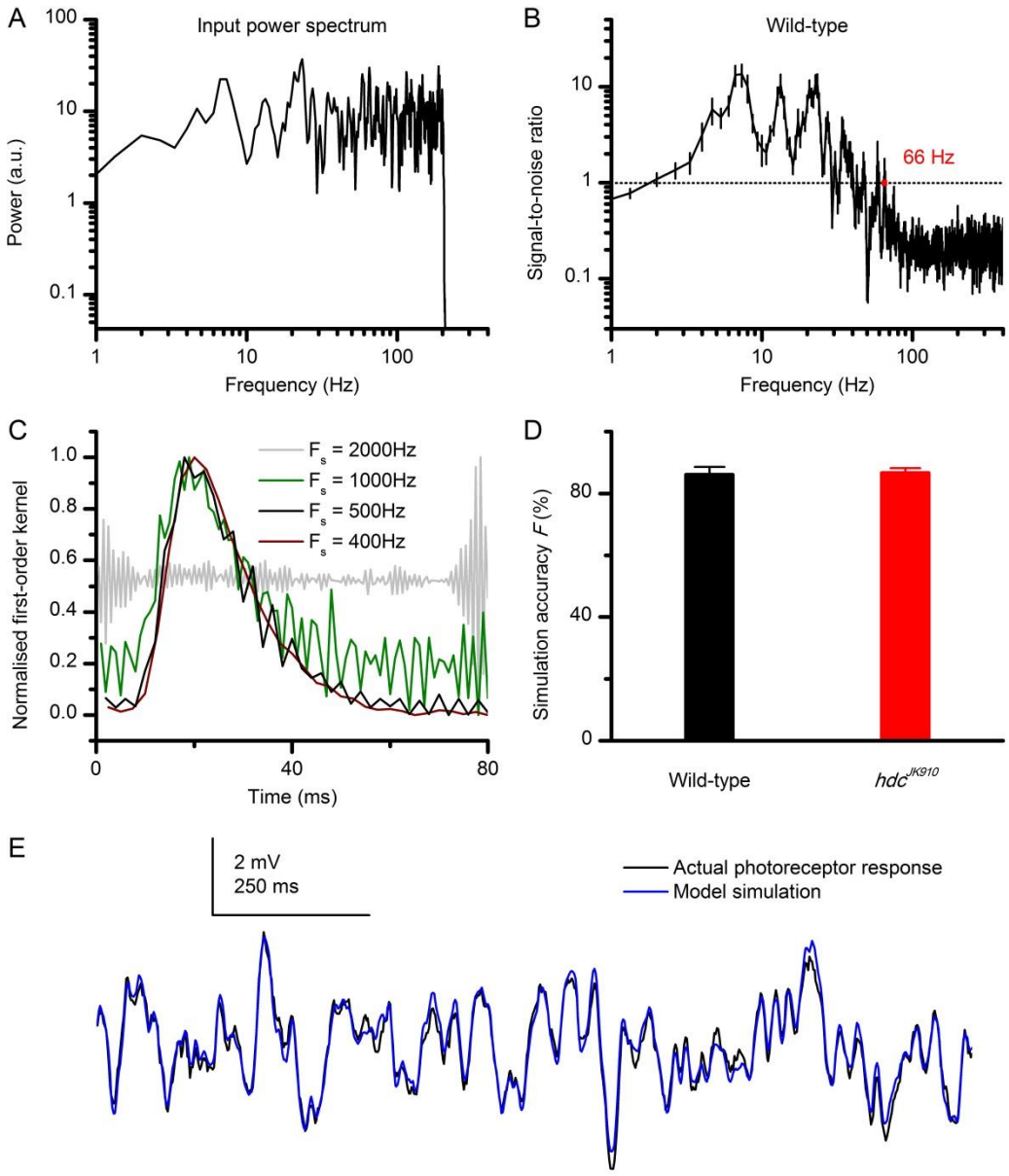

Figure 5-6. **(A)** Power spectrum of the Gaussian White-noise light stimuli with a cut-off frequency of 200 Hz.

(B) Signal-to-noise ratio of wild-type photoreceptor response. Noise power started to be larger than signal content at frequency around 66 Hz. Responses of *hdc*^{JK910} photoreceptor exhibited the same characteristic (data not shown for clarity).

(C) Example of kernels computed from data of different sampling rate, all of which originated from one set of raw data.

(D) Accuracy of GWN response simulation by Volterra series models for wild-type and *hdc*^{JK910} photoreceptors. $F_{\text{wild-type}}$ = 86 ± 2.5%, F_{hdc} = 86.6 ± 1.6%.
(E) Simulations of *Drosophila* photoreceptor response to GWN stimuli matched actual data closely.
B,D: Mean ± SEM, $n_{\text{wild-type}}$ = 9, n_{hdc} = 8.

Firstly, to examine whether the selected input bandwidth of 200 Hz (**Fig. 5-6A**) was appropriate, signal-to-noise (SNR) ratios of photoreceptor outputs were analysed. As shown in **Fig. 5-6B**, SNR decayed below one, at which point photoreceptor response started to contain more noise than signal, at around 66 Hz. Hence, it could be safely concluded that the GWN stimuli indeed activated the whole frequency range of photoreceptor dynamics.

Secondly, different values of data sampling rate were assessed. According to the Nyquist-Shannon sampling theorem, a signal with no frequencies higher than *B* Hz could be perfectly sampled and reconstructed by a sampling rate F_s of 2*B* Hz (Shannon, 1949). Since the bandwidth of interest was 0-66 Hz, data could be processed, in theory, at any sampling rate from 132 Hz to the recorded rate of 10 kHz without compromising any meaningful information.

I found that higher sampling rates tend to yield models which predict photoreceptor output with slightly higher accuracy. However, their kernels also exhibited larger fluctuations and kernel values did not decayed to zero over time, most likely due to the irrelevant components at high frequencies. For F_s = 1000 Hz and higher, such fluctuations undermined the physiological meaning the Volterra first-order kernel (**Fig. 5-6C**), which is an impulse response of photoreceptor (Victor, 1992). Thus, kernels computed from too richly-sampled data would be useful only for prediction of photoreceptor response to this particular type of light stimuli (GWN).

On the other hand, while computations performed with data of lower F_s would produce smoother kernel, a low sampling rate would also limit other application of the model. For example, Volterra series models were used to simulate photoreceptor response to the image of moving objects created by the 25 lighting point array. For an object moving at 409 º/s, its travelling time across the array was 100ms, or 4ms per lighting point. As the simulation required at least 2 data points per lighting-point, F_s was chosen to be 500 Hz, at which rate reasonably smooth kernels could still be produced (**Fig. 5-6C**).

Moreover, because value of first-order kernels decayed to zero at 50-60 ms, kernel length of 80 ms was sufficient for computations.

Volterra series models, computed from data sampled at 500 Hz, were able to consistently predict response of *Drosophila* photoreceptors to GWN stimuli (for example, see **Fig. 5-6E**). On average, accuracies of model simulations, given by equation (5-5), were ~86% in wild-type and hdc^{JK910} photoreceptor (**Fig. 5-6D**). These high values of F confirmed that it was appropriate to approximate output of light-adapted *Drosophila* photoreceptors with a linear Volterra series model.

5.3.5 Simulation of *Drosophila* photoreceptor response to moving objects

Based on the spatial stimuli approximated directly from measurements of photoreceptor receptive field and temporal dynamics modelled by Volterra series, response of *Drosophila* photoreceptor to motion were computed (see Materials and Methods).

In the case of simulating voltage response to single moving point-object, model predictions were not as consistent as for GWN stimuli. For example, **Fig. 5-7A&B** depicts simulations of high and low accuracies together with actual photoreceptor intracellular responses. Moreover, the effects of motion on resolution of retinal images were also calculated from these simulations and compared to real data (**Fig. 5-7C**), which were taken from **Fig 5-4B**. While the trend of motion blurring increase rapidly with object speed and the difference between wild-type and mutant performances were predicted well by the models, occasionally simulation and actual data were noticeably different.

In addition, Volterra series models were unreliable in predicting response of photoreceptor to two moving objects. Typically, model simulation exhibited lower resolvability than that of actual photoreceptor response (**Fig. 5-7D**). Such discrepancy reflects the drawbacks of the modelling method. While system's memory is deduced from experiments with GWN input that constantly stimulate the photoreceptor, realistic light stimuli often contain dark periods, which can enhance temporal resolution of responses (phase coding). Specifically, the interval between the two point-objects allows many microvilli to recover from their refractory periods, thus the second peak of actual photoreceptor responses are often larger than that of computer simulations, resulting in higher resolvability. Therefore, it is most probable

that models which take into account biophysical properties of the phototransduction machinery would yield better theoretical predictions (Song et al., 2012).

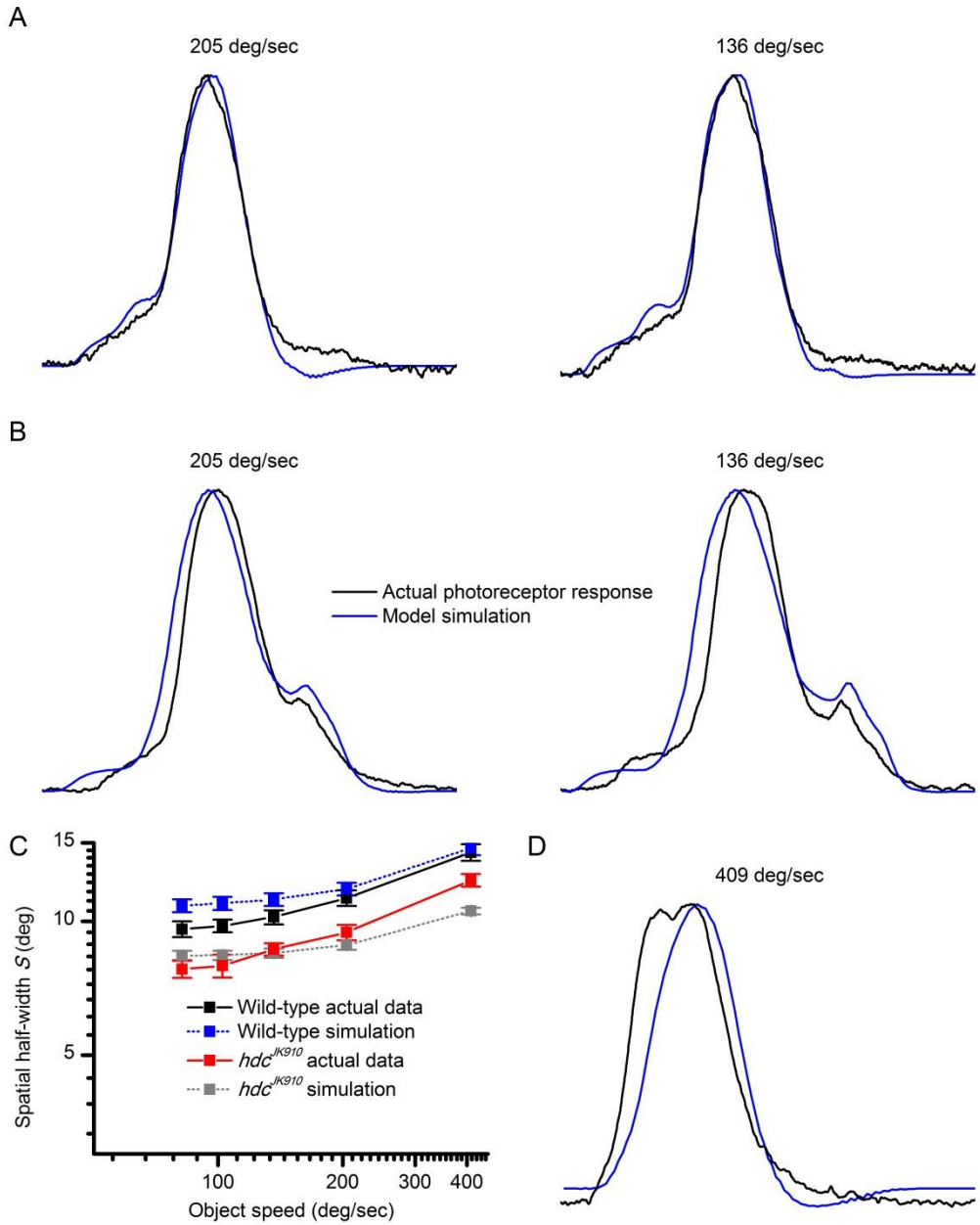

Figure 5-7. **(A)** Examples in which model simulations were very close to actual photoreceptor response to one point-object moving.

(B) Examples in which model simulations were clearly different from actual photoreceptor response to one point-object moving.

(C) Actual and model simulation of spatial half-width of retinal image as functions of object speed. Mean ± SEM, $n_{wild\text{-}type} = 9$, $n_{hdc} = 8$.

(D) Volterra series models failed to predict response of photoreceptor to two objects moving together. Typically, model simulation exhibited lower resolvability than that of actual data.

5.4 Discussions

In this chapter, neural images of moving objects in the fly retina were studied by examining intracellular response of photoreceptors and mathematical modelling. Compensation of neural latency and directional selectivity were not found at the fly retina, emphasising that the primary task of photoreceptors is to sample environmental light stimuli. To find out the stage in the visual system where such neural computations of motion processing first occur, it is recommended to next perform similar experiments and analysis on large monopolar cells. Although LMCs were shown to exhibit great similarity to bipolar cells in vertebrate (Laughlin, 1976), one could speculate that due to the small size of insect brain, LMCs might also undertake some computational functions of ganglion cells, in which firing rate could follow moving objects closely (Berry et al., 1999).

While in both dim and moderately bright condition, retinal images in the *hdc* mutant compound eye exhibited higher resolutions than those of wild-type (**Fig. 5-4B** and **Fig. 5-5D&E**), resolvability of wild-type photoreceptors showed remarkable improvements when ambient light increased (**Fig. 5-5F**). Since the drastic increase of lateral inhibition, which could significantly sharpen neural images, was observed in LMCs under wide-field illumination (Zettler and Järvilehto, 1972, Dubs, 1982, Srinivasan et al., 1990), it is highly suggestive that the difference between wild-type and hdc^{JK910} performance originated from top-down regulation. This hypothesis is also in good agreement with theories of sensory coding, which directly imply that the coding strategy in dim is to integrate information (increase sensitivity at the cost of acuity) whereas in bright, information should be differentiated to enhance image sharpness (Srinivasan et al., 1982, van Hateren, 1992c, Warrant, 1999). Nevertheless, the underlying mechanisms remained mysterious. As discussed in Chapter 3 and Chapter 4, further morphological and physiological studies to comprehensively compare the eye of wild-type *Drosophila* and hdc^{JK910} mutant are essential.

For long, It has been shown that animals counter the detrimental effect of motion blurring by moving their eyes to compensate for head and body's movement, so that position of retinal images are stationary for as long as possible (Land, 1999b). Interestingly, response of fly photoreceptor to two moving objects represents a case in which motion could be beneficial. In order to separate two stationary objects, at least three photoreceptors are required so that the dip of intensity in between could be detected. This would not be possible for two objects with an angular distance of

6.8º, given that *Drosophila* inter-ommatidial angle is ~5.8º (Land, 1997) and average half-width of receptive field is ~9.4º (Chapter 4). However, responses of single photoreceptors to two moving objects with a large enough dip in temporal axis strongly suggest that the objects could be well resolved. Indeed, outputs of several adjacent photoreceptors would have to be processed together in order to "see" two moving objects differently from one stationary object with brightness changing over time. This example highlights the inseparability of spatiotemporal information processing.

The unique advantage of the present study was the experimental set-up that allowed photoreceptor to be stimulated by images of actual moving objects, instead of using simulated light intensity series. Thus, it was possible to confirm the theoretically predicted relationship between resolution of retinal image and object speed (Srinivasan and Bernard, 1975, Juusola and French, 1997) by experimental data (**Fig. 5-4**). However, the equipment also had several limitations to be improved in future research. Wider range of object speed is necessary, especially for experiments on insects with fast visual dynamics. Owing to the long transient time, each lighting point could not be reliably turn on and off in shorter than 2 ms. Consequently, the minimum travelling time was 50 ms and upper limit for object speed in experiments with *Calliphora* was 334 º/s, which was far slower than the limit of animal's behaviour at 2000 º/s (Hateren and Schilstra, 1999, Schilstra and Hateren, 1999). Positioning the lighting point array closer to the fly might help to increase object angular speed, but would also compromise resolution of the stimuli because fewer lighting points would lie within the cell's receptive field. Moreover, it would also be more natural to stimulate the animal by images of dark objects moving against a bright background, rather than bright objects against dark background as being used in the present study.

Supplement Figures

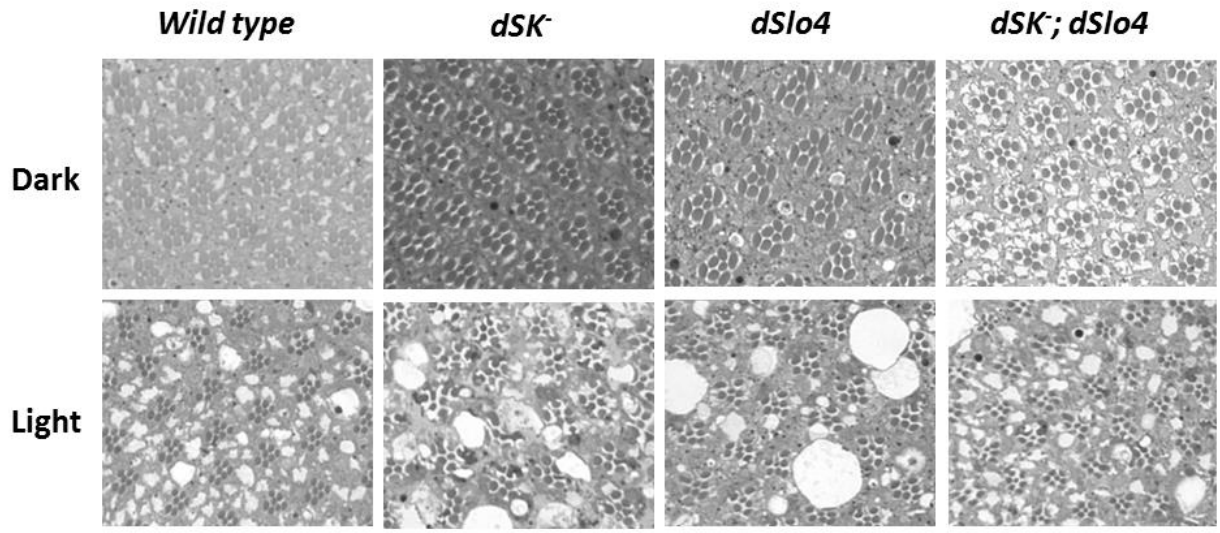

Figure S2-1. ***dSK*** **and** ***dSlo4*** **mutants undergo light-dependent retinal degeneration**

Retinal cross sections (1 µm) of wild-type flies or mutants, which were either dark- or light-reared for 10 days. Unlike wild-type, mutant light-reared eyes show several signs of retinal degeneration, including vacuolization, distorted ommatidia, and a decrease in rhabdomeric size.

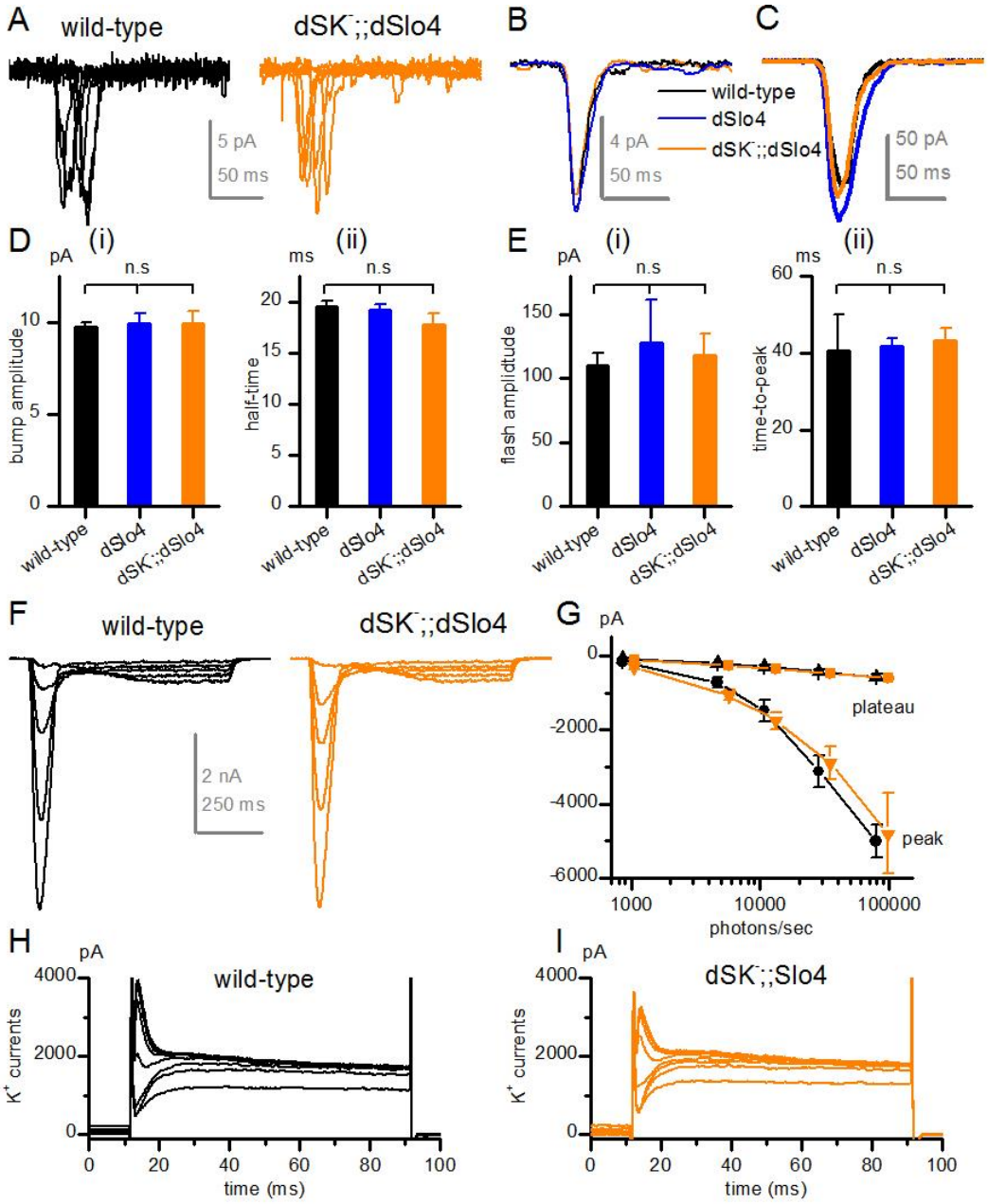

Figure S2-2. ***dSlo4* and *dSK-;;dSlo4* showed wild-type phototransduction process and normal photo-insensitive membrane properties**

(A) Superimposed quantum bumps induced by 1ms brief flashes.

(B) Averaged bumps waveform.

(C) Response to 1ms flash containing ca 20 photons.

(D) Bump statistic (amplituide and halftime).

(E) Flash response statistic (amplirude and time-to-peak).

(F) Responses to 1s steps of icnreasing intensity.

(G) Stats for peak response and plateau.

(H& I) Examples of potassium channel profiles: *Shaker* current is smaller in mutant photoreceptors, while delayed rectifier is unaffected.

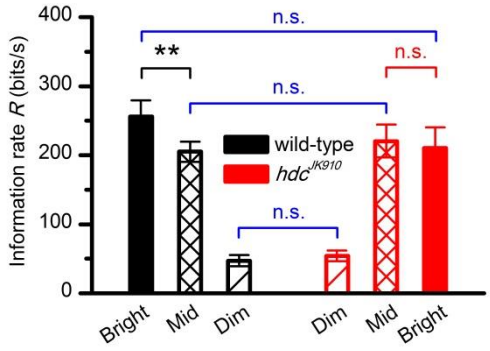

Figure S3-1. Information transfer rate calculated by using Shannon Information Theory

Dim: $R_{\text{wild-type}}$ = 47 ± 8.12, R_{hdc} = 53.88 ± 7.93; Mid: $R_{\text{wild-type}}$ = 205 ± 14.78, R_{hdc} = 220.38 ± 23.71; Bright: $R_{\text{wild-type}}$ = 256.29 ± 22.98, R_{hdc} = 210.25 ± 30.05, all in bits/second, p>0.05, t-test; Mean ± SEM, $n_{\text{wild-type}}$ = 7, n_{hdc} = 8.

Bibliography

ABBOTT, L. & LEMASSON, G. 1993. Analysis of neuron models with dynamically regulated conductances. *Neural Computation,* 5**,** 823-842.

ABOU TAYOUN, A. N., LI, X. F., CHU, B., HARDIE, R. C., JUUSOLA, M. & DOLPH, P. J. 2011. The Drosophila SK Channel (dSK) Contributes to Photoreceptor Performance by Mediating Sensitivity Control at the First Visual Network. *Journal of Neuroscience,* 31**,** 13897-13910.

ALLEN, D., NAKAYAMA, S., KUROIWA, M., NAKANO, T., PALMATEER, J., KOSAKA, Y., BALLESTEROS, C., WATANABE, M., BOND, C. T. & LUJÁN, R. 2011. SK2 channels are neuroprotective for ischemia-induced neuronal cell death. *Journal of Cerebral Blood Flow & Metabolism,* 31**,** 2302-2312.

ASYALI, M. H. & JUUSOLA, M. 2005. Use of meixner functions in estimation of Volterra kernels of nonlinear systems with delay. *IEEE Trans Biomed Eng,* 52**,** 229-37.

ATKINSON, N. S., ROBERTSON, G. A. & GANETZKY, B. 1991. A component of calcium-activated potassium channels encoded by the Drosophila slo locus. *Science,* 253**,** 551-5.

ATTNEAVE, F. 1954. Some informational aspects of visual perception. *Psychological review,* 61**,** 183.

BARLOW, H. B. 1961. Possible principles underlying the transformation of sensory messages. *Sensory communication***,** 217-234.

BAUSENWEIN, B. & FISCHBACH, K. 1992. Separation of functional pathways in the fly's medulla: combination of 2-deoxyglucose studies with anatomical fine analysis. *Nervous systems: principles of design and function. Bombay: Wiley Eastern. p***,** 223-240.

BECKER, M. N., BRENNER, R. & ATKINSON, N. S. 1995. Tissue-specific expression of a Drosophila calcium-activated potassium channel. *J Neurosci,* 15**,** 6250-9.

BERRY, M. J., BRIVANLOU, I. H., JORDAN, T. A. & MEISTER, M. 1999. Anticipation of moving stimuli by the retina. *Nature,* 398**,** 334-338.

BLONDEAU, J. & HEISENBERG, M. 1982. The three-dimensional optomotor torque system ofDrosophila melanogaster. *Journal of comparative physiology,* 145**,** 321-329.

BORST, A. 2009. *Drosophila*'s View on Insect Vision. *Current biology,* 19**,** R36-R47.

BORST, A. & HAAG, J. 2002. Neural networks in the cockpit of the fly. *Journal of Comparative Physiology A,* 188**,** 419-437.

BORST, A. & HAAG, J. 2007. 5 Optic Flow Processing in the Cockpit of the Fly. *Cold Spring Harbor Monograph Archive,* 49**,** 101-122.

BOSCHEK, G. B. 1971. On the fine structure of the peripheral retina and lamina ganglionaris of the fly, Musca domestica. *Zeitschrift für Zellforschung und mikroskopische Anatomie,* 118**,** 369-409.

BRAITENBERG, V. & DEBBAGE, P. 1974. A regular net of reciprocal synapses in the visual system of the fly, Musca domestica. *Journal of comparative physiology,* 90**,** 25-31.

BRAITENBERG, V. V. 1967. Patterns of projection in the visual system of the fly. I. Retina-lamina projections. *Experimental Brain Research,* 3**,** 271-298.

BRENNER, E. & SMEETS, J. B. 2000. Motion extrapolation is not responsible for the flash–lag effect. *Vision research,* 40**,** 1645-1648.

BRINKWORTH, R. S., MAH, E. L., GRAY, J. P. & O'CARROLL, D. C. 2008. Photoreceptor processing improves salience facilitating small target detection in cluttered scenes. *J Vis,* 8**,** 8 1-17.

BURG, M. G., SARTHY, P. V., KOLIANTZ, G. & PAK, W. L. 1993. Genetic and molecular identification of a Drosophila histidine decarboxylase gene required in photoreceptor transmitter synthesis. *EMBO J,* 12**,** 911-9.

BURKHARDT, D. 1977. Vision of Insects. *Journal of Comparative Physiology,* 120**,** 33-50.

BURKHARDT, D. A. 1993. Synaptic Feedback, Depolarization, and Color Opponency in Cone Photoreceptors. *Visual Neuroscience,* 10**,** 981-989.

BURTON, B. G. & LAUGHLIN, S. B. 2003. Neural images of pursuit targets in the photoreceptor arrays of male and female houseflies Musca domestica. *J Exp Biol,* 206**,** 3963-77.

BURTON, B. G., TATLER, B. W. & LAUGHLIN, S. B. 2001. Variations in photoreceptor response dynamics across the fly retina. *Journal of Neurophysiology,* 86**,** 950-960.

BUSCHBECK, E. K. & FRIEDRICH, M. 2008. Evolution of insect eyes: tales of ancient heritage, deconstruction, reconstruction, remodeling, and recycling. *Evolution: Education and Outreach,* 1**,** 448-462.

CLANDININ, T. R. & ZIPURSKY, S. L. 2002. Making connections in the fly visual system. *Neuron,* 35**,** 827-841.

CLARK, B. D., KURTH-NELSON, Z. L. & NEWMAN, E. A. 2009. Adenosine-evoked hyperpolarization of retinal ganglion cells is mediated by G-protein-coupled inwardly rectifying K+ and small conductance Ca2+-activated K+ channel activation. *J Neurosci,* 29**,** 11237-45.

CLARK, D. A., BURSZTYN, L., HOROWITZ, M. A., SCHNITZER, M. J. & CLANDININ, T. R. 2011. Defining the computational structure of the motion detector in Drosophila. *Neuron,* 70**,** 1165-77.

DE POLAVIEJA, G. G. 2002. Errors drive the evolution of biological signalling to costly codes. *J Theor Biol,* 214**,** 657-64.

DIRNAGL, U., IADECOLA, C. & MOSKOWITZ, M. A. 1999. Pathobiology of ischaemic stroke: an integrated view. *Trends in neurosciences,* 22**,** 391-397.

DOUGLASS, J. K. & STRAUSFELD, N. J. 2003. Anatomical organization of retinotopic motion-sensitive pathways in the optic lobes of flies. *Microscopy research and technique,* 62**,** 132-150.

DUBS, A. 1982. The spatial integration of signals in the retina and lamina of the fly compound eye under different conditions of luminance. *Journal of comparative physiology,* 146**,** 321-343.

DUBS, A., LAUGHLIN, S. & SRINIVASAN, M. 1981. Single photon signals in fly photoreceptors and first order interneurones at behavioral threshold. *The Journal of Physiology,* 317**,** 317-334.

ECKERT, H. 1982. The vertical-horizontal neurone (VH) in the lobula plate of the blowfly, Phaenicia. *Journal of comparative physiology,* 149**,** 195-205.

ECKERT, H. & BISHOP, L. G. 1975. Nonlinear dynamic transfer characteristics of cells in the peripheral visual pathway of flies. I. The retinula cells. *Biol Cybern,* 17**,** 1-6.

EGELHAAF, M. & BORST, A. 1993. A look into the cockpit of the fly: visual orientation, algorithms, and identified neurons.

EGELHAAF, M., KERN, R., KRAPP, H. G., KRETZBERG, J., KURTZ, R. & WARZECHA, A.-K. 2002. Neural encoding of behaviourally relevant visual-motion information in the fly. *Trends in neurosciences,* 25**,** 96-102.

EGUCHI, E. & HORIKOSHI, T. 1984. Comparison of Stimulus-Response (V-Log-I) Functions in 5 Types of Lepidopteran Compound Eyes (46 Species). *Journal of Comparative Physiology,* 154**,** 3-12.

ELYADA, Y. M. 2009. *Intracellular processing of motion information in a network of blowfly visual interneurons.* lmu.

FABER, E. S., DELANEY, A. J. & SAH, P. 2005. SK channels regulate excitatory synaptic transmission and plasticity in the lateral amygdala. *Nat Neurosci,* 8**,** 635-41.
FABER, E. S. & SAH, P. 2003. Calcium-activated potassium channels: multiple contributions to neuronal function. *Neuroscientist,* 9**,** 181-94.
FISCHBACH, K.-F. & HIESINGER, P. R. 2008. Optic lobe development. *Brain development in Drosophila melanogaster.* Springer.
FRY, S. N., SAYAMAN, R. & DICKINSON, M. H. 2003. The aerodynamics of free-flight maneuvers in Drosophila. *Science,* 300**,** 495-498.
GEMPERLEIN, R. & MCCANN, G. D. 1975. A study of the response properties of retinula cells of flies using nonlinear identification theory. *Biol Cybern,* 19**,** 147-58.
GENGS, C. X., LEUNG, H. T., SKINGSLEY, D. R., IOVCHEV, M. I., YIN, Z., SEMENOV, E. P., BURG, M. G., HARDIE, R. C. & PAK, W. L. 2002. The target of Drosophila photoreceptor synaptic transmission is a histamine-gated chloride channel encoded by ort (hclA). *Journal of Biological Chemistry,* 277**,** 42113-42120.
GOLUB, G. H. & REINSCH, C. 1970. Singular value decomposition and least squares solutions. *Numerische Mathematik,* 14**,** 403-420.
GONZALEZ-BELLIDO, P. T., WARDILL, T. J. & JUUSOLA, M. 2011. Compound eyes and retinal information processing in miniature dipteran species match their specific ecological demands. *Proceedings of the National Academy of Sciences of the United States of America,* 108**,** 4224-4229.
GOTZ, K. G. 1964. [Optomoter studies of the visual system of several eye mutants of the fruit fly Drosophila]. *Kybernetik,* 2**,** 77-92.
GREINER, B., RIBI, W. A. & WARRANT, E. J. 2005. A neural network to improve dim-light vision? Dendritic fields of first-order interneurons in the nocturnal bee Megalopta genalis. *Cell Tissue Res,* 322**,** 313-20.
GRIBKOFF, V. K., STARRETT, J. E. & DWORETZKY, S. I. 2001. Maxi-K potassium channels: form, function, and modulation of a class of endogenous regulators of intracellular calcium. *The Neuroscientist,* 7**,** 166-177.
GRIMES, W. N., LI, W., CHAVEZ, A. E. & DIAMOND, J. S. 2009. BK channels modulate pre- and postsynaptic signaling at reciprocal synapses in retina. *Nat Neurosci,* 12**,** 585-92.
HARDIE, R., FRANCESCHINI, N., RIBI, W. & KIRSCHFELD, K. 1981. Distribution and properties of sex-specific photoreceptors in the flyMusca domestica. *Journal of comparative physiology,* 145**,** 139-152.
HARDIE, R. & POSTMA, M. 2008. 1.05 Phototransduction in Microvillar Photoreceptors of Drosophila and Other Invertebrates.
HARDIE, R. & WECKSTRÖM, M. 1990. Three classes of potassium channels in large monopolar cells of the blowfly Calliphora vicina. *Journal of Comparative Physiology A,* 167**,** 723-736.
HARDIE, R. C. 1979. Electro-Physiological Analysis of Fly Retina .1. Comparative Properties of R1-6 and R7 and 8. *Journal of Comparative Physiology,* 129**,** 19-33.
HARDIE, R. C. 1987. Is Histamine a Neurotransmitter in Insect Photoreceptors. *Journal of Comparative Physiology a-Sensory Neural and Behavioral Physiology,* 161**,** 201-213.
HARDIE, R. C. 1989. A Histamine-Activated Chloride Channel Involved in Neurotransmission at a Photoreceptor Synapse. *Nature,* 339**,** 704-706.
HARDIE, R. C. 1991a. Voltage-Sensitive Potassium Channels in Drosophila Photoreceptors. *Journal of Neuroscience,* 11**,** 3079-3095.
HARDIE, R. C. 1991b. Whole-Cell Recordings of the Light-Induced Current in Dissociated Drosophila Photoreceptors - Evidence for Feedback by Calcium

Permeating the Light-Sensitive Channels. *Proceedings of the Royal Society B-Biological Sciences,* 245**,** 203-210.
HARDIE, R. C. 2001. Phototransduction in Drosophila melanogaster. *J Exp Biol,* 204**,** 3403-9.
HARDIE, R. C. & RAGHU, P. 2001. Visual transduction in Drosophila. *Nature,* 413**,** 186-193.
HARDIE, R. C., VOSS, D., PONGS, O. & LAUGHLIN, S. B. 1991. Novel potassium channels encoded by the Shaker locus in Drosophila photoreceptors. *Neuron,* 6**,** 477-86.
HATEREN, J. H. & SCHILSTRA, C. 1999. Blowfly flight and optic flow. II. Head movements during flight. *J Exp Biol,* 202 (Pt 11)**,** 1491-500.
HATEREN, J. V. 1984. Waveguide theory applied to optically measured angular sensitivities of fly photoreceptors. *Journal of Comparative Physiology A: Neuroethology, Sensory, Neural, and Behavioral Physiology,* 154**,** 761-771.
HEISENBE.M 1971. Separation of Receptor and Lamina Potentials in Electroretinogram of Normal and Mutant Drosophila. *Journal of Experimental Biology,* 55**,** 85-&.
HENGSTENBERG, R., HAUSEN, K. & HENGSTENBERG, B. 1982. The number and structure of giant vertical cells (VS) in the lobula plate of the blowflyCalliphora erythrocephala. *Journal of comparative physiology,* 149**,** 163-177.
HOFBAUER, A. & BUCHNER, E. 1989. Does Drosophila have seven eyes? *Naturwissenschaften,* 76**,** 335-336.
HORNSTEIN, E. P., O'CARROLL, D. C., ANDERSON, J. C. & LAUGHLIN, S. B. 2000. Sexual dimorphism matches photoreceptor performance to behavioural requirements. *Proc Biol Sci,* 267**,** 2111-7.
HORRIDGE, D., MIMURA, K. & HARDIE, R. C. 1976. Fly Photoreceptors. III. Angular Sensitivity as a Function of Wavelength and the Limits of Resolution. *Proc R Soc Lond B Biol Sci,* 194**,** 151-177.
HOTTA, Y. & BENZER, S. 1969. Abnormal Electroretinograms in Visual Mutants of Drosophila. *Nature,* 222**,** 354-&.
JACKMAN, S. L., BABAI, N., CHAMBERS, J. J., THORESON, W. B. & KRAMER, R. H. 2011. A Positive Feedback Synapse from Retinal Horizontal Cells to Cone Photoreceptors. *Plos Biology,* 9.
JOESCH, M., PLETT, J., BORST, A. & REIFF, D. F. 2008. Response properties of motion-sensitive visual interneurons in the lobula plate of Drosophila melanogaster. *Current Biology,* 18**,** 368-374.
JOESCH, M., SCHNELL, B., RAGHU, S. V., REIFF, D. F. & BORST, A. 2010. ON and OFF pathways in Drosophila motion vision. *Nature,* 468**,** 300-U186.
JUUSOLA, M. & DE POLAVIEJA, G. G. 2003. The rate of information transfer of naturalistic stimulation by graded potentials. *Journal of General Physiology,* 122**,** 191-206.
JUUSOLA, M. & FRENCH, A. S. 1997. Visual acuity for moving objects in first- and second-order neurons of the fly compound eye. *J Neurophysiol,* 77**,** 1487-95.
JUUSOLA, M. & HARDIE, R. C. 2001a. Light adaptation in Drosophila photoreceptors: I. Response dynamics and signaling efficiency at 25 degrees C. *J Gen Physiol,* 117**,** 3-25.
JUUSOLA, M. & HARDIE, R. C. 2001b. Light adaptation in Drosophila photoreceptors: II. Rising temperature increases the bandwidth of reliable signaling. *J Gen Physiol,* 117**,** 27-42.
JUUSOLA, M., KOUVALAINEN, E., JARVILEHTO, M. & WECKSTROM, M. 1994. Contrast gain, signal-to-noise ratio, and linearity in light-adapted blowfly photoreceptors. *J Gen Physiol,* 104**,** 593-621.

JUUSOLA, M., NIVEN, J. E. & FRENCH, A. S. 2003. Shaker K+ channels contribute early nonlinear amplification to the light response in Drosophila photoreceptors. *Journal of neurophysiology,* 90**,** 2014-2021.
JUUSOLA, M., WECKSTROM, M., UUSITALO, R. O., KORENBERG, M. J. & FRENCH, A. S. 1995. Nonlinear models of the first synapse in the light-adapted fly retina. *J Neurophysiol,* 74**,** 2538-47.
KATZ, B. & MINKE, B. 2009. Drosophila photoreceptors and signaling mechanisms. *Frontiers in cellular neuroscience,* 3.
KIRSCHFELD, K. 1967. Die Projektion der optischen Umwelt auf das Raster der Rhabdomere im Komplexauge von Musca. *Experimental Brain Research,* 3**,** 248-270.
KIRSCHFELD, K. & FRANCESCHINI, N. 1969a. Ein Mechanismus zur Steuerung des Lichtflusses in den Rhabdomeren des Komplexauges von Musca. *Kybernetik,* 6**,** 13-22.
KIRSCHFELD, K. & FRANCESCHINI, N. 1969b. [A mechanism for the control of the light flow in the rhabdomeres of the complex eye of Musca]. *Kybernetik,* 6**,** 13-22.
KLAUS, A. & WARRANT, E. J. 2009. Optimum spatiotemporal receptive fields for vision in dim light. *J Vis,* 9**,** 18 1-16.
KLOCKER, N., OLIVER, D., RUPPERSBERG, J. P., KNAUS, H. G. & FAKLER, B. 2001. Developmental expression of the small-conductance Ca(2+)-activated potassium channel SK2 in the rat retina. *Mol Cell Neurosci,* 17**,** 514-20.
KOLODZIEJCZYK, A., SUN, X. J., MEINERTZHAGEN, I. A. & NASSEL, D. R. 2008. Glutamate, GABA and Acetylcholine Signaling Components in the Lamina of the Drosophila Visual System. *Plos One,* 3.
KORENBERG, M. J., BRUDER, S. B. & MCILROY, P. J. 1988. Exact orthogonal kernel estimation from finite data records: extending Wiener's identification of nonlinear systems. *Ann Biomed Eng,* 16**,** 201-14.
KORENBERG, M. J., JUUSOLA, M. & FRENCH, A. S. 1998. Two methods for calculating the responses of photoreceptors to moving objects. *Ann Biomed Eng,* 26**,** 308-14.
KORENBERG, M. J. & PAARMANN, L. D. 1989. Applications of fast orthogonal search: time-series analysis and resolution of signals in noise. *Ann Biomed Eng,* 17**,** 219-31.
KREKELBERG, B. & LAPPE, M. 2001. Neuronal latencies and the position of moving objects. *Trends in neurosciences,* 24**,** 335-339.
KRETZMER, E. 1954. Redundancy in television. *Bell Lab Record***,** 401-404.
LAND, M. & ECKERT, H. 1985. Maps of the acute zones of fly eyes. *Journal of Comparative Physiology A,* 156**,** 525-538.
LAND, M. & NILSSON, D. 2002. Animal eyes Oxford. UK: Oxford University Press.
LAND, M. F. 1989. Variations in the structure and design of compound eyes. *Facets of vision.* Springer.
LAND, M. F. 1997. Visual acuity in insects. *Annu Rev Entomol,* 42**,** 147-77.
LAND, M. F. 1999a. Compound eye structure: Matching eye to environment. *Adaptive Mechanisms in the Ecology of Vision.* Springer Netherlands.
LAND, M. F. 1999b. Motion and vision: why animals move their eyes. *Journal of Comparative Physiology A,* 185**,** 341-352.
LAND, M. F. & COLLETT, T. 1974. Chasing behaviour of houseflies (Fannia canicularis). *Journal of Comparative Physiology,* 89**,** 331-357.
LAUGHLIN, S. 1976. Adaptations of the dragonfly retina for contrast detection and the elucidation of neural principles in the peripheral visual system. *Neural principles in vision.* Springer.
LAUGHLIN, S. B. 1989. The role of sensory adaptation in the retina. *J Exp Biol,* 146**,** 39-62.

LAUGHLIN, S. B. 1992. Retinal information capacity and the function of the pupil. *Ophthalmic Physiol Opt,* 12**,** 161-4.
LAUGHLIN, S. B., DE RUYTER VAN STEVENINCK, R. R. & ANDERSON, J. C. 1998. The metabolic cost of neural information. *Nat Neurosci,* 1**,** 36-41.
LAUGHLIN, S. B. & HARDIE, R. C. 1978. Common Strategies for Light Adaptation in the Peripheral Visual Systems of Fly and Dragonfly. *Journal of Comparative Physiology,* 128**,** 319-340.
LAWSON, C. L. & HANSON, R. J. 1974. *Solving least squares problems*, SIAM.
LEMASSON, G., MARDER, E. & ABBOTT, L. F. 1993. Activity-dependent regulation of conductances in model neurons. *Science,* 259**,** 1915-7.
MARDER, E. & GOAILLARD, J. M. 2006. Variability, compensation and homeostasis in neuron and network function. *Nat Rev Neurosci,* 7**,** 563-74.
MARMARELIS, P. Z. & MCCANN, G. D. 1973. Development and application of white-noise modeling techniques for studies of insect visual nervous system. *Kybernetik,* 12**,** 74-89.
MATIC, T. & LAUGHLIN, S. B. 1981. Changes in the Intensity-Response Function of an Insects Photoreceptors Due to Light Adaptation. *Journal of Comparative Physiology,* 145**,** 169-177.
MEINERTZHAGEN, I. A. & ONEIL, S. D. 1991. Synaptic Organization of Columnar Elements in the Lamina of the Wild-Type in Drosophila-Melanogaster. *Journal of Comparative Neurology,* 305**,** 232-263.
MEINERTZHAGEN, I. A. & SORRA, K. E. 2001. Synaptic organization in the fly's optic lamina: few cells, many synapses and divergent microcircuits. *Prog Brain Res,* 131**,** 53-69.
MELNATTUR, K. V. & LEE, C. H. 2011. Visual circuit assembly in Drosophila. *Dev Neurobiol,* 71**,** 1286-96.
MELZIG, J., BUCHNER, S., WIEBEL, F., WOLF, R., BURG, M., PAK, W. L. & BUCHNER, E. 1996. Genetic depletion of histamine from the nervous system of Drosophila eliminates specific visual and mechanosensory behavior. *J Comp Physiol A,* 179**,** 763-73.
MELZIG, J., BURG, M., GRUHN, M., PAK, W. L. & BUCHNER, E. 1998. Selective histamine uptake rescues photo- and mechanoreceptor function of histidine decarboxylase-deficient Drosophila mutant. *J Neurosci,* 18**,** 7160-6.
MIMURA, K. 1981. Receptive-Field Patterns in Photoreceptors of the Fly. *Journal of Comparative Physiology,* 141**,** 349-362.
MINKE, B. & COOK, B. 2002. TRP channel proteins and signal transduction. *Physiological reviews,* 82**,** 429-472.
MORANTE, J. & DESPLAN, C. 2005. Photoreceptor axons play hide and seek. *Nature neuroscience,* 8**,** 401-402.
NGO-ANH, T. J., BLOODGOOD, B. L., LIN, M., SABATINI, B. L., MAYLIE, J. & ADELMAN, J. P. 2005. SK channels and NMDA receptors form a Ca2+-mediated feedback loop in dendritic spines. *Nat Neurosci,* 8**,** 642-9.
NIJHAWAN, R. 1994. Motion extrapolation in catching. *Nature*.
NIJHAWAN, R. 2002. Neural delays, visual motion and the flash-lag effect. *Trends in cognitive sciences,* 6**,** 387-393.
NIKOLAEV, A., ZHENG, L., WARDILL, T. J., O'KANE, C. J., DE POLAVIEJA, G. G. & JUUSOLA, M. 2009. Network adaptation improves temporal representation of naturalistic stimuli in Drosophila eye: II mechanisms. *PLoS One,* 4**,** e4306.
NILSSON, D. E. 1989. Optics and evolution of the compound eye. *In:* STAVENGA, D. G. & HARDIE, R. C. (eds.) *Facets of vision.* Berlin: Springer.
NILSSON, D. E. & RO, A. I. 1994. Did neural pooling for night vision lead to the evolution of neural superposition eyes? *Journal of Comparative Physiology a-Neuroethology Sensory Neural and Behavioral Physiology,* 175**,** 289-302.

NIVEN, J. E., ANDERSON, J. C. & LAUGHLIN, S. B. 2007. Fly photoreceptors demonstrate energy-information trade-offs in neural coding. *PLoS biology,* 5**,** e116.

NIVEN, J. E., VÄHÄSÖYRINKI, M., JUUSOLA, M. & FRENCH, A. S. 2004. Interactions between light-induced currents, voltage-gated currents, and input signal properties in Drosophila photoreceptors. *Journal of neurophysiology,* 91**,** 2696-2706.

NIVEN, J. E., VÄHÄSÖYRINKI, M., KAURANEN, M., HARDIE, R. C., JUUSOLA, M. & WECKSTRÖM, M. 2003. The contribution of Shaker K+ channels to the information capacity of Drosophila photoreceptors. *Nature,* 421**,** 630-634.

PELUCCHI, B., GRIMALDI, A. & MORIONDO, A. 2008. Vertebrate rod photoreceptors express both BK and IK calcium-activated potassium channels, but only BK channels are involved in receptor potential regulation. *J Neurosci Res,* 86**,** 194-201.

PICK, B. & BUCHNER, E. 1979. Visual movement detection under light- and dark-adaptation in the fly, musca domestica. *journal of comparative physiology,* 134**,** 45-54.

RAGHU, S. V. & BORST, A. 2011. Candidate glutamatergic neurons in the visual system of Drosophila. *PLoS One,* 6**,** e19472.

RIBI, W. A. 1978. Gap junctions coupling photoreceptor axons in the first optic ganglion of the fly. *Cell and tissue research,* 195**,** 299-308.

RISTER, J., PAULS, D., SCHNELL, B., TING, C. Y., LEE, C. H., SINAKEVITCH, I., MORANTE, J., STRAUSFELD, N. J., ITO, K. & HEISENBERG, M. 2007. Dissection of the peripheral motion channel in the visual system of Drosophila melanogaster. *Neuron,* 56**,** 155-70.

RIVERA-ALBA, M., VITALADEVUNI, S. N., MISCHENKO, Y., LU, Z. Y., TAKEMURA, S. Y., SCHEFFER, L., MEINERTZHAGEN, I. A., CHKLOVSKII, D. B. & DE POLAVIEJA, G. G. 2011. Wiring Economy and Volume Exclusion Determine Neuronal Placement in the Drosophila Brain. *Current Biology,* 21**,** 2000-2005.

ROEBROEK, J. & STAVENGA, D. 1990. Insect pupil mechanisms. *Journal of Comparative Physiology A,* 166**,** 537-543.

SAH, P. 1996. Ca (2+)-activated K+ currents in neurones: types, physiological roles and modulation. *Trends in neurosciences,* 19**,** 150-154.

SALKOFF, L. 2006. A tail of multiple calcium-sensing domains. *J Gen Physiol,* 128**,** 387-8.

SCHETZEN, M. 1980. The Volterra and Wiener theories of nonlinear systems.

SCHILSTRA, C. & HATEREN, J. H. 1999. Blowfly flight and optic flow. I. Thorax kinematics and flight dynamics. *J Exp Biol,* 202 (Pt 11)**,** 1481-90.

SHANNON, C. E. 1948. A Mathematical Theory of Communication. *Bell System Technical Journal,* 27**,** 379-423.

SHANNON, C. E. 1949. Communication in the presence of noise. *Proceedings of the IRE,* 37**,** 10-21.

SHATZ, C. J. 1990. Competitive interactions between retinal ganglion cells during prenatal development. *Journal of neurobiology,* 21**,** 197-211.

SHAW, S. 1984. Early visual processing in insects. *Journal of Experimental Biology,* 112**,** 225-251.

SINAKEVITCH, I. & STRAUSFELD, N. J. 2004. Chemical neuroanatomy of the fly's movement detection pathway. *Journal of Comparative Neurology,* 468**,** 6-23.

SKORUPSKI, P. & CHITTKA, L. 2010. Differences in photoreceptor processing speed for chromatic and achromatic vision in the bumblebee, Bombus terrestris. *J Neurosci,* 30**,** 3896-903.

SMAKMAN, J. G. J. & STAVENGA, D. G. 1987. Angular Sensitivity of Blowfly Photoreceptors - Broadening by Artificial Electrical Coupling. *Journal of*

Comparative Physiology a-Sensory Neural and Behavioral Physiology, 160**,** 501-507.

SMAKMAN, J. G. J., VANHATEREN, J. H. & STAVENGA, D. G. 1984. Angular Sensitivity of Blowfly Photoreceptors - Intracellular Measurements and Wave-Optical Predictions. *Journal of Comparative Physiology,* 155**,** 239-247.

SNYDER, A. 1977. Acuity of compound eyes: physical limitations and design. *Journal of Comparative Physiology,* 116**,** 161-182.

SNYDER, A. W. & MILLER, W. H. 1977. Photoreceptor diameter and spacing for highest resolving power. *JOSA,* 67**,** 696-698.

SNYDER, A. W., STAVENGA, D. G. & LAUGHLIN, S. B. 1977. Spatial Information Capacity of Compound Eyes. *Journal of Comparative Physiology,* 116**,** 183-207.

SONG, Z. Y., POSTMA, M., BILLINGS, S. A., COCA, D., HARDIE, R. C. & JUUSOLA, M. 2012. Stochastic, Adaptive Sampling of Information by Microvilli in Fly Photoreceptors. *Current Biology,* 22**,** 1371-1380.

SRINIVASAN, M., PINTER, R. & OSORIO, D. 1990. Matched filtering in the visual system of the fly: large monopolar cells of the lamina are optimized to detect moving edges and blobs. *Proceedings of the Royal Society of London. B. Biological Sciences,* 240**,** 279-293.

SRINIVASAN, M. V. & BERNARD, G. D. 1975. The effect of motion on visual acuity of the compound eye: a theoretical analysis. *Vision research,* 15**,** 515-525.

SRINIVASAN, M. V. & DVORAK, D. 1980. Spatial processing of visual information in the movement-detecting pathway of the fly. *Journal of Comparative Physiology a-Neuroethology Sensory Neural and Behavioral Physiology,* 140**,** 1-23.

SRINIVASAN, M. V., LAUGHLIN, S. B. & DUBS, A. 1982. Predictive coding: a fresh view of inhibition in the retina. *Proc R Soc Lond B Biol Sci,* 216**,** 427-59.

STAVENGA, D. G. 2003a. Angular and spectral sensitivity of fly photoreceptors. I. Integrated facet lens and rhabdomere optics. *J Comp Physiol A Neuroethol Sens Neural Behav Physiol,* 189**,** 1-17.

STAVENGA, D. G. 2003b. Angular and spectral sensitivity of fly photoreceptors. II. Dependence on facet lens F-number and rhabdomere type in Drosophila. *J Comp Physiol A Neuroethol Sens Neural Behav Physiol,* 189**,** 189-202.

STAVENGA, D. G. 2004a. Angular and spectral sensitivity of fly photoreceptors. III. Dependence on the pupil mechanism in the blowfly Calliphora. *Journal of Comparative Physiology a-Neuroethology Sensory Neural and Behavioral Physiology,* 190**,** 115-129.

STAVENGA, D. G. 2004b. Visual acuity of fly photoreceptors in natural conditions--dependence on UV sensitizing pigment and light-controlling pupil. *J Exp Biol,* 207**,** 1703-13.

STERLING, P. 1983. Microcircuitry of the Cat Retina. *Annual Review of Neuroscience,* 6**,** 149-185.

STOCKER, M. 2004. Ca(2+)-activated K+ channels: molecular determinants and function of the SK family. *Nat Rev Neurosci,* 5**,** 758-70.

STRAUSFELD, N. & CAMPOS-ORTEGA, J. 1973. The L4 monopolar neurone: a substrate for lateral interaction in the visual system of the fly musca domestica. *Brain research,* 59**,** 97-117.

STRAUSFELD, N. J. & BRAITENBERG, V. 1970. The compound eye of the fly (Musca domestica): connections between the cartridges of the lamina ganglionaris. *Zeitschrift für vergleichende Physiologie,* 70**,** 95-104.

STRAW, A. D., WARRANT, E. J. & O'CARROLL, D. C. 2006. A 'bright zone' in male hoverfly (Eristalis tenax) eyes and associated faster motion detection and increased contrast sensitivity. *Journal of Experimental Biology,* 209**,** 4339-4354.

TAKEMURA, S. Y., KARUPPUDURAI, T., TING, C. Y., LU, Z. Y., LEE, C. H. & MEINERTZHAGEN, I. A. 2011. Cholinergic Circuits Integrate Neighboring Visual Signals in a Drosophila Motion Detection Pathway. *Current Biology,* 21**,** 2077-2084.

TAKEMURA, S. Y., LU, Z. & MEINERTZHAGEN, I. A. 2008. Synaptic circuits of the Drosophila optic lobe: the input terminals to the medulla. *Journal of Comparative Neurology,* 509**,** 493-513.

TANG, S. & GUO, A. 2001. Choice behavior of Drosophila facing contradictory visual cues. *Science,* 294**,** 1543-1547.

THORESON, W. B., BABAI, N. & BARTOLETTI, T. M. 2008. Feedback from horizontal cells to rod Photoreceptors in vertebrate retina. *Journal of Neuroscience,* 28**,** 5691-5695.

THORESON, W. B. & MANGEL, S. C. 2012. Lateral interactions in the outer retina. *Progress in Retinal and Eye Research,* 31**,** 407-441.

UGARTE, G., DELGADO, R., O'DAY, P., FARJAH, F., CID, L., VERGARA, C. & BACIGALUPO, J. 2005. Putative ClC-2 chloride channel mediates inward rectification in Drosophila retinal photoreceptors. *The Journal of membrane biology,* 207**,** 151-160.

VAHASOYRINKI, M., NIVEN, J. E., HARDIE, R. C., WECKSTROM, M. & JUUSOLA, M. 2006. Robustness of neural coding in Drosophila photoreceptors in the absence of slow delayed rectifier K+ channels. *J Neurosci,* 26**,** 2652-60.

VAN HATEREN, J. 1986. Electrical coupling of neuro-ommatidial photoreceptor cells in the blowfly. *Journal of Comparative Physiology A,* 158**,** 795-811.

VAN HATEREN, J. 1993a. Spatiotemporal contrast sensitivity of early vision. *Vision research,* 33**,** 257-267.

VAN HATEREN, J. 1993b. Three modes of spatiotemporal preprocessing by eyes. *Journal of Comparative Physiology A,* 172**,** 583-591.

VAN HATEREN, J. 1997. Processing of natural time series of intensities by the visual system of the blowfly. *Vision research,* 37**,** 3407-3416.

VAN HATEREN, J. H. 1992a. Real and optimal neural images in early vision. *Nature,* 360**,** 68-70.

VAN HATEREN, J. H. 1992b. Theoretical predictions of spatiotemporal receptive fields of fly LMCs, and experimental validation. *Journal of Comparative Physiology a-Neuroethology Sensory Neural and Behavioral Physiology,* 171**,** 157-170.

VAN HATEREN, J. H. 1992c. A theory of maximizing sensory information. *Biol Cybern,* 68**,** 23-9.

VAN HATEREN, J. H. & SNIPPE, H. P. 2001. Information theoretical evaluation of parametric models of gain control in blowfly photoreceptor cells. *Vision Res,* 41**,** 1851-65.

VICTOR, J. D. 1992. Nonlinear systems analysis in vision: Overview of kernel methods. *Nonlinear vision: Determination of neural receptive fields, function, and networks***,** 1-37.

VOGT, N. & DESPLAN, C. 2007. The First Steps in *Drosophila* Motion Detection. *Neuron,* 56**,** 5-7.

WANG, G. Y., OLSHAUSEN, B. A. & CHALUPA, L. M. 1999. Differential effects of apamin- and charybdotoxin-sensitive K+ conductances on spontaneous discharge patterns of developing retinal ganglion cells. *J Neurosci,* 19**,** 2609-18.

WARDILL, T. J., LIST, O., LI, X., DONGRE, S., MCCULLOCH, M., TING, C. Y., O'KANE, C. J., TANG, S., LEE, C. H., HARDIE, R. C. & JUUSOLA, M. 2012. Multiple spectral inputs improve motion discrimination in the Drosophila visual system. *Science,* 336**,** 925-31.

WARRANT, E. & MCINTYRE, P. 1992. The trade-off between resolution and sensitivity in compound eyes. *Nonlinear vision***,** 391-421.
WARRANT, E. & NILSSON, D.-E. 2006. *Invertebrate vision,* Cambridge, Cambridge University Press.
WARRANT, E., POROMBKA, T. & KIRCHNER, W. H. 1996. Neural image enhancement allows honeybees to see at night. *Proceedings of the Royal Society B-Biological Sciences,* 263**,** 1521-1526.
WARRANT, E. J. 1999. Seeing better at night: life style, eye design and the optimum strategy of spatial and temporal summation. *Vision Research,* 39**,** 1611-1630.
WARRANT, E. J. & MCINTYRE, P. D. 1991. Strategies for retinal design in arthropod eyes of low F-number. *Journal of Comparative Physiology A,* 168**,** 499-512.
WARRANT, E. J. & MCINTYRE, P. D. 1993. Arthropod Eye Design and the Physical Limits to Spatial Resolving Power. *Progress in Neurobiology,* 40**,** 413-461.
WASHIZU, Y., BURKHARDT, D. & STRECK, P. 1964. Visual Field of Single Retinula Cells and Interommatidial Inclination in the Compound Eye of the Blowfly Calliphora-Erythrocephala. *Zeitschrift Fur Vergleichende Physiologie,* 48**,** 413-428.
WASSLE, H. 2004. Parallel processing in the mammalian retina. *Nature Reviews Neuroscience,* 5**,** 747-757.
WERNET, M. F., LABHART, T., BAUMANN, F., MAZZONI, E. O., PICHAUD, F. & DESPLAN, C. 2003. Homothorax Switches Function of Drosophila Photoreceptors from Color to Polarized Light Sensors. *Cell,* 115**,** 267-279.
WIJNGAARD, W. & STAVENGA, D. 1975. On optical crosstalk between fly rhabdomeres. *Biological Cybernetics,* 18**,** 61-67.
WILLIAMS, D. S. 1982. Ommatidial structure in relation to turnover of photoreceptor membrane in the locust. *Cell Tissue Res,* 225**,** 595-617.
WILSON, M. 1975. Angular Sensitivity of Light and Dark Adapted Locust Retinula Cells. *Journal of Comparative Physiology,* 97**,** 323-328.
WOLFF, T. & READY, D. 1993. Pattern formation in the Drosophila retina. *The development of Drosophila melanogaster,* 2**,** 1277-1325.
XU, J. W. & SLAUGHTER, M. M. 2005. Large-conductance calcium-activated potassium channels facilitate transmitter release in salamander rod synapse. *J Neurosci,* 25**,** 7660-8.
YASUYAMA, K. & MEINERTZHAGEN, I. 1999. Extraretinal photoreceptors at the compound eye's posterior margin in Drosophila melanogaster. *Journal of Comparative Neurology,* 412**,** 193-202.
ZETTLER, F. & JÄRVILEHTO, M. 1972. Lateral inhibition in an insect eye. *Zeitschrift für vergleichende Physiologie,* 76**,** 233-244.
ZHENG, L., DE POLAVIEJA, G. G., WOLFRAM, V., ASYALI, M. H., HARDIE, R. C. & JUUSOLA, M. 2006. Feedback network controls photoreceptor output at the layer of first visual synapses in Drosophila. *J Gen Physiol,* 127**,** 495-510.
ZHENG, L., NIKOLAEV, A., WARDILL, T. J., O'KANE, C. J., DE POLAVIEJA, G. G. & JUUSOLA, M. 2009. Network adaptation improves temporal representation of naturalistic stimuli in Drosophila eye: I dynamics. *PLoS One,* 4**,** e4307.